A fluorescent nanodiamond foundation for quantum sensing in cells

Hemelaar, Simon Robert

A FLUORESCENT NANODIAMOND FOUNDATION for QUANTUM SENSING in CELLS

Simon Hemelaar

Colophon

Cover artwork:	Nora Höppener
Printing:	Ipskamp Printing B.V., *www.proefschriften.net*
ISBN:	978-94-034-1014-2
ISBN (digital):	978-94-034-1013-5

The research presented in this thesis was carried out at the Department of Biomedical Engineering of the University of Groningen. Financial support for printing this thesis was received from the University Library and the Graduate School of Medical Sciences of the University of Groningen.

rijksuniversiteit
groningen

A fluorescent nanodiamond foundation for quantum sensing in cells

Proefschrift

ter verkrijging van de graad van doctor aan de
Rijksuniversiteit Groningen
op gezag van de
rector magnificus prof. dr. E. Sterken
en volgens besluit van het College voor Promoties.

De openbare verdediging zal plaatsvinden op

woensdag 10 oktober 2018 om 12.45 uur

door

Simon Robert Hemelaar

geboren op 24 april 1989
te Weert

Promotor
Prof. dr. R. Schirhagl

Copromotor
Prof. dr. G.M. van Dam

Beoordelingscommisie
Prof. dr. L.F.M.H. de Leij
Prof. dr. H.C. van der Mei
Prof. dr. F. Treussart

Paranimfen
Felipe P. Perona-Martinez
Michael M. Lerch

CONTENTS

1. General introduction
2. The interaction of fluorescent nanodiamond probes with cellular media
3. Generally applicable transformation protocols for fluorescent nanodiamond internalization into cells
4. The response of HeLa cells to fluorescent nanodiamond uptake
5. Intracellular targeting and tracking of fluorescent nanodiamonds
6. Nanodiamonds as multi-purpose labels for microscopy
7. Discussion
8. Summary
Acknowledgements
CURRICULUM VITAE

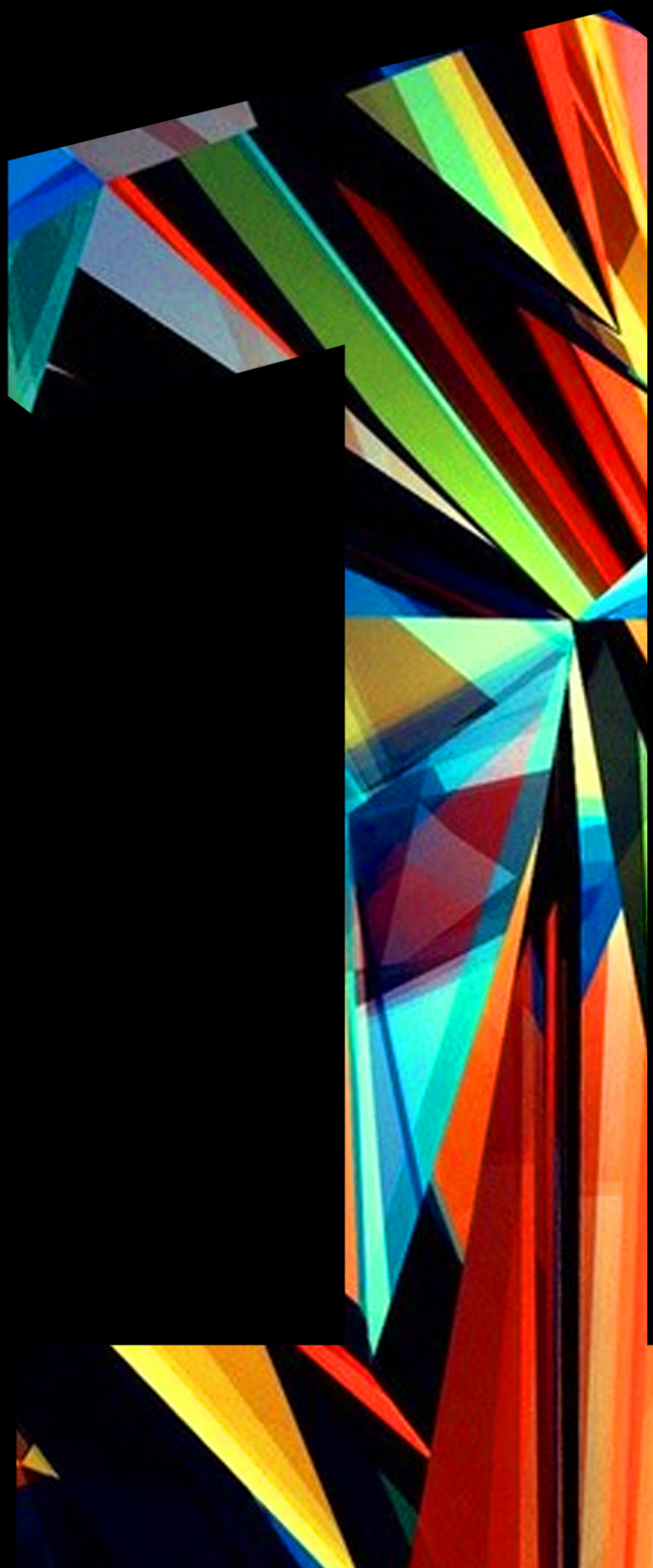

General Introduction

Simon R. Hemelaar

"Growing old with diamonds"

Getting old while staying young

"Who wants to live forever?" (Brian May, 1986) Mankind's search for immortality has already provided us with scientific clues for lengthening cellular life,[1–3] but eternal living still seems to be a far future goal. And so researchers have been focusing on improving life at later age: healthy ageing. A class of molecules involved in almost all processes of cellular ageing are free radicals.[4–6] A balance in production and scavenging of these oxidative products is imperative for a healthy intracellular environment.[7] The free electron of these molecules results in extremely high reactivity and a short lifetime (usually in the nanosecond range), which hinder temporal and spatial detection by conventional methods. This is where the Nitrogen-Vacancy center (NV-center) of fluorescent nanodiamonds (FNDs) comes into play.

Diamonds

In most people's minds, thinking about diamonds initiates a train of thoughts revolving around jewelry, marriages, money and crime in Africa. In the field of diamond science however, important distinctions need to be made in the range of diamonds. First of all, diamonds can be either produced chemically or dug up in mines. Chemically creating diamonds is a controlled process, and so it is preferred for using it in scientific applications. Synthetic diamonds can be produced by explosions and are dubbed: detonation nanodiamonds (DNDs).[8] Other nanodiamonds can be grown by High Pressure High Temerature (HPHT)[9] and be ground down to nanosize, from now on referred to simply as nanodiamonds (NDs). Although both types can have Nitrogen-Vacancy centers implanted, the differences and distinction between nanodiamonds and detonation nanodiamonds are of utmost importance. DNDs generally have a diameter of 5nm and are oval in shape. Due to their small shape and chemical surface composition they tend to aggregate easily.[10] Further, they contain relatively many impurities and the internal defects can be unstable. HPHT nanodiamonds have a bigger variation in size; ranging from 10nm to 1µm. These diamonds are very pure and have sharp edges, in a flake-like structure.[11] They have a modifiable surface[12] and can be implanted with helium for the generation of NV-centers in a high-throughput and relatively cheap manner.[13] Therefore, in this thesis all research performed uses HPHT fluorescent nanodiamonds.

The Nitrogen-Vacancy center

In 2008, the exceptional sensing capabilities of the Nitrogen-Vacancy center were first theoretically described by Christian Degen.[14] This defect consisting of a nitrogen atom replacing a carbon atom with an adjacent vacancy, exists within diamond particles. The NV-center is a fluorescent defect, and its red fluorescence is influenced by quantum parameters in the direct nanoscale environment of the diamond particle. Of particular interest in biology are the measurement of temperature[15] and magnetic sensing.[16–19] With a sensitive microscope magnetic resonances can be detected optically from the NV-center. This means that we can detect magnetic resonances using a microscope

without the need of conventional magnetic resonance equipment. In this thesis we detected magnetic resonances by using a microwave sweep, where the signal is decreased at the resonance. The distance between the two resonance lines of the NV-center is a measure for the magnetic field. A second method we are preparing in our research group is the so-called T1 measurement. This approach brings the NV-center in the ground state and observes how long it takes until the system is back to its initial state. The more reactive molecules there are in the surrounding that can interact with the NV, the faster this relaxation will be. An example of this can be found in **Figure 1.** These parameter shifts are in turn relative to the change in temperature or the size, direction and distance of a magnetic field.

Biology research with FNDs

Because diamond is an inert carbon material, cells normally do not respond to the diamonds as they would to toxic stimuli. The diamonds can even stay for prolonged times inside cells and micro-organisms, without having any toxic side-effects.[21] When cells readily take up diamond particles they are taken up through an endosomal route. The cell membrane invaginates upon contact with a diamond particle and forms an endosome. It has been speculated that due to their sharp edges, the diamonds can 'escape' the endosome and move around freely in the cytosol.[22] When the diamond is not readily taken up, which happens in different cell lines and notably in microorganisms with a cell wall, a forced uptake procedure is required. Once in the cytosol, the diamond moves seemingly at random, here, specific targeting of the particle would greatly increase the chance of locating high free radical production sites in the cell. In addition, it should be made sure that the diamond itself is not stimulating the cell to produce extra radicals, thus adding

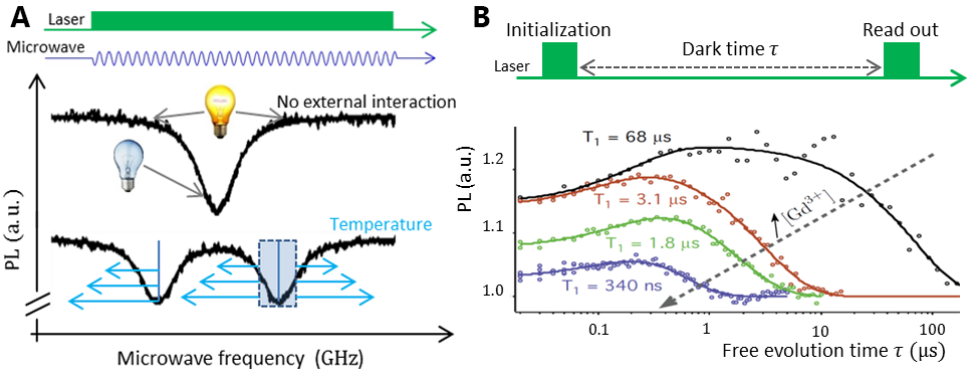

Figure 1. Theorized Quantum Measurements. Reproduced and modified from Chipaux et al.[20] **A**. The left diagram examples an ESR spectrum, which is created by analyzing the photo luminescence during a microwave sweep. For example: when the local temperature increases, the spectrum shifts to the left, when it decreases it shifts to the right. **B**. On the right a T1 curve is shown, which is created by pulsing a yellow-green light and measuring the emitted red light from the nanodiamond. The black line exemplifies a control situation, without any present stimuli. An increase of the concentration of a molecule with a 'nonzero' spin such as gadolinium (Gd^{3+}) or free radicals for example, shifts the curve to the left (red to green to blue).

a bias in the measurement. Finally, there is still a lot of uncharted territory in the possible applications for intracellular measurements using FNDs. The field of cellular magnetometry using fluorescent nanodiamonds is relatively young, with a high potential and many aspects still to be explored.

Aim of this thesis

This thesis lays the groundwork for future intracellular quantum measurements using Fluorescent Nanodiamonds. The topics of this thesis move in a gradient from chemical and biological compatibility towards applications. A key process is the taking up of diamond particles by cells. In **Chapter 2** the behavior of FNDs in cellular medium is studied, to increase the understanding of diamond interactions and reduce aggregation of the particles. **Chapter 3** focuses on the forced uptake mechanism of chemical transformation in yeast cells. The influence of the transformation procedure and diamond uptake is analyzed to probe the biocompatibility of the used method. To distinguish the cellular responses of the cell to the uptake of the diamond particle, **Chapter 4** handles the genetic, proteomic, oxidative and metabolic response of HeLa cells to diamond uptake. In **Chapter 5** we compare adsorption and covalently immobilized antibodies on the diamond surface in its targeting efficiency in both living and fixated HeLa cells. In addition, we show an ingenious way to track diamond particles inside cells and segment their trajectories into understandable factors. Obviously, 'Diamonds are forever' (Shirley Bassey, 1971) so this is especially valuable in electron microscopic applications. **Chapter 6** presents the survival of nanodiamonds after a staining and embedding technique for electron microscopy. While conventional organic dyes bleach during this procedure, FNDs remain fluorescent. The cathodoluminescent ability of the nitrogen vacancy center is presented in combination with an indirect antibody targeting technique of the diamonds. Finally, in **Chapter 7** the findings of this thesis are discussed in the light of other recent findings and opportunities for future studies are given.

References

1. Roake, C. M. & Artandi, S. E. Control of Cellular Aging, Tissue Function, and Cancer by p53 Downstream of Telomeres. *Cold Spring Harb. Perspect. Med.* a026088 (2017). doi:10.1101/cshperspect.a026088
2. Carnero, A. *et al.* Disruptive chemicals, senescence and immortality. *Carcinogenesis* **36,** S19–S37 (2015).
3. Sturm, Á., Perczel, A., Ivics, Z. & Vellai, T. The Piwi-piRNA pathway: road to immortality. *Aging Cell* (2017). doi:10.1111/acel.12630
4. Monacelli, F., Acquarone, E., Giannotti, C., Borghi, R. & Nencioni, A. Vitamin C, aging and Alzheimer's disease. *Nutrients* **9,** (2017).
5. Bu, H., Wedel, S., Cavinato, M. & Jansen-dürr, P. MicroRNA Regulation of Oxidative Stress-Induced Cellular Senescence. *Oxid. Med. Cell. Longev.* 2017, (2017).
6. Egea, J. *et al.* European contribution to the study of ROS: A summary of the findings and prospects for the future from the COST action BM1203 (EU-ROS). *Redox Biol.* **13,** 94–162 (2017).
7. Vajapey, R., Rini, D., Walston, J. & Abadir, P. The impact of age-related dysregulation of the angiotensin system on mitochondrial redox balance. *Frontiers in Physiology* **5,** (2014).
8. Mochalin, V. N., Shenderova, O., Ho, D. & Gogotsi, Y. The properties and applications of nanodiamonds. *Nat. Nanotechnol.* **7,** 11–23 (2011).
9. Boudou, J.-P. *et al.* High yield fabrication of fluorescent nanodiamonds. *Nanotechnology* **20,** 359801–359801 (2009).
10. Krüger, A. *et al.* Unusually tight aggregation in detonation nanodiamond: Identification and disintegration. *Carbon N. Y.* **43,** 1722–1730 (2005).
11. Ong, S. Y., Chipaux, M., Nagl, A. & Schirhagl, R. Shape and crystallographic orientation of nanodiamonds for quantum sensing. *Phys. Chem. Chem. Phys.* (2017). doi:10.1039/C6CP07431F
12. Nagl, A., Hemelaar, S. R. & Schirhagl, R. Improving Surface and Defect Center Chemistry of Fluorescent Nano-Diamonds for Imaging Purposes – A Review. *Anal. Bioanal. Chem.* (2015). doi:10.1007/s00216-015-8849-1
13. Chang, Y.-R. *et al.* Mass production and dynamic imaging of fluorescent nanodiamonds. *Nat. Nanotechnol.* **3,** 284–288 (2008).
14. Degen, C. L. Scanning magnetic field microscope with a diamond single-spin sensor. *Appl. Phys. Lett.* **92,** 22–24 (2008).
15. Kucsko, G. *et al.* Nanometre-scale thermometry in a living cell. *Nature* **500,** 54–8 (2013).
16. Schirhagl, R., Chang, K., Loretz, M. & Degen, C. L. Nitrogen-vacancy centers in diamond: nanoscale sensors for physics and biology. *Annu. Rev. Phys. Chem.* **65,** 83–105 (2014).
17. Le Sage, D. *et al.* Optical magnetic imaging of living cells. *Nature* **496,** 486–489 (2013).
18. Glenn, D. R. *et al.* Single-cell magnetic imaging using a quantum diamond microscope. **12,** 12–16 (2015).
19. Van der Laan, K., Hasani, M., Zheng, T. & Schirhagl, R. Nanodiamonds for In Vivo Applications. *Small* (2018). doi:10.1002/smll.201703838 (2018).
20. Chipaux, M. *et al.* Nanodiamonds and Their Applications in Cells. *Small* 1704263

(2018). doi:10.1002/smll.201704263
21. Mohan, N., Chen, C. S., Hsieh, H. H., Wu, Y. C. & Chang, H. C. In vivo imaging and toxicity assessments of fluorescent nanodiamonds in caenorhabditis elegans. *Nano Lett.* **10,** 3692–3699 (2010).
22. Chu, Z. *et al.* Unambiguous observation of shape effects on cellular fate of nanoparticles. *Sci. Rep.* **4,** 4495 (2014).

The interaction of fluorescent nanodiamond probes with cellular media

Simon R. Hemelaar[1], Andreas Nagl[1], François Bigot[1], Melissa M. Rodríguez-García[1], Marcel P. de Vries[2], Mayeul Chipaux[1] & Romana Schirhagl[1]

[1]Department of Biomedical Engineering, University Medical Center Groningen, The Netherlands.
[2]European Research Institute for the Biology of Ageing, University Medical Center Groningen, The Netherlands.

Microchimica Acta **184:4** 1001-1009 (2017)

"*Diamonds' supercape allows him to work independently*"

Abstract

Fluorescent nanodiamonds (FNDs) are promising tools to image cells, bioanalytes and physical quantities such as temperature, pressure and electric or magnetic fields with nanometer resolution. To exploit their potential for intracellular applications, the FNDs have to be brought into contact with cell culture media. The interactions between the medium and the diamonds crucially influence sensitivity as well as the ability to enter cells. The authors demonstrate that certain proteins and salts spontaneously adhere to the FNDs and may cause aggregation. This is a first investigation on the fundamental questions on how (a) FNDs interact with the medium, and (b) which proteins and salts are being attracted. A differentiation between strongly binding and weakly binding proteins is made. Not all proteins participate in the formation of FND aggregates. Surprisingly, some main components in the medium seem to play no role in aggregation. Simple strategies to prevent aggregation are discussed. These include adding the proteins, which are naturally present in the cell culture to the diamonds first and then inserting them in the full medium.

Introduction

The nitrogen vacancy center (NV-center), a lattice defect in diamond, is responsible for the stable, non-bleaching fluorescence of the diamond. It acts as a versatile quantum sensor.[1] Fluorescent nanodiamonds (FNDs) have already been used to measure several quantities including magnetic resonances,[2] temperature,[3,4] pressure and to detect external NMR and ESR signals as well as electric or magnetic fields.[5,6] Depending on the diamond surface quality, magnetic fields, for instance from a single electron spin,[7] can be detected up to tens of nm from the defect. First attempts for nanoscale intracellular measurements have been made for temperature[8] and magnetic resonances.[9,10] As a sensor probe, FNDs have several advantages: they allow unprecedented spatial resolution,[3,7] they are non-toxic[11] while they also have a modifiable surface.[10,12] The field of using nanoparticles for bioimaging has been reviewed by Wolfbeis.[13]

However, when introduced to cellular media, formation of aggregates occurs, thus greatly increasing the hydrodynamic diameter of the particles. This phenomenon is particularly relevant as aggregates reduce cellular uptake, since endocytosis is size dependent.[14] Furthermore, it is desired for sensing applications to have the FND probe as close as possible to the analyte of interest, which is impeded by the aggregation process. Forming of aggregates or the formation of a protein layer on the diamond can increase the distance between the NV-center and the target molecule. It has to be noted that our study is different from well-known aggregation in detonation nanodiamonds.[15,16] These aggregate during synthesis without the presence of other molecules. We did not investigate detonation nanodiamonds in our study.

For NDs, until now only salting out was considered in physiological salt conditions.[17] In cellular media, however, the situation is much more complex. For various nanoparticles, the formation of a so-called "protein corona" of medium components is known.[18–21] It determines the nanoparticle's physicochemical properties, including hydrodynamic size, surface charge, and aggregation behavior.[22] Proteins have already been used as coating for diamond particles.[23–26] Furthermore, the adhesion of proteins to diamond has been utilized in protein separation.[27,28] However, which of the naturally present proteins in cell medium adhere to the diamond surface plays a role in intracellular sensing applications has not been studied. Here we first observe and characterize protein corona formation and the aggregation phenomenon for diamond nanoparticles. The complex interplay between the medium components leads to the formation of aggregates of notable size (see **Figure 1**).

We investigated the influence of salts and proteins present in the medium in the aggregation process and suggest strategies to avoid or mitigate the aggregation phenomenon. We analyzed size distributions, protein presence and the surface composition of the aggregates. While working with severely aggregated particles is completely impossible for most medical applications, for the typical applications of FNDs (as sensing different quantities in cell biology) some aggregation is tolerable.[29]

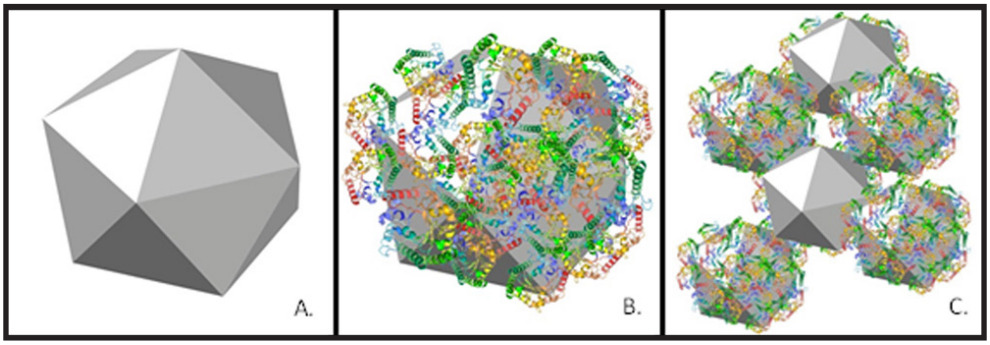

Figure 1. Schematic representation of nanodiamond aggregation. A depicts the bare Nanodiamond particle. In figure **B** the nanodiamond particle with proteins adhering to the surface is shown. Figure **C** represents the nanodiamond aggregation by interaction between multiple diamond particles through protein connections

Thus we not only looked at dispersed particles but considered it important to also analyze the composition of aggregates. Some ground breaking work has been done without considering aggregation or corona formation.[30] However, for future applications it is important to account for this effect when interpreting signals or when overcoming the current limits of the technique.

Materials and methods

Fluorescent nanodiamond (FND) starting material

FNDs with a diameter of 25 nm (later abbreviated as FND_{25}) purchased from Microdiamant AG (Lengwil, Switzerland, MSY 0–0.05 µm GAF, reference: 129,578, www.microdiamant.com), are acid cleaned and have an oxygen terminated surface. These diamond particles have a zeta potential of approximately −22 mV (see also **Table S1**). The surface charge is very important for the interaction of the diamonds with other molecules.[31,32] These particles with a flake structure[33] were used as received from the manufacturer for all experiments, except for cell uptake, because these are not detectable using normal confocal techniques due their low NV-center content. They are currently the smallest diamonds available that can be engineered so that every diamond hosts an NV-center. For cell uptake we used FNDs (end concentration 1 µg/ml) with a diameter of 70 nm (later abbreviated as FND_{70}) for better visibility due to the high number of NV-centers. They were purchased from Adámas Nanotechnologies, Inc. (NC, USA; ND-NV-70, >300 NV-centers / diamond particle, www.adamasnano.com) and used as received.

Aggregate/corona formation

We chose to analyze the interaction with DMEM (Dulbecco's Modified Eagle Medium) since it is the most common standard cell medium for culturing mammalian cells. It is a complex mixture providing cells with nutrients. It contains amino acids, vitamins,

salts, antibiotics as well as bovine serum (which itself contains a complex mixture of over 3700 proteins). Aggregates were created by dispersing the $FNDs_{25}$ to an end concentration of 200 µg mL^{-1} in different media. The different media were (1) DMEM Complete (consisting of DMEM + complements: Glutamax (1%), Pen/Strep (1%), Foetal bovine serum (FBS) (10%), Gibco Life Technologies, Bleiswijk, the Netherlands, www.thermofisher.com/ch/en/home/brands/gibco). (2) DMEM without complements and (3) pure or diluted (10%) FBS. To wash samples, we centrifuged for 10 minutes at 12.000 xG. Then we discarded the supernatant and added distilled water, shook it and sonicated it for 10 minutes, resuspending the pellet. The centrifugation was repeated and the supernatant was removed once again. The final aggregates were either resuspended again or dried to perform further experiments.

Characterization of size and appearance

Dynamic light scattering

Dynamic light scattering (DLS) measurements were performed using a Malvern ZetaSizer Nano system (Malvern Instruments Ltd., Malvern, UK, www.malvern.com) to determine the hydrodynamic diameter of the particles. Samples were measured at least in triplicate in folded capillary cells and mixed intermediary to prevent sedimentation of larger particles. Sizes were calculated using the number mean. We are aware of the fact that DLS is not ideal to determine sizes of large heterogeneous aggregate particles. Nevertheless, we found the technique very useful to screen whether or not aggregation took place qualitatively and to a small degree, quantitatively. We also confirmed the size of larger particles by TEM.

Electron microscopy

Bare $FNDs_{25}$ were prepared on a silicon surface and visualized using SEM (pictures taken in a Leo 1530 Gemini, Carl Zeiss AG, Jena, Germany, www.zeiss.com). This was done by diluting the stock solution 1:200 in methanol and dropping 5 uL of of this solution onto a 1 × 1 cm silicon wafer piece. Inlens detection and a voltage of 10 kV were used to record the images. FND_{25} aggregates with DMEM complete medium were prepared on a holey carbon coated grid (Quantifoil 1.2/1.3, Quantifoil, Jena, Germany, www.quantifoil.com). This was achieved by placing the grids for 5 minutes on a drop of the solution, removing the grid and drying for a few minutes in air. Finally, we imaged these with a TEM Philips CM12 (Philips, Eindhoven, The Netherlands, www.philips.com) equipped with a slow CCD camera to show how the proteins assemble around the crystalline diamonds (the identity of the FNDs was confirmed by selected area electron diffraction (SAED)).

Characterization of particles composition

Mass spectrometry

The following samples have been investigated: (1) FBS (as control sample), (2) 10% FBS + FNDs and (3) DMEM + FBS + FND. Samples (2) and (3) were also analyzed after washing. Samples were prepared and then washed in DI water or using a sucrose cushion. The latter method[27] removes the 'soft' protein corona. Afterwards all samples were freeze dried and prepared for HPLC and MS/MS. For a detailed description of the technique, please review **Figure S1** and **text S1** (supporting information).

X-ray photoelectron spectroscopy

Three samples were prepared by mixing diamond and medium: (a) Pure FND, (b) FND_{25} in DMEM, (c) FND_{25} in DMEM + 10% FBS, freeze dried and analyzed using a S-Probe (Surface Science Instr., Mountain View, CA, USA).

Characterization of behavior during uptake

HeLa cells (grown in DMEM complete medium) were incubated with 1 µg/ml FND_{70} for 5 h at 37°C, 5% CO_2. The $FNDs_{70}$ were prepared by dispersing them in DMEM or DMEM complete. Alternatively a sample was prepared by first mixing the diamonds in 100% FBS (end concentration 10%) followed by resuspension in DMEM. Afterwards cells were fixed with 3.7% PFA and permeabilized using 1% Triton X-100 in PBS (containing 0.9% NaCl). Cells were stained using Phalloidin-FITC (stains the actin cytoskeleton) and DAPI (stains the nucleus). Cells were imaged using a Zeiss LSM780 microscope (Zeiss, Jena, Germany, www.zeiss.com). Standard settings were used for imaging the respective dyes. Since diamond particles do not bleach, they were imaged after imaging the dyes using the highest gain settings. Diamond particles are excited with a 532 nm laser and emit a broad band above 600 nm. Magnification steps were made to visualize diamond particles.

Results and discussions

Size distribution

The first parameter we analyzed was size and appearance of our particles. This was investigated using DLS measurements. **Figure 2** shows the results of these measurements. To investigate which part of the sample is involved in aggregation we tested the components $FNDs_{25}$ in water (1) and FBS (2) as reference, and the complete DMEM medium (3) as well as composites formed from diamonds with different parts from the medium: the uncomplemented DMEM medium (4), 100% FBS (5) and 10% FBS (6). Thus, influence of salts as well as proteins on the hydrodynamic diameter was explored. To investigate how stable these aggregates are and to find out if washing is useful to reduce aggregate sizes we also washed the samples with DI water. The

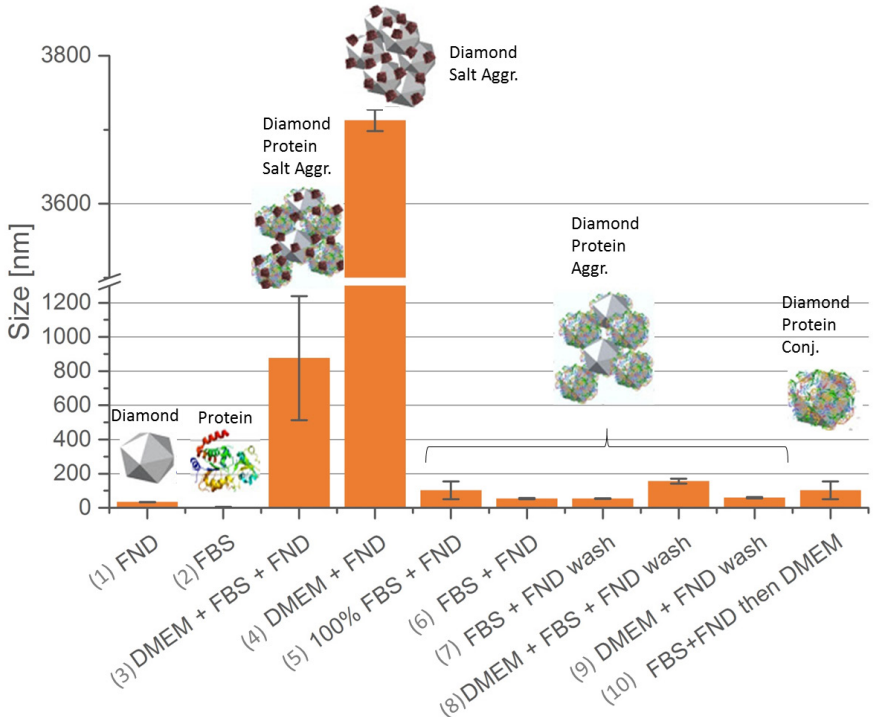

Figure 2. Hydrodynamic diameters measured using cumulant analysis for ND particles (Microdiamant MSY 0–0.05, hydrodynamic diameter 25 nm) in different media. Error bars correspond to the standard deviation. The schematics above show the composition of the particles we found. Samples (1) and (2) are reference measurements, the diamonds were suspended in water. Unless stated otherwise the concentration of FBS was 10% (prepared in distilled water to eliminate the salt effect). The samples which are labeled with "wash" are measured after resuspending the particles.

size data ((7)–(9)) in Figure 2 were taken after redispersing the washed particles in water. In the last row in Figure 2 we first mixed the $FNDs_{25}$ with FBS and then added the particles with the protein corona to DMEM medium. This method turned out to be useful to prevent aggregation.

The measurements in DI water yielded particle sizes close to the supplier information and no big increase was observed. Thus we conclude that the starting material (in agreement with the claims of the supplier) does not aggregate in water. However, when adding different medium components, the sizes increase due to either formation of a corona or aggregation. Aggregates formed from adding diamonds to salt solution (4) showed the highest hydrodynamic diameter (in the micron regime) compared to aggregates containing diamonds and proteins (samples (5) and (6)) or aggregates containing diamonds, proteins and salts (sample (3) and (10)). In sample (3), which represents the conditions in which the cells are normally cultured, we find relevant aggregation, which is however, still lower than in sample (4). Indeed proteins

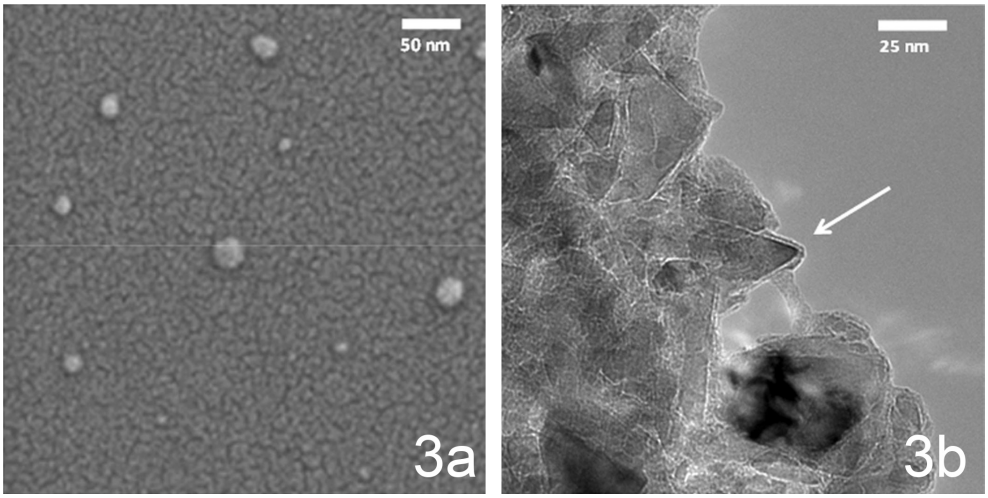

Figure 3. Electron microscopy images of FND and FND aggregates. Fluorescent nanodiamonds spotted on a silicon surface and imaged with an SEM (Leo 1530 Gemini, Carl Zeiss AG) (**3a**). FND aggregate imaged using Philips CM12 (Philips, Eindhoven, The Netherlands) on holey carbon grids (**3b**). The arrow indicates the protein corona.

mitigate the aggregation tendency to a certain degree. Introducing FNDs first to proteins to allow the formation of the protein corona followed by adding the DMEM (sample (10)) is efficiently reducing the aggregation. Washing reduces the aggregate sizes (most efficiently in sample (4). The corresponding zeta potential as well as polydispersity indices of measured particles can be found in Table S1.

Aggregate morphology

Imaging of the aggregates using electron microscopy revealed huge aggregates with proteins between the $FNDs_{25}$. In **Figure 3a** dispersed $FNDs_{25}$ (as received) can be seen on a silicon surface under a SEM (sample (1) from Figure 2). The samples were imaged at least 3 times and different areas were chosen for imaging to avoid imaging artefacts in order to find representative areas for imaging. **Figure 3b** shows the proteins assembling around the crystalline diamonds (on a holey carbon coated grid), imaged with a TEM Philips CM12 (sample (3) from Figure 2).

Composition of aggregates.

The presence of proteins on the aggregates was confirmed by Fourier transformed infrared spectroscopy (in attenuated total reflection mode and matrix-assisted laser desorption/ionization, see **Figure S4**). Proteins were analyzed after trypsin digestion using a label free mass spectrometry technique (for a detailed description of the analysis methods see text S1 and Figure S1) with a semi-quantitative assessment of relative protein amounts using normalized spectral counts.[34–36]

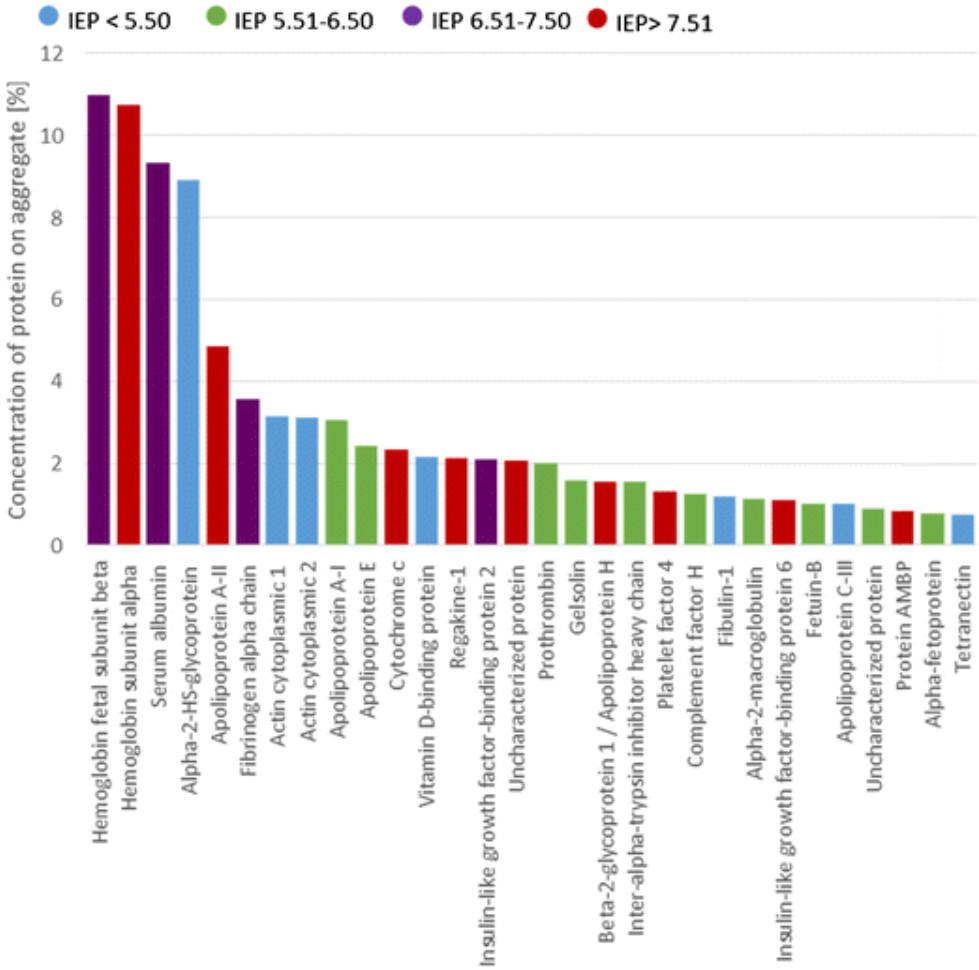

Figure 4. Most abundant proteins and their theoretical isoelectrical point present in aggregates from FND in DMEM +10% FBS (sample 3) calculated from a typical mass spectrum (for details see supplementary information)

A large number of different proteins were found in the aggregates. Interestingly, we find a great range of proteins that participate in the aggregation process that are not among the most abundant proteins of the serum, thus suggesting a certain selectivity of the nanodiamond surface towards some proteins. This selective adsorption of certain proteins onto nanoparticles is also commonly observed for other nanoparticles.[19] While in pure FBS only a total number of 25 proteins were identified. The reason is that the sample is dominated by the most abundant proteins (also known from literature[34,37]) to be serum albumin and Alpha-2-HS-glycoprotein, which make up 66% of the normalized spectral counts. Relatively rare proteins, however, can be found in the aggregates.

Figure 4 shows an overview of the most abundant proteins we found in the medium aggregates. For a detailed overview of the most important proteins in the medium and on the respective aggregate, their properties and their functions, see **table S2**. In sample DMEM + FBS + FNDs 66 proteins were identified. Similar numbers of proteins involved in the corona formation have also been found for other nanoparticles.[38] This reflects the complexity of the components involved in the aggregation process (and the crucial role of inorganic salts). Washing of samples with DI water decreases the amount of proteins by washing away the "soft" corona (loosely bound proteins). Only proteins with higher affinity remain on the diamond surface. While before washing the sample is still dominated by more abundant proteins, after washing we can identify more of the low abundance proteins. This results in over 200 proteins, which were identified. We investigated these proteins further to find any similarities between binding or non-binding proteins. Surprisingly, no correlation between the adsorption and the theoretical isoelectric point (IEP) (see Figure 4), (from http://web.expasy.org/compute_pi/) or the molecular mass of the proteins was established. Also, no significant difference between the IEP of the 25 most abundant proteins in the medium and in the diamond aggregates was found. This is in agreement with similar studies on other nanoparticles.[39,40] It can be explained by the fact that proteins have an inhomogeneous distribution of charges at their surfaces. Even with an overall negative net charge of the protein, positive charge domains may allow an electrostatic interaction with the particle surface. For multiple layers protein-protein interactions also have to be taken into account, possibly reducing the importance of the charge and polarity of the nanodiamonds. Proteins present in the aggregates, which are marked green in Table S2 show a molecular function related to binding to negative compounds (e.g. heparin or ATP). This is a possible explanation for the favored adsorption on the oxygen-terminated FNDs with a negative zeta potential. An overview of the proteins found in the aggregates is given in Figure 4.

Additionally, we investigated proteins that are even more tightly bonded to the diamond particles. These were separated by using a cleaning method suggested by Docter et al.[38] To this end the aggregates were centrifuged through a sucrose cushion to completely remove loosely bound proteins. The results (which were qualitatively similar to Figure 4) as well as some more details on the method are shown in **Figure S2.**

Surface analysis of bare particles

The analysis of bare nanodiamonds reveals oxygen groups on the surface of the diamond (hydrogen is not shown in XPS analysis). This conclusion is also supported by the FTIR spectra of the bare particles. Although diamond bands dominate the spectrum some surface groups are also visible. The broad band at 3600 cm^{-1} most likely comes from O-H groups. C = O is visible as a shoulder of the diamond peak at 1700 cm^{-1}. The peak at 1100 cm^{-1} indicates the presence of C-O groups. This indicates the presence of COOH and other oxygen containing groups, which corresponds to the manufacturers carboxylation of the particle.

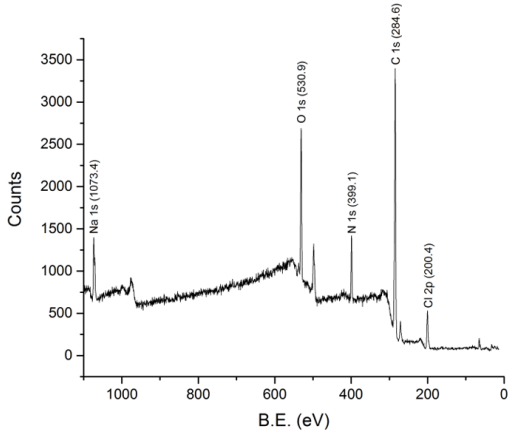

	DMEM	FND in DMEM	FND in DMEM + 10% FBS
N [%]	13	47.1	6.5
Mg [%]	0.2	-	-
Na [%]	41.4	27	18.6
P [%]	0.3	-	-
S [%]	4.7	-	-
Cl [%]	38.9	25.9	6.3
K [%]	1.3	-	-
Ca [%]	0.3	-	6.2

Figure 5. Determining the salt contribution in aggregates. Left: XPS spectrum of FND in DMEM +10% FBS (sample 3). Also here, sodium chloride remains the main compound in the aggregates (apart from the carbon mainly present as diamond, protein and amino acids). Right: Comparison of the element composition of DMEM medium, and the measured elemental ratios (which do not naturally occur on the diamond surface) in aggregate samples.

Aggregate surface analysis

The aggregates were analyzed using X-Ray Photoelectron Spectroscopy in order to determine the element composition (especially inorganic salts involved). For the results see **Figure S3** and **table S3**. Sodium chloride is the major salt component in the aggregates. While this is not surprising, calcium, magnesium, potassium and phosphorus – although in great quantity present in the medium - seem to be less abundant (if at all) in the aggregates. Together with the fact that far less aggregation is observed when leaving out sodium chloride, this suggests a central role of sodium chloride in the aggregation process. **Figure 5** lists the elements present in the measured samples compared to the salts in DMEM.

Prevention of aggregation

A simple method we found to improve aggregation is adding the FBS to diamonds first. Once a thin coating of proteins has formed on the diamond surface they can safely be introduced in the full medium. Coating the diamond with proteins from FBS is an effective option to prevent inter-particle aggregation and achieve size reduction. Indeed, the resuspension of $FNDs_{25}$ in FBS and following dilution in DMEM (end concentration 200 ng mL−1) showed an average size 90 nm, resembling the situation of diamonds in water or in 10% FBS. Compared to other methods to prevent aggregation of nanodiamonds coating with FBS first and then adding the coated protein into DMEM has an advantage; no additional proteins are introduced. If additional proteins are introduced, an exchange of proteins can occur when inserted in the final medium.

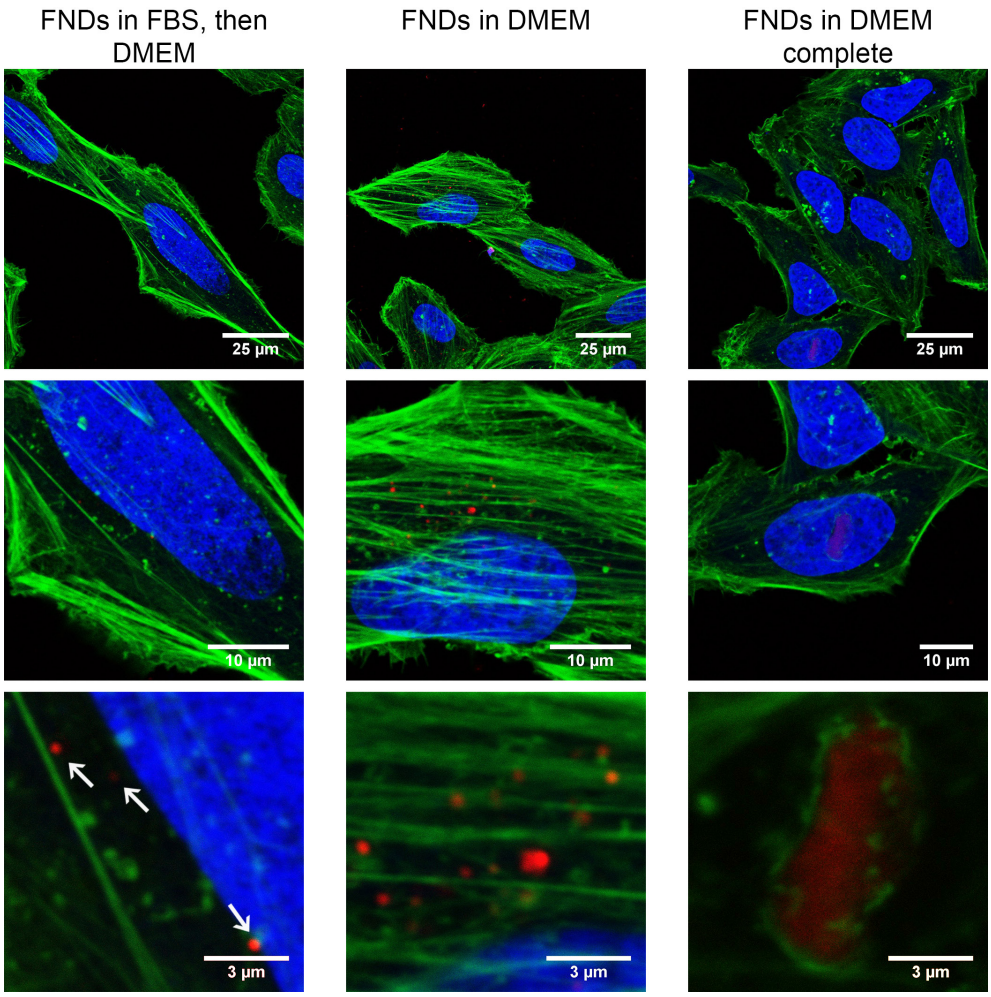

Figure 6. Cellular uptake of nanodiamonds into HeLa Cells. (red: nanodiamonds, green: Phalloidin-FITC (stains the actin cytoskeleton), blue: DAPI (stains the nucleus)). Arrows indicate diamond particles. In the lower right pane, a large diamond aggregate (occupying almost the entire area of the pane) can be seen precipitating on the cell (as it is surrounded by the actin filaments of the cytoskeleton) (DAPI was omitted to make the diamond more visible).

Cellular uptake

The reduction of fluorescent nanodiamond aggregate size greatly increases chances of having a single FND taken up inside a cell. We tested the impact of aggregation on uptake into HeLa cells using FNDs with a 70 nm diameter (manufacturer information, on average). The results of these uptake experiments are shown in the confocal image **Figure 6**, with the cells actin cytoskeleton in green, the nucleus in blue and the diamonds in red.

In the serum-free DMEM medium, there are more aggregates. In the DMEM complete medium hardly any diamond particles are taken up, however a large aggregate is shown which is precipitating on the cell (there is part of the cellular membrane around it, lower right pane, DAPI signal not shown for visualization purposes). These images are typical for the whole sample, indicating that uptake of the aggregates in HeLa cells is possible. However, for other cell types and sensing applications, single diamonds are preferred. With the resuspension of $FNDs_{70}$ in FBS before DMEM, we were able to obtain the smallest (diffraction limited) particle signal (indicating no/very little aggregation). Other options to achieve size reduction might encompass lower particle concentrations or using an inert solution as medium. Alternatively, using a less concentrated medium or a medium lacking NaCl and certain proteins found in the aggregates might prevent or improve aggregation as well.

Conclusions

Here we have for the first time performed an in depth analysis of the composition of FND aggregates and protein coronas for use in biological systems. The consideration of different sizes of diamond particles is very important in achieving the most efficient uptake in cellular systems. In this research we have mainly analyzed 25 nm particles, since these approach the limit of diamond size with stable NV-centers inside. Although larger particles will have a lower surface to volume ratio, we believe that the aggregation is mostly determined by the surface chemistry. These results can thus be extrapolated to larger particles with the same surface composition. We provide a detailed analysis of which components contribute to the aggregation and which components form a corona on the diamond surface. This information can be taken into account in the future when sensitivity is estimated. Furthermore, we suggest a simple method to improve aggregation. When particles are first suspended in Foetal Bovine Serum and then diluted in DMEM, the resulting particle size decreases. In this situation the interactions between different protein-diamond aggregates is prevented through coating the diamond with FBS, before adding to a salt rich solution. The LC-MS/MS data shows that different proteins adhere to the diamond surface and thus participate in the aggregate formation. Ultimately, we have shown that the presence of salts in a protein rich environment results in much larger aggregates (compared to an environment without salts).

References

1. Balasubramanian, G. *et al.* Ultralong spin coherence time in isotopically engineered diamond. *Nat. Mater.* **8,** 383–387 (2009).
2. Gruber, A. Scanning Confocal Optical Microscopy and Magnetic Resonance on Single Defect Centers. *Science* **276,** 2012–2014 (1997).
3. Acosta, V. M. *et al.* Temperature dependence of the nitrogen-vacancy magnetic resonance in diamond. *Phys. Rev. Lett.* **104,** (2010).
4. Rondin, L. *et al.* Magnetometry with nitrogen-vacancy defects in diamond. *Rep. Prog. Phys.* **77,** 56503 (2014).
5. Degen, C. L. Scanning magnetic field microscope with a diamond single-spin sensor. *Appl. Phys. Lett.* **92,** 22–24 (2008).
6. Grinolds, M. S. *et al.* Nanoscale magnetic imaging of a single electron spin under ambient conditions. *Nat. Phys.* **9,** 215–219 (2013).
7. Doherty, M. W. *et al.* Temperature shifts of the resonances of the NV-center in diamond. *Phys. Rev. B - Condens. Matter Mater. Phys.* **90,** (2014).
8. Schirhagl, R., Chang, K., Loretz, M. & Degen, C. L. Nitrogen-vacancy centers in diamond: nanoscale sensors for physics and biology. *Annu. Rev. Phys. Chem.* **65,** 83–105 (2014).
9. Nagl, A., Hemelaar, S. R. & Schirhagl, R. Improving Surface and Defect Center Chemistry of Fluorescent Nano-Diamonds for Imaging Purposes – A Review. *Anal. Bioanal. Chem.* (2015). doi:10.1007/s00216-015-8849-1
10. Mohan, N., Chen, C. S., Hsieh, H. H., Wu, Y. C. & Chang, H. C. In vivo imaging and toxicity assessments of fluorescent nanodiamonds in caenorhabditis elegans. *Nano Lett.* **10,** 3692–3699 (2010).
11. Bradac, C., Gaebel, T., Naidoo, N., Rabeau, J. R. & Barnard, A. S. Prediction and measurement of the size-dependent stability of fluorescence in diamond over the entire nanoscale. *Nano Lett.* **9,** 3555–3564 (2009).
12. Zhang, S., Li, J., Lykotrafitis, G., Bao, G. & Suresh, S. Size-dependent endocytosis of nanoparticles. *Adv. Mater.* **21,** 419–424 (2009).
13. Krüger, A. *et al.* Unusually tight aggregation in detonation nanodiamond: Identification and disintegration. *Carbon N. Y.* **43,** 1722–1730 (2005).
14. Korobov, M. V *et al.* Improving the dispersity of detonation nanodiamond: differential scanning calorimetry as a new method of controlling the aggregation state of nanodiamond powders. *Nanoscale* **5,** 1529–36 (2013).
15. Lee, J. W. *et al.* Preparation of non-aggregated fluorescent nanodiamonds (FNDs) by non-covalent coating with a block copolymer and proteins for enhancement of intracellular uptake. *Mol. Biosyst.* **9,** 1004–11 (2013).
16. Capriotti, A. L. *et al.* Analytical methods for characterizing the nanoparticle-protein corona. *Chromatographia* **77,** 755–769 (2014).
17. Monopoli, M. P., Aberg, C., Salvati, A. & Dawson, K. a. Biomolecular coronas provide the biological identity of nanosized materials. *Nat. Nanotechnol.* **7,** 779–86 (2012).
18. Petri-Fink, A., Steitz, B., Finka, A., Salaklang, J. & Hofmann, H. Effect of cell media on polymer coated superparamagnetic iron oxide nanoparticles (SPIONs): Colloidal stability, cytotoxicity, and cellular uptake studies. *Eur. J. Pharm. Biopharm.* **68,** 129–137 (2008).
19. Lesniak, A. *et al.* Effects of the presence or absence of a protein corona on silica

nanoparticle uptake and impact on cells. *ACS Nano* **6,** 5845–5857 (2012).
20. Ritz, S. *et al.* The Protein Corona of Nanoparticles: Distinct Proteins Regulate the Cellular Uptake. *Biomacromolecules* 150320125141006 (2015). doi:10.1021/acs.biomac.5b00108
21. Rehor, I. *et al.* Fluorescent nanodiamonds with bioorthogonally reactive protein-resistant polymeric coatings. *Chempluschem* **79,** 21–24 (2014).
22. Perevedentseva, E. *et al.* Effect of surface adsorbed proteins on the photoluminescence of nanodiamond. *J. Appl. Phys.* **109,** (2011).
23. Tzeng, Y. K. *et al.* Superresolution imaging of albumin-conjugated fluorescent nanodiamonds in cells by stimulated emission depletion. *Angew. Chemie - Int. Ed.* **50,** 2262–2265 (2011).
24. Sotoma, S. *et al.* Selective labeling of proteins on living cell membranes using fluorescent nanodiamond probes. *Nanomaterials* **6,** (2016).
25. Chen, W. H. *et al.* Solid-phase extraction and elution on diamond (SPEED): A fast and general platform for proteome analysis with mass spectrometry. *Anal. Chem.* **78,** 4228–4234 (2006).
26. Kong, X. L. *et al.* High-affinity capture of proteins by diamond nanoparticles for mass spectrometric analysis. *Anal. Chem.* **77,** 259–265 (2005).
27. Zhang, X. Q. *et al.* Polymer-functionalized nanodiamond platforms as vehicles for gene delivery. *ACS Nano* **3,** 2609–2616 (2009).
28. McGuinness, L. P. *et al.* Quantum measurement and orientation tracking of fluorescent nanodiamonds inside living cells. *Nat. Nanotechnol.* **6,** 358–363 (2011).
29. Petrakova, V. *et al.* Charge-sensitive fluorescent nanosensors created from nanodiamonds. *Nanoscale* **7,** 12307–11 (2015).
30. Petráková, V. *et al.* Luminescence of nanodiamond driven by atomic functionalization: Towards novel detection principles. *Adv. Funct. Mater.* **22,** 812–819 (2012).
31. Sakulkhu, U. *et al.* Ex situ evaluation of the composition of protein corona of intravenously injected superparamagnetic nanoparticles in rats. *Nanoscale* (2014). doi:10.1039/C4NR02793K
32. Hofmann, H. Significance of surface charge and shell material of superparamagnetic iron oxide nanoparticle (SPION) based core/shell nanoparticles on the composition of the protein corona. *Biomater. Sci.* **3,** 265–278 (2015).
33. Zhu, W., Smith, J. W. & Huang, C. M. Mass spectrometry-based label-free quantitative proteomics. *J. Biomed. Biotechnol.* **2010,** (2010).
34. Zheng, X. *et al.* Proteomic analysis for the assessment of different lots of fetal bovine serum as a raw material for cell culture. Part IV. Application of proteomics to the manufacture of biological drugs. *Biotechnol. Prog.* **22,** 1294–1300 (2006).
35. Tenzer, S. *et al.* Rapid formation of plasma protein corona critically affects nanoparticle pathophysiology. *Nat. Nanotechnol.* **8,** 772–81 (2013).
36. Ge, C. *et al.* Towards understanding of nanoparticle–protein corona. *Arch. Toxicol.* 519–539 (2015). doi:10.1007/s00204-015-1458-0
37. Shannahan, J. H. *et al.* Silver Nanoparticle Protein Corona Composition in Cell Culture Media. *PLoS One* **8,** (2013).
38. Pham, M. D., Yu, S. S.-F., Han, C.-C. & Chan, S. I. Improved Mass Spectrometric Analysis of Membrane Proteins Based on Rapid and Versatile Sample Preparation on Nanodiamond Particles. *Anal. Chem.* **85,** 6748–6755 (2013)

Supplementary Information

Sample	Mean	Std. Deviation	PdI
25nm FND	-22.20	3.439	0.19 ± 0.07
FBS	-15.95	0.520	0.53 ± 0.06
FBS + FND	-18.13	0.208	0.18 ± 0.00
FBS + FND washed	-27.90	1.153	0.31 ± 0.02
FBS + DMEM + FND	-9.85	0.882	0.52 ± 0.06
FBS + DMEM + FND washed	-28.08	0.591	0.52 ± 0.06
DMEM + FND	-19.83	1.193	0.26 ± 0.07
DMEM + FND washed	-37.43	0.306	0.12 ± 0.00

Supplementary Table 1. Average Zeta-potential in mV and standard deviation for each sample are displayed. Zeta potential of all samples reduced significantly after washing ($P < 0.01$), the polydispersity indices are listed.

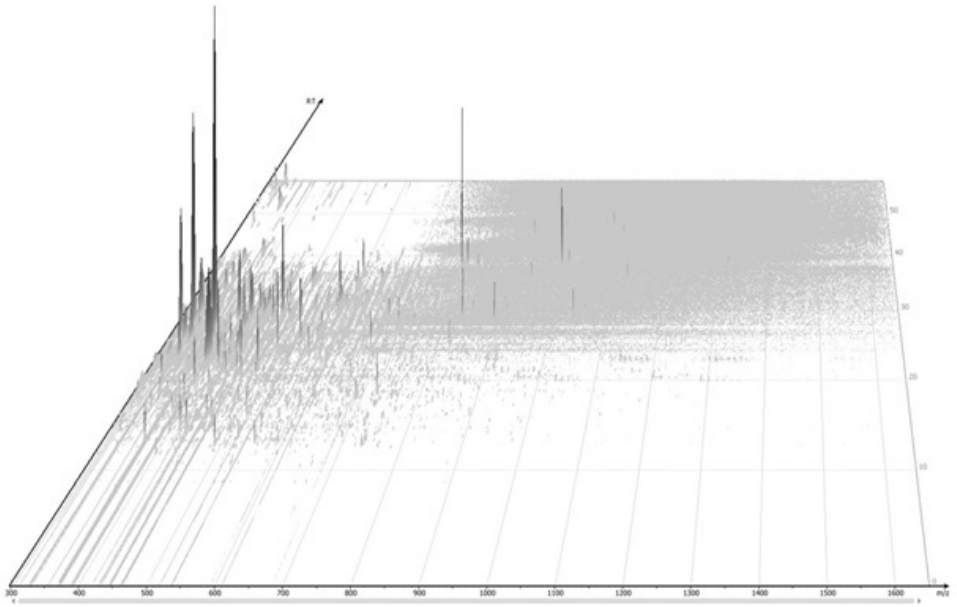

Supplementary Figure 1. Example of a chromatogram of the protein corona of nanodiamond particles after trypsin digestion. The X-axis shows the M/Z while the Y-axis shows the retention time of the column. The height of the peaks corresponds to the intensity of the signal in MS/MS

Supplementary text S1: LC-MS/MS methods

Samples were analyzed by nanoLC–MS/MS on an Ultimate 3000 system (Dionex, Amsterdam, The Netherlands) interfaced on-line with a Q-ExactivePlus mass spectrometer (ThermoFisher Scientific., San Jose, CA). Peptide mixtures were loaded onto a 5 mm × 300 µm i.d. trapping micro column packed with C18 PepMAP100 5 µm particles (Dionex) in 2% AcN in 0.1% FA at the flow rate of 20 µL/minute. After loading and washing for 3 minutes, peptides were back-flush eluted onto a 15 cm × 75 µm i.d. nanocolumn, packed with C18 PepMAP100 1.8 µm particles (Dionex). The following mobile phase gradient was delivered at the flow rate of 300 nl/minute: 2–50% of solvent B in A for 60 minutes; 50–90% B in A for 7 minutes; 90% B in A during 10 minutes, and back to 2% B in A in 5 minutes. Solvent A was 100:0 H_2O/acetonitrile (v/v) with 0.1% formic acid and solvent B was 0:100 H_2O/acetonitrile (v/v) with 0.1% formic acid.

Peptides were infused into the mass spectrometer via dynamic nanospray probe (ThermoElectron Corp.) with a stainless steel emitter (Thermo). Typical spray voltage was 1.8 kV with no sheath and auxiliary gas flow; ion transfer tube temperature was 275°C. Mass spectrometer was operated in data-dependent mode. DDA cycle consisted of the survey scan within m/z 300–1650 at the Orbitrap analyzer with target mass resolution of 70,000 (FWHM, full width at half maximum at m/z 200) followed by MS/MS fragmentations of the top10 precursor ions. Singly charged ions were excluded from MS/MS experiments and m/z of fragmented precursor ions were dynamically excluded for further 20 s.

The software PEAKS Studio (version 7) was applied to the spectra generated by the Q-exactive plus mass spectrometer to search against either the protein sequence database UniProtKB/Trembl of the UniProt Knowledgebase (UniProtKB), limited to protein sequences of Bos Taurus. Searching for the fixed modification carbamidomethylation of cysteine and the variable post translational modifications oxidation of methionine was done with a maximum of 5 posttranslational modifications per peptide at a parent mass error tolerance of 10 ppm and a fragment mass tolerance of 0.02 Da. False discovery rate was set at 0.1%.

Protein	Accession	Avg. Mass [Da]	IEP	Sample 1 $NpSpC_x$ [%]	Sample 2 $NpSpC_x$ [%]	Sample 3 $NpSpC_x$ [%]	Sample 4 $NpSpC_x$ [%]	Sample 5 $NpSpC_x$ [%]	Molecular function
Hemoglobin fetal subunit beta	P02081|HBBF_BOVIN	15859	6.51	2.87		8.68	10.97	6.20	Heme binding, iron binding, oxygen binding, oxygen transporter activity
Hemoglobin subunit alpha	P01966|HBA_BOVIN	15184	8.19	5.24	4.79	5.67	10.74	4.71	Heme binding, iron binding, oxygen binding, oxygen transporter activity
Serum albumin	P02769|ALBU_BOVIN	69294	5.60	32.32	22.56	16.64	9.34	2.10	DNA binding, drug binding, fatty acid binding, metal ion binding, oxygen binding, pyridoxal phosphate binding, toxic substance binding
Alpha-2-HS-glycoprotein	P12763|FETUA_BOVIN	38419	5.10	34.02	38.32	15.46	8.92	1.34	Cysteine-type endopeptidase inhibitor activity
Apolipoprotein A-II	P81644|APOA2_BOVIN	11202	7.80	2.03		1.54	4.85	1.90	Cholesterol binding, cholesterol transporter activity, high-density lipoprotein particle binding, lipase inhibitor activity, phosphatidylcholine binding, phosphatidylcholine-sterol O-acyltransferase activator activity, protein heterodimerization, triglyceride binding
Fibrinogen alpha chain	P02672|FIBA_BOVIN	67012	6.73			0.90	3.57		N/A
Actin cytoplasmic 1	P60712|ACTB_BOVIN	41737	5.29	0.54		0.62	3.13	1.77	ATP binding
Actin cytoplasmic 2	P63258|ACTG_BOVIN	41793	5.31	0.54		0.62	3.12	1.76	ATP binding, structural constituent of cytoskeleton
Apolipoprotein A-I	P15497|APOA1_BOVIN	30276	5.71			1.14	3.05	5.02	Beta-amyloid binding, chemorepellent activity, cholesterol binding, cholesterol transporter activity, high-density lipoprotein particle binding, high-density lipoprotein particle receptor binding, phosphatidylcholine binding, phosphatidylcholine-sterol O-acyltransferase activator activity
Apolipoprotein E	Q03247|APOE_BOVIN	35980	5.55			0.72	2.42	2.58	Antioxidant activity, beta-amyloid binding , cholesterol binding, cholesterol transporter activity, heparin binding, lipoprotein particle binding, low-density lipoprotein particle receptor binding, metal chelating activity, phosphatidylcholine-sterol O-acyltransferase activator activity, phospholipid binding, very-low-density lipoprotein particle receptor binding
Cytochrome c	P62894|CYC_BOVIN	11704	9.52	3.88	10.87	4.41	2.32	0.29	Electron carrier activity Source, heme binding, iron ion binding
Vitamin D-binding protein	Q3MHN5|VTDB_BOVIN	53342	5.36			2.10	2.14		Vitamin D binding, vitamin transporter activity
Regakine-1	P82943|REG1_BOVIN	10281	8.80		5.30		2.12	0.43	Heparin binding
Insulin-like growth factor-binding protein 2	P13384|IBP2_BOVIN	34015	7.13				2.08	1.51	Insulin-like growth factor I binding, insulin-like growth factor II binding
Uncharacterized protein	tr|F1N4M7|F1N4M7_BOVIN	68905	8.07			0.62	2.05	1.35	Scavenger receptor activity, serine-type endopeptidase activity
Prothrombin*	P00735|THRB_BOVIN	70506	5.97	0.48			2.00	1.47	Calcium ion binding, fibrinogen binding, serine-type endopeptidase activity, thrombospondin receptor activity
Gelsolin*	tr|F1N1I6|F1N1I6_BOVIN	85687	5.86			0.70	1.59	2.33	Calcium ion binding
Beta-2-glycoprotein 1 / Apolipoprotein H	P17690|APOH_BOVIN	38252	8.53		1.90	2.25	1.56	0.88	Heparin binding Source, lipoprotein lipase activator activity, phospholipid binding
Inter-alpha-trypsin inhibitor heavy chain	Q3T052|ITIH4_BOVIN	101513	6.22	0.22		0.59	1.55	1.68	Serine-type endopeptidase inhibitor activity
Platelet factor 4*	tr|F1MD83|F1MD83_BOVIN	12567	9.30	3.62	5.78		1.30	1.42	CXCR3 chemokine receptor binding, heparin binding
Complement factor H	Q28085|CFAH_BOVIN	140374	6.43			0.43	1.24	1.15	N/A
Fibulin-1 *	tr|F1MYN5|F1MYN5_BOVIN	77486	4.94	1.47	0.70		1.19	0.37	Calcium ion binding, peptidase activator activity
Alpha-2-macroglobulin	Q7SIH1|A2MG_BOVIN	167575	5.71			1.95	1.14	1.01	Serine-type endopeptidase inhibitor activity
Insulin-like growth factor-binding protein 6	Q05718|IBP6_BOVIN	24967	8.73				1.09	0.63	N/A
Fetuin-B	Q58D62|FETUB_BOVIN	42663	5.59	0.80		3.63	1.02	0.76	Cysteine-type endopeptidase inhibitor activity, metalloendopeptidase inhibitor activity
Apolipoprotein C-III	P19035|APOC3_BOVIN	10692	5.02				1.02	0.84	Lipase inhibitor activity, phospholipid binding
Uncharacterized protein	tr|Q3ZBS7|Q3ZBS7_BOVIN	53575	5.92				0.91	1.06	Extracellular matrix binding, polysaccharide binding, scavenger receptor activity
Protein AMBP	P00978|AMBP_BOVIN	39235	7.81	2.03	2.78		0.83		Heme binding, IgA binding, protein homodimerization activity, serine-type endopeptidase inhibitor activity, small molecule binding
Alpha-fetoprotein	Q3SZ57|FETA_BOVIN	68588	5.92			2.01	0.79	0.28	Metal ion binding
Tetranectin*	Q2KIS7|TETN_BOVIN	22144	5.47				0.74	1.06	Calcium ion binding, carbohydrate binding, heparin binding

*Ca-binding function

< **Supplementary Table 2. The most abundant proteins in the FND aggregation.** Sample 1 = FBS, sample 2 = 10% FBS + FNDs, sample 3 = 10% FBS + FNDs washed, sample 4 = DMEM + FBS + FNDs, sample 5 = DMEM + FBS + FNDs washed. Proteins which are marked with green show a molecular function related to binding to negative compounds (e.g. heparin or ATP). See next page for detailed information.

In table S2 an overview of the identified proteins is given, ordered by the 30 most abundant proteins of sample 4 (DMEM + FBS+ FNDs). The full list of proteins of samples is available upon request. A semi-quantitative assessment of (relative) protein amounts was conducted using normalized spectral counts given by the following equation: [1–3]

$$NpSpC_k = \left(\frac{(SpC/M_w)_k}{\sum_{i=1}^{n}(SpC/M_w)_i}\right) * 100$$

where $NpSpC_k$ is the normalized percentage of spectral count for protein k, SpC is the spectral count identified, and M_W is the molecular weight (in Da) of the protein k. The protein corona does not reflect the relative abundance of proteins of sample 1, which is the pure FBS, suggesting some specificity of the adsorption process.

Sample 1 revealed the most abundant proteins (also known from literature[2,4]): Serum albumin and Alpha-2-HS-glycoprotein make up 66% of the normalized spectral counts. Sample 2 and Sample 3 reflect that with pure FBS, hardly any aggregation is happening. The protein pattern closely resembles the one from sample 1.

Amongst the proteins of sample 4, Prothrombin, Gelsolin, Platelet factor 4, Fibulin-1 and Tetranectin (marked with a star) are known to be binding to calcium, which is present in DMEM medium and was proven to play a role in the agglomeration process by XPS analysis.

Identifying hard corona:

In order to differentiate between hard and soft corona we also performed sedimentation through a sucrose cushion to remove loosely bound proteins. To this end we first mixed 5 µl of 20 mg/ml FND_{25} with 495 µl of DMEM Complete Medium. Then we incubated the samples for 5 minutes and centrifuged them through a 0.7M Sucrose cushion (500 µl) for 20 minutes at 15.400xG. After removing the supernatant we resuspended the pellet in 1x PBS (pH 7.4) and centrifuged it again 20 minutes at 15.400xG. This step was repeated once. After the last washing step, the samples were stored at -20 degrees until freeze drying (for 2 hours). For freeze drying: first the samples were cooled down to -50°C for 1 hour and 15 minutes. Then a vacuum of 0.055 mbar was applied and the samples were left over night. The next day the samples were gradually brought to room temperature and the vacuum was released. Then we continued the protein analysis as described for the other samples in the main manuscript.

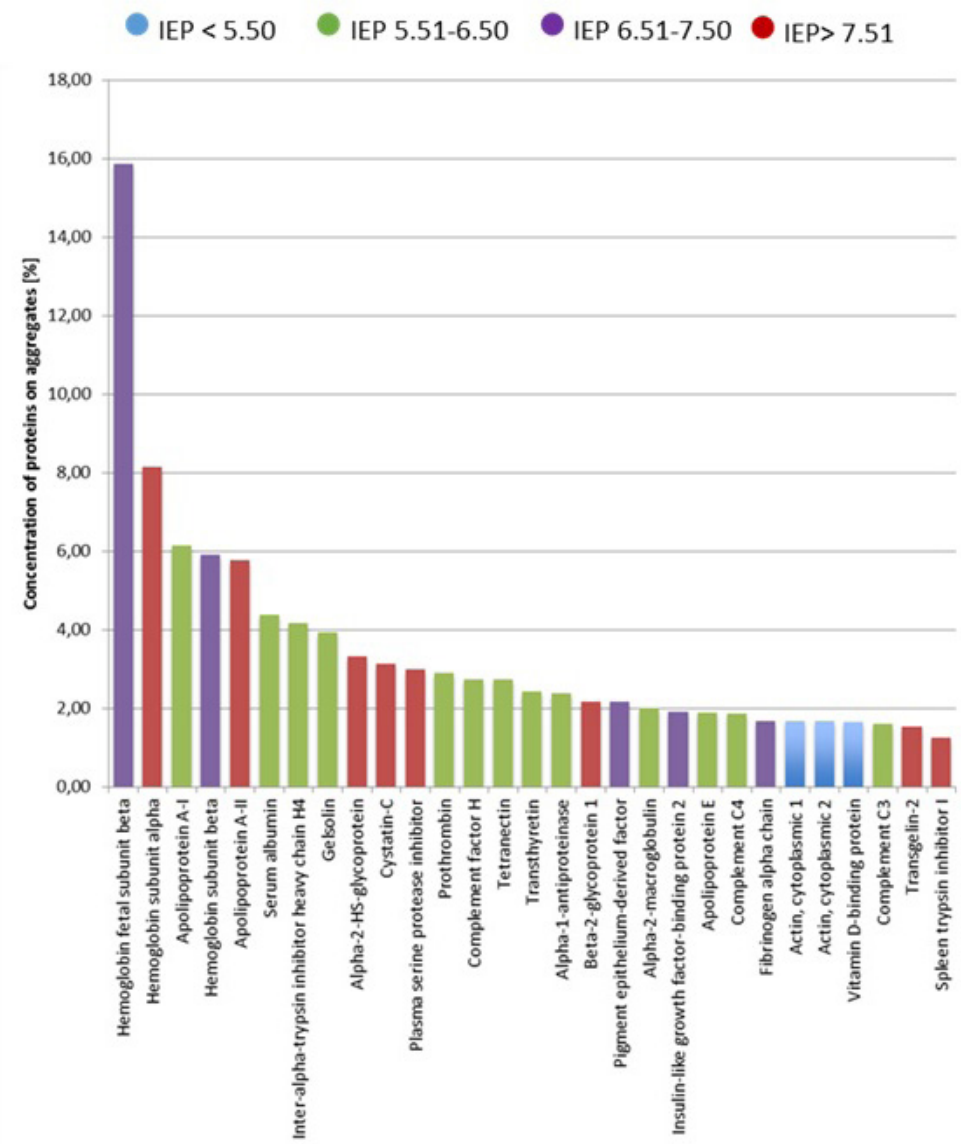

Supplementary Figure 2. Hardest bound proteins identified by sedimenting diamond aggregates through a sucrose cushion

XPS Methods

Instruments, Scienta Scientific, Uppsala, Sweden), X-ray production set to 10 kV, 22 mA with a spot size of 250 by 1000 µm using an aluminum anode. Wide scans were performed with an energy range of 0 to 1200 eV at low resolution (pass energy,

150 eV). The area under each peak, after Shirley background subtraction, was used to calculate peak intensities, yielding elemental surface concentration ratios for nitrogen (N), oxygen (O), and phosphorus (P) to carbon (C). Narrow scans for C, O and N were made at a pass energy of 50 eV, these where used for peak fitting of the carbon and oxygen peak. The sample was checked for contamination by monitoring the increase of the C-C peak after repeating measurements of the carbon peak.

We can see the typical XPS spectrum of oxygen-terminated and acid-cleaned FNDs. Small amounts of P, N and Si (contaminations, possibly also from the production process of the FNDs) can be identified. The peak fitting of carbon and oxygen reveal the presence of carboxylate groups and carboxylic acid and alcohol groups, all of which are likely to be present on the surface. Figure 5b on the other hand shows the presence of inorganic salts, especially sodium chloride alongside calcium, nitrogen and again small amounts of Si. As seen in Figure 5c, with FBS present, also sodium chloride alongside N are the main inorganic elements to be found. In such a complex mixture as DMEM (+ 10% FBS) peak fittings of carbon and oxygen only reveal the adsorption of proteins and other organic components present in the medium: Further differentiation is virtually impossible. Nitrogen is present both in form of inorganic nitrogen salts as well as amino acids and proteins (in case of Sample (c)).

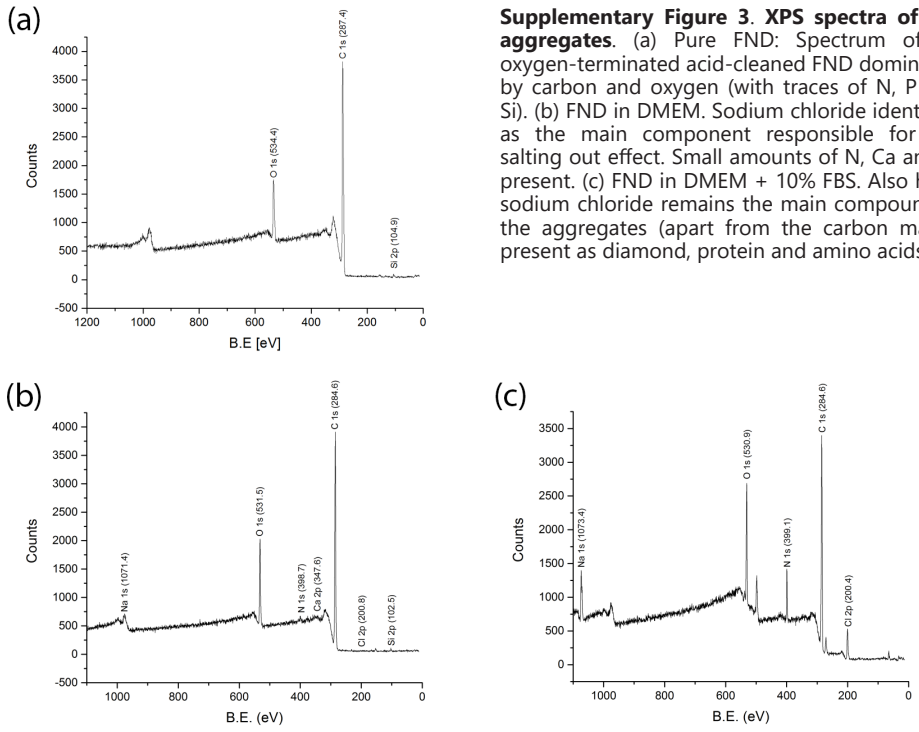

Supplementary Figure 3. **XPS spectra of the aggregates**. (a) Pure FND: Spectrum of an oxygen-terminated acid-cleaned FND dominated by carbon and oxygen (with traces of N, P and Si). (b) FND in DMEM. Sodium chloride identified as the main component responsible for the salting out effect. Small amounts of N, Ca and Si present. (c) FND in DMEM + 10% FBS. Also here, sodium chloride remains the main compound in the aggregates (apart from the carbon mainly present as diamond, protein and amino acids).

Supplementary Table3. Elements present at the surface of FND/medium aggregates.

Present elements	FNDs (control sample)	Aggregates DMEM without FBS	Aggregates DMEM with serum proteins
Carbon	86.07%	80.39%	65.73%
Oxygen	11.65%	12.59%	16.45%
Sodium		2.31%	4.82%
Nitrogen	0.45%	1.93%	8.39%
Chloride		1.31%	4.61%
Calcium		0.64%	
Silicon	1.65%	0.83%	
Phosphrous	0.18%		

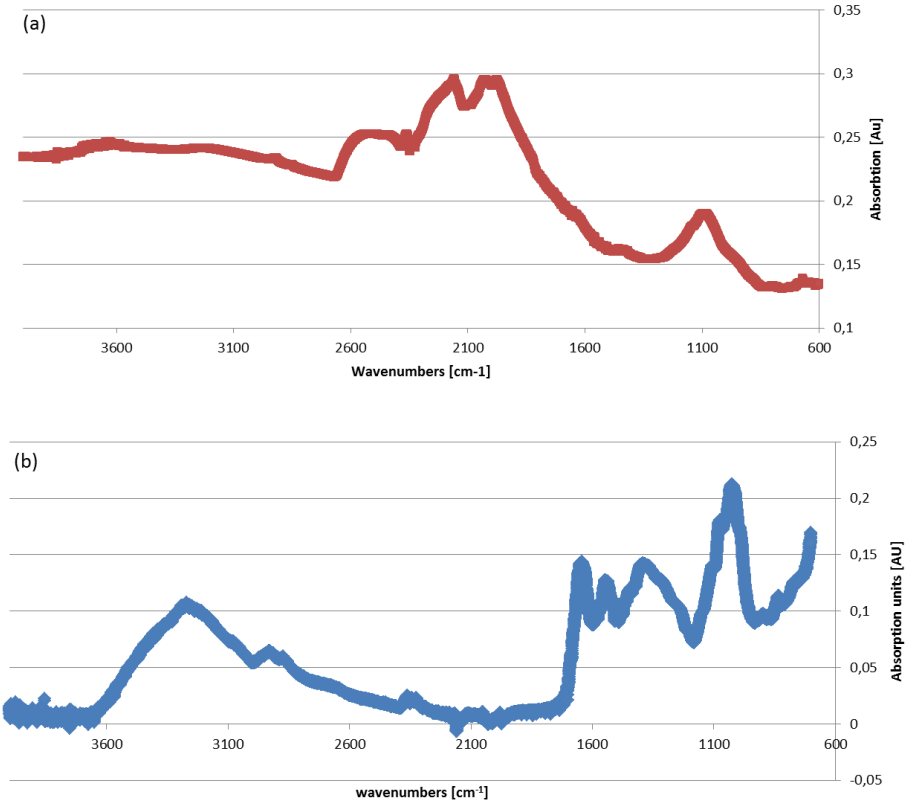

Supplementary Figure 4. IR spectra of (a) pure diamond powder and (b) aggregates formed in complete DMEM +FBS. The second spectrum is dominated by protein bands.

References

1. Sakulkhu, U. *et al.* Ex situ evaluation of the composition of protein corona of intravenously injected superparamagnetic nanoparticles in rats. *Nanoscale* (2014). doi:10.1039/C4NR02793K
2. Usawadee, S. *et al.* Significance of surface charge and shell material of superparamagnetic iron oxide nanoparticle (SPION) based core/shell nanoparticles on the composition of the protein corona. *Biomater. Sci.* **3,** 265–278 (2015).
3. Zhu, W., Smith, J. W. & Huang, C. M. Mass spectrometry-based label-free quantitative proteomics. *J. Biomed. Biotechnol.* **2010,** (2010).
4. Zheng, X. *et al.* Proteomic analysis for the assessment of different lots of fetal bovine serum as a raw material for cell culture. Part IV. Application of proteomics to the manufacture of biological drugs. *Biotechnol. Prog.* **22,** 1294–1300 (2006).

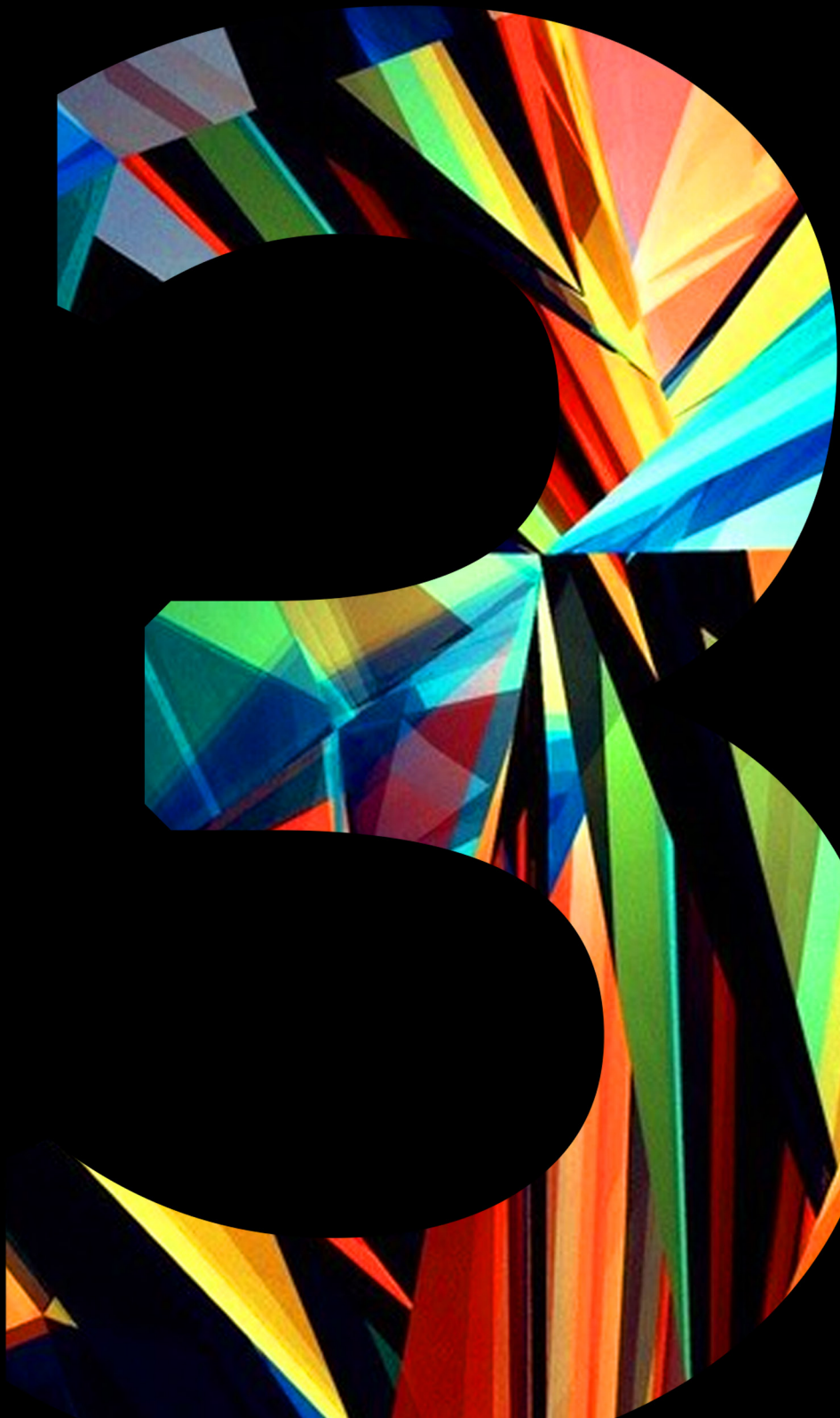

Generally applicable transformation protocols for fluorescent nanodiamond internalization into cells

Simon R. Hemelaar[1#], Kiran J. van der Laan[1#], Sophie R. Hinterding[1], Manon V. Koot[1], Else Ellermann[1], Felipe P. Perona-Martinez[1], David Roig[1], Severin Hommelet[1], Daniele Novarina[2], Hiroki Takahashi[3], Michael Chang[2] & Romana Schirhagl[1]

[1]Department of Biomedical Engineering, University Medical Center Groningen, The Netherlands. [2]European Research Institute for the Biology of Ageing, University Medical Center Groningen, The Netherlands. [3]Department of Physics, ETH-Zurich, Switzerland

[#]These authors contributed equally

Scientific Reports **7:1** 5862-5868 (2017)

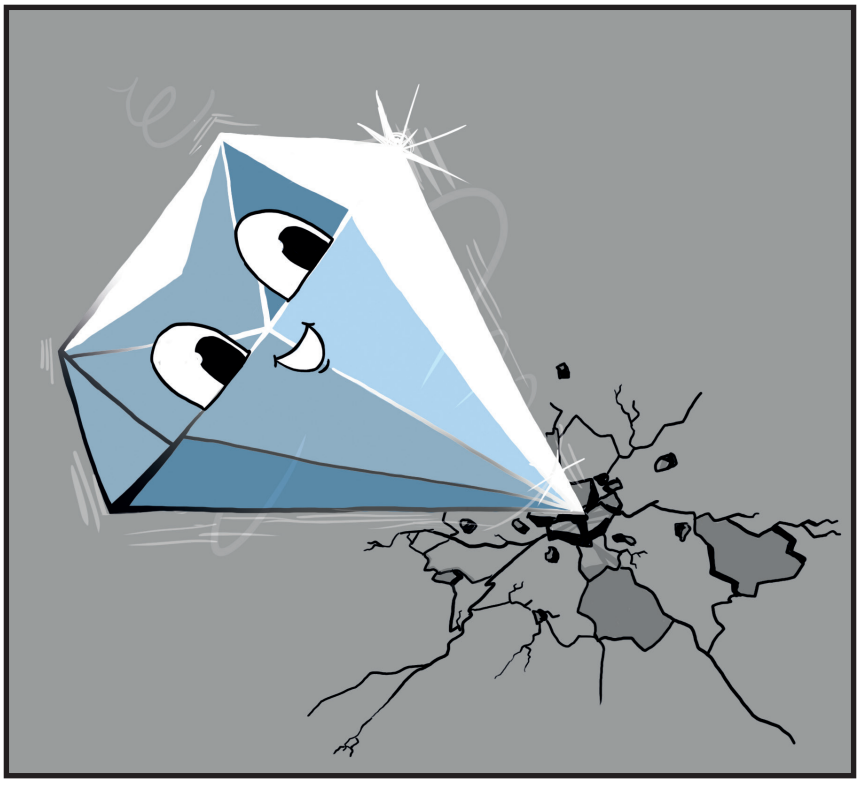

"*Diamond breaking through the cell wall*"

Abstract

Fluorescent nanodiamonds (FNDs) are promising nanoprobes, owing to their stable and magnetosensitive fluorescence. Therefore they can probe properties such as magnetic resonances, pressure, temperature or strain. The unprecedented sensitivity of diamond defects can detect the faint magnetic resonance of a single electron or even a few nuclear spins. However, these sensitivities are only achieved if the diamond probe is close to the molecules that need to be detected. In order to utilize its full potential for biological applications, the diamond particle has to enter the cell. Some model systems, like HeLa cells, readily ingest particles. However, most cells do not show this behavior. In this article we show for the first time generally applicable methods, which are able to transport fluorescent nanodiamonds into cells with a thick cell wall. Yeast cells, in particular *Saccharomyces cerevisiae*, are a favored model organism to study intracellular processes including ageing on a cellular level. In order to introduce FNDs in these cells, we evaluated electrical transformation and conditions of chemical permeabilization for uptake efficiency and viability. 5% DMSO (dimethyl sulfoxide) in combination with optimized chemical transformation mix leads to high uptake efficiency in combination with low impact on cell biology. We have evaluated all steps in the procedure.

Introduction

In recent years fluorescent nanodiamonds (FNDs) have gained a great deal of attention.[1] Their stable fluorescence permits long-term tracking and their magneto-optical behavior allows them to be used as sensors for different properties in the environment, owing to nitrogen vacancy (NV) centers inside the nanodiamond particle.[2] Diamond defects are so sensitive that nanoscale temperature measurements (accuracies down to 1 mK)[3] or measuring the magnetic fields of single electron spins[4] are possible. Other advantages are the biocompatibility of FNDs and their excellent inertness while the surface is modifiable.[5–7] However, to fully deploy their potential for bioapplications the diamond particles need to enter cells. Some mammalian cells, for instance HeLa cells or macrophages, readily ingest diamond nanoparticles without surface modification or chemical stimulus.[8–11] A few selected other cells show a similar behavior and readily take up particles.[12–14]

In case the cells of interest do not readily ingest particles, only a limited set of methods is currently available. One way is to inject cells with nanodiamonds using a silicon nanowire.[15] This was achieved for human embryonic fibroblast WS1 cells. Tzeng *et al*. introduced BSA-coated diamonds by electroporation into (HeLa) cells.[16] An additional way to control diamond uptake is to treat the cells with different chemicals, such as NaN3, sucrose or filipin.[17,18]

Most of these techniques have only been applied to HeLa cells or similar and none of these methods have been tested to achieve uptake in non-mammalian cells. For multicellular organisms or very large cells (e.g. egg cells), nanodiamonds can simply be injected.[19] However, this approach is quite invasive and not applicable for average-sized single cells.

In this study we focused on *Saccharomyces cerevisiae*, which is considered one of the most important model organisms to study a wide range of biological processes. In particular, they are a favored model organism to study ageing. Their high turnover rate and the suitability for genetic manipulation,[20] as well as the many basic biological processes which are highly conserved from yeast to humans, make the study of them extremely relevant to humans. Additionally, the fact that young and old cells can be separated relatively easy also offers great potential to study ageing. Furthermore, yeast is widely used in food industries as well as in biotechnology to produce different pharmaceutical products.[21–23] Unlike human cells, yeast cells have a thick cell wall. In order to introduce FNDs into these cells, this obstacle needs to be overcome.
In this study, we show for the first time broadly applicable approaches, which enable the nanodiamond particles to enter cells which do not readily ingest particles. We demonstrate different uptake methods, which were optimized with regard to their success rate as well as their impact on cell viability.

Methods

Cell cultures and materials

Experiments were performed using an Hxt6-GFP *S. cerevisiae* strain from the Yeast GFP Clone Collection from ThermoScientific.[25] This strain expresses a fusion of HeXose Transporter 6 (HXT6, a glucose transporter in the cellular membrane) with Green Fluorescent Protein, allowing the visualization of the cell membrane. Cells were grown overnight in synthetic dextrose complete medium (SD medium) at 30 °C, 200 rpm. Cellular concentration at the start of experiments was determined by measuring the optical density at 600 nm. $1.05 * 10^7$cells/mL were used to return the cellular population to mid log phase (indicating the linear part of a logarithmic scale in the growth curve). Cells were then grown for an additional 2 h at 30 °C, 200 rpm. At the end of each experiment, cells were fixed in 3.7% paraformaldehyde for microscopic analysis. 1 M sorbitol was used as a buffer.

Diamond particle characterization

The diamonds used in this study have an average diameter of 70 nm (FND_{70}, Adámas Nanotechnologies, available as aqueous solution). They contain approximately 300 nitrogen vacancies per particle. They are produced by the manufacturer by grinding larger HPHT diamond and performing a selection of sizes. Since they are cleaned with oxidizing acids they have a carboxylated surface. Their fluorescence spectra are typical for NV-centers with a broad emission of the phonon side band above 600 nm. Their recorded spectrum is shown in **Supplementary Figure 1** and a schematic of the fluorescent mechanism of the diamond is shown in refence [26] and in **Supplementary Figure 2**, reproduced from Nagl., *et al*.[27]

Trials to achieve uptake without permeabilizing the cell wall

Yeast cells were washed twice with H_2O. Next, 2 µg of FNDs were added to the cells. FNDs were diluted with sorbitol to a total volume of 1 mL to avoid formation of FND aggregates. This mixture was then incubated for 2 hours at 30 °C to ensure maximum interaction between cells and diamonds. Under these conditions, no uptake can be expected so these samples served as negative controls. Next to this control condition, other physical and chemical options were tested to see if any influenced cellular uptake. First, instead of 1 M sorbitol as a solvent for the FNDs, H_2O was used. Second, FNDs were coated with glucose before incubation. Since glucose can be utilized by yeast, they might have an incentive to ingest them. Third, FNDs were coated with FBS as described by Hemelaar *et al*.[5] The glucose / FBS coated FND particles were made by incubating diamonds with a sterilized 0.1% w/v glucose solution or a 100% FBS-HI solution in a 1:10 ratio for several minutes. Fourth, cells were incubated in the dark instead of in the light. Finally, FNDs were incubated for 4 hours instead of 2. Internalized FNDs were found in none of the samples (see **Supplementary Figure 3**).

Optimizing removal of diamonds on the cell surface

To prevent overestimating uptake, a detergent washing method to remove diamond particles from the cell surface was optimized. After adding 2 µg of FNDs to the washed yeast cells and incubating for 2 hours at 30 °C, three different detergents (Triton, Tween and SDS) were tested at concentrations of 1%, 0.5%, 0.1%, 0.05% and 0.01%. These detergents were added to the cell-FND suspensions and incubated for 30 minutes at RT. Removing surface diamonds reduces overestimation of uptake due to extracellular FNDs for microscopic analysis. Samples were compared to a non-washed suspension of yeast cells and diamonds. The most efficient detergent and concentration to wash diamond particles off the cellular exterior was Triton 0.01% (confirmed qualitatively by confocal microscopy, **Supplementary Figure 4**). In addition, the influence of the different detergents on the viability was tested. A concentration-dependent effect of the soap on the cell viability, tested using colony forming units, see below, was found for all soaps (**Supplementary Figure 5**). The 0.01% Triton solution was used in the chemical transformation protocol for further experiments.

Chemical transformation TMIX

To achieve permeabilization of the yeast cells, we adapted and optimized a common protocol for chemical transformation of yeast cells from gene transfection. Mid log phase cells were washed in H_2O and resuspended in 0.1 M LiAc in order to improve the chemical transformation efficiency.[28] The cells were spun down at 1000 × G and resuspended in H_2O. The used transformation mix consists of 66.6% w/v PEG4000 and 1 M lithium acetate (LiAc). TMIX, FND_{70}, DMSO 5% and 1 M sorbitol were added to yeast aliquots and the samples were incubated for 20 minutes at 42 °C. DMSO 5% was used to increase uptake efficiency and TMIX was added to weaken the cell wall. Afterwards the samples were washed with H_2O and processed for microscopy or viability assays.

Electroporation

Mid log phase cells were washed in H_2O and resuspended in 0.1 M LiAc. The cells were spun down for 4 minutes at 1000xG and resuspended in sterile H_2O. Aliquots of the yeast suspension were mixed with 2 µg FND_{70} in 1 M sorbitol solution. Electroporation was performed using an electroporation cuvette (Bio-Rad, Veenendaal, the Netherlands, catalog no. description 165/2089) and applying 1, 2, 4, 8, 12 or 16 pulses (25 µF/200 Ω/900 V) in a Bio-Rad Gene Pulser XcellTM Electroporation System, an adjustment of the electroporation protocol by E.L Rech *et al*.[29] Afterwards the cells were centrifuged for 4 minutes at 1000xG and prepared for confocal microscopy by fixation or incubated on YPD plates (see below).

Biocompatibility

To investigate the biocompatibility of the uptake and washing methods, colony forming units (CFUs) were counted after 48 hours of incubation at 30 °C on YPD plates (in triplicates) after a dilution series to prevent overcrowding. The respective controls for chemical and electrical transformation were produced with the exact same amount of pipetting and washing steps as for the transformation experiments. In order to check for cellular damage as a result of the used treatment, cells were imaged using SEM (FEI Magellan 400 XHR Scanning Electron Microscope, USA). In preparation, cells fixed in 1% glutaraldehyde and 4% paraformaldehyde in 0.1 M cacodylic acid were dried on a cover slip and coated with a 4 nm gold layer for 30 seconds at 20 °C, 40 mA in a Balzers SCD050 sputter coater.

FND uptake quantification

Uptake was analyzed by fixing the cells in between a polylysine coated slide and a cover glass and imaging them using a Zeiss LSM 780 confocal laser scanning microscope (Zeiss, Germany). GFP was imaged at ex/em 488/525 nm and FNDs were imaged at 561/650 nm. To quantify the uptake of FNDs, the confocal images were analyzed by using the software Fiji (https://fiji.sc/). The Fiji protocol which has also been used in another study[8] is described in the following. The analysis was divided into three phases: cell selection, masking and particle analysis. During the first phase, the images were visually inspected and 2 times approximately 100 random cells were selected for the analysis. Cells with large aggregates associated with the cell membrane were rejected post-hoc to prevent false positive results. The images were composed of several slices (z-stacks) and the cell's region was defined in all the three dimensions. In the horizontal plane, the selection considered an area containing only the cell of interest. In the z-direction, the first and last slices containing the cell were manually identified using only the signal from the GFP channel to prevent biased selection. As a result, the first phase defines a volume that holds only the cell of interest. In the masking phase, that volume is molded in order to resemble the spheroid shape of the cell. The image is converted to binary (using the Isodata algorithm to calculate the threshold)[30] and the cell's perimeter is detected in every slice. To find the inner volume of the cell, the program shrinks the cell's region in order to exclude the cell membrane from the analysis. The final step uses a special function of Fiji, which analyzes the particles found in a region. By applying this function to the masked image, it is possible to directly obtain the number of objects (connected components) in the specified region. The performance of this process is set mainly by the parameter "threshold" which is used to separate the background light from the signal emitted by the FNDs. Every pixel with intensity less than the threshold is assumed as background and deleted from the image (set as black), while every pixel with an intensity greater than or equal to the threshold is assumed as part of a particle. To find an adequate value for this parameter, the image was visually inspected and different values were probed. Finally, the decision was made in favor of removing more background signal, but without deleting clearly identified particles.

As a result, images containing no particles show no particles in the analysis. The process provides the number of objects, corresponding to the connected FND signal positive areas, and the number of particles, reflecting the actual number of diamonds, calculated from the total intensity of the objects. After finding the right conditions for particle counting the same algorithm was applied to all conditions. Finally, in all samples the 10 cells with most particles located in the membrane regions were excluded, to prevent false positives from large aggregates at the surface.

Embedding

Z-stacks in confocal microscopy give a good indication on the position of diamond particles. However, in order to be absolutely certain that diamond particles were inside the yeast cells, thin slices of the cell material were prepared. Finding diamond particles in slices taken in the middle of the cell confirms uptake. Samples fixed in 1% glutaraldehyde and 4% paraformaldehyde in 0.1 M cacodylic acid were resuspended in low melt agarose and cut to 1 mm^3 sections. The samples were postfixed in 1% osmiumtetroxide/2.5% potassiumferrocyanide/0.1 M cacodylate buffer mixture for 2 hours. Next, the samples were dehydrated through an increasing graded ethanol series and left overnight in 1:1 ethanol and Epon (Serva) mixture at room temperature, which was replaced by pure Epon (4 times) and finally polymerized overnight at 58 °C.[31] After this, the samples were cut into semi-thin (approximately 0.8 µm) sections using an Ultracut E396879/M91103 microtome. Using a LSM780 confocal microscope, cell borders could be identified using differential interference contrast (DIC) and internalized nanodiamonds were detected using a 651 nm laser.

Results

FND uptake

The uptake of FNDs in yeast cells was confirmed both by confocal microscopy and additionally by sectioning of embedded samples (**Figure 1**). The absolute amount of FND uptake could not be measured, as a diffraction limited spot is at least one particle but could also be a small cluster of particles. An estimation to value the number of particles was modelled through a home written FIJI based script (see methodology section: FND uptake quantification). **Figure 2** shows the uptake of objects (adjacent FND positive pixels) and particles. The amount of particles is estimated by the total intensity of the aforementioned objects. In Figure 2A,B the absolute amount of objects and particles are shown as estimated by our FIJI protocol. The control should be considered as a background measurement, as it is not possible to completely eliminate noise and the signal of membrane bound diamond particles due to limited Z-resolution. The chemical transformation is highly successful in introducing diamond into yeast cells. Notably, the electroporation protocol actually reduced uptake of diamond particles after multiple pulses, possibly due to the reduced viability of the cell. Dead cells lose their membrane integrity and internalized diamond particles are washed away by the washing steps in the electroporation protocol. In Figure 2C,D we

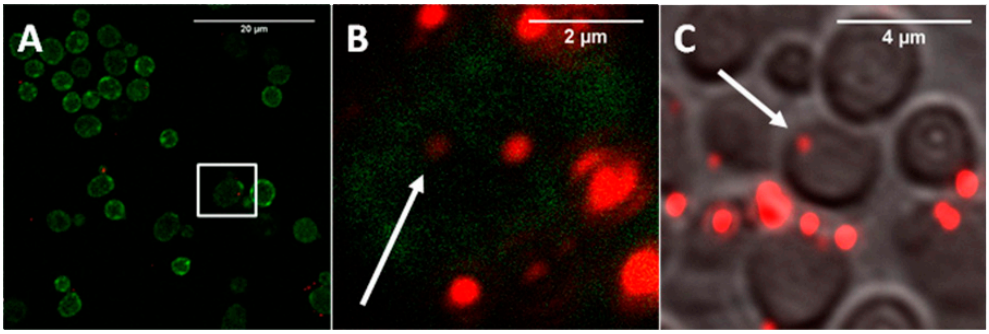

Figure 1. Qualitative analysis of uptake of FNDs by Hxt6-GFP-expressing yeast cells. (**A**) Overview of FNDs and Hxt6-GFP-expressing cells after treatment with TMIX, incubation at 42 °C and treatment with 5% DMSO. (**B**) Close up of the boxed cell from A, with diamond particles inside (for better visibility of the diamond particles the contrast of the red channel has been increased). The arrow shows a particle that was not at any place associated with the cell membrane. (**C**) Embedded and sectioned (approximately 0.8 µm thickness) cells, visualized using Differential Interference Contrast. The diamond particle indicated by the arrow is internalized.

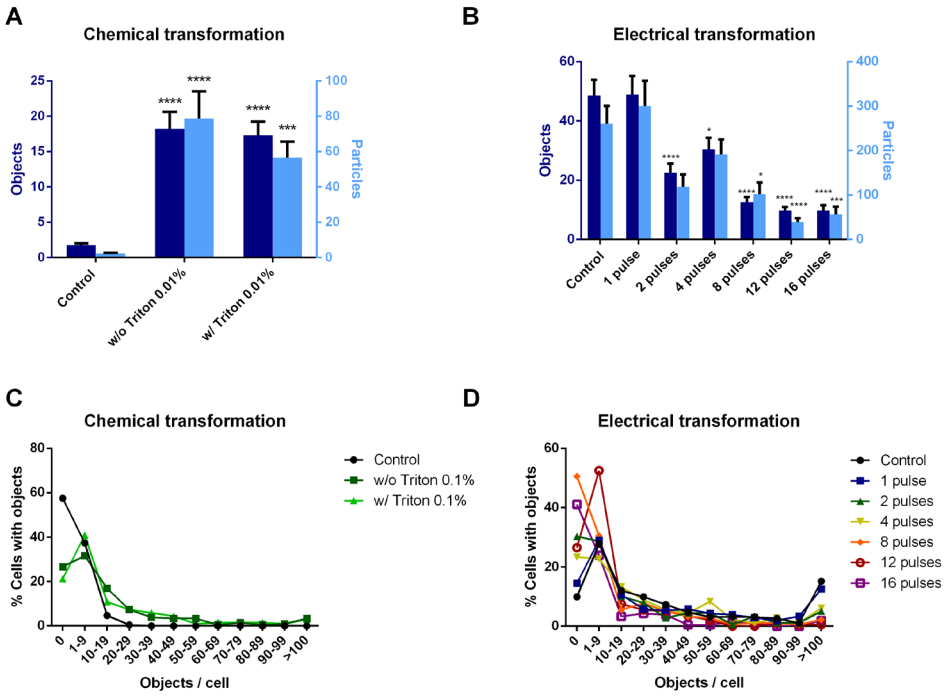

Figure 2. Quantitative analysis of FND uptake by Hxt6-GFP-expressing Saccharomyces cerevisiae cells. The number of objects (adjacent FND positive pixels are counted as an object) and particles (an object can also be an aggregate consisting of more than one particle) is estimated through our home written FIJI protocol (see Method section: FND uptake quantification). For all situations, 2 times approximately 100 cells were selected and cells with obvious large aggregates on the exterior were excluded post-hoc. (**A** and **B**) show the absolute numbers of objects (dark blue) or particles (light blue) for both types of transformations. T In (**C** and **D**) a grouped distribution of the percentage of cells carrying a range of objects is shown. Significance is tested compared to the control situation. *$p < 0.05$, ***$p < 0.001$, ****$p < 0.0001$.

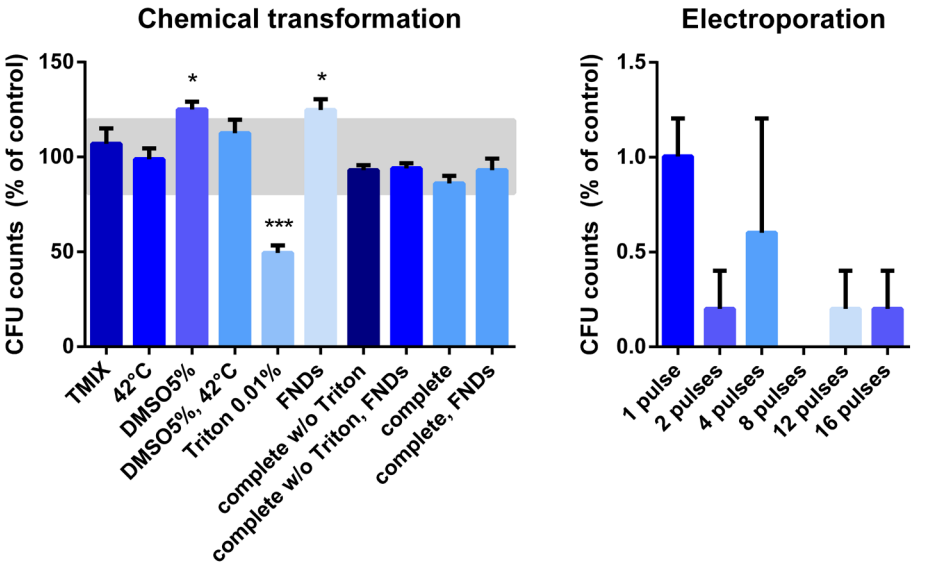

Figure 3. Survival of yeast cells after performing the interventions and different steps in the transformation protocols separately. Colony forming units (CFUs) are a measure of the survival of viable cells after either the chemical transformation or the electroporation protocol. (**A**) The greatest reduction in viability occurs after the addition of 0.01% Triton. The addition of FNDs to the treatment does not decrease the viability. Bars represent averages of triplicates out of two independent experiments. An area of +/−20% around 100% is deemed as 'normal viability,' (**B**). Electroporation reduces viability by a factor 10^2. In all samples FNDs were also added. In the case of 8 pulses, cell viability was completely reduced. For the electroporation protocol all decreases were significant ($p < 0.0001$). Bars represent averages of replicates out of two independent experiments, error bars show the Standard Error of the Mean. Significance is tested compared to the control situation. *$p < 0.05$, ***$p < 0.001$.

show a distribution of the percentage of cells with a certain number of internalized objects. For both transformation methods, there is a larger percentage of cells with a high amount of particles compared to the control.

Biocompatibility

The impact of the different interventions involved in the transformation methods on cell viability were analyzed by counting the amount of colony forming units (CFUs) after the interventions. The CFUs represent the number of viable cells that survived the transformation. Since the cells not only need to be alive but also be able to proliferate, CFUs are generally considered to be the most stringent form of viability measurements.[24] For the chemical transformation technique, the different steps were tested separately and most of them were shown to have a low impact on the viability (**Figure 3A**). Only the use of 0.01% Triton negatively affected the viability of the cells. However, this significant decline in viability was not observed when the complete treatment (including Triton) was performed. The addition of diamond particles to the chemical transformation did not negatively influence the viability, moreover the addition of either 5% DMSO or FNDs was shown to increase the viability. The

electroporation protocol drastically affected the cell viability (**Figure 3B**) with a factor 100 lower compared to the control sample.

Impact on cell morphology

The morphology of Hxt6-GFP-expressing cells after transformation is shown in **Figure 4**. Visual inspection revealed that the vast majority of cells remained visually intact after addition of FNDs (Figure 4A), 2% DMSO and TMIX (Figure 4B), FNDs and 0.1% Triton (Figure 4C) and complete chemical transformation (4D). The crystals on the cells in Figure 4B,C display remaining salt crystals from the drying process (salts contained in the medium). The transformation using electroporation resulted in damage to the cell wall (Figure 4E–G). The most severely damaged cells can clearly be seen since they visibly lose cell wall integrity and cellular content (Figure 4G, after 8 pulses electroporation). Nanodiamond particles on the surface could only rarely be seen in a few areas (Figure 4H). The SEM results confirm the viability data qualitatively.

Discussion

The forced internalization of nanodiamond sensors can prove extremely useful to study intracellular processes in yeast cells, or any other cells, which do not readily ta up diamonds. We have assessed a variety of protocols to overcome the thick cell wall obstacle. We show for the first time that yeast cells can take up fluorescent nanodiamond particles using a defined transformation mix combined with DMSO. Furthermore, we have evaluated the impact of different internalization protocols on cell viability. The techniques here are demonstrated in yeast cells, but will theoretically allow nanodiamonds to enter all kinds of cells with a cell wall, such as *E. coli* bacteria or plant cells.

The most effective and least-invasive method to induce fluorescent nanodiamond uptake in yeast cells is the use of a chemical transformation mix in combination with DMSO that weakens the cell wall. Electroporation could be the optimum method if some of the reagents of the chemical transformation protocol are not compatible with the used cell. In this case the cellular response and its functioning should be closely monitored. Electroporation can also be useful when cell viability is secondary. For instance, this is for instance the case if one wants to detect how other cells react to (dead) yeast cells. Small numbers of cells with internalized FNDs or cells with a low number of internalized FNDs are useful for single cell studies. This is possible in the case of NV-sensing, as this is usually done with one or very few particles. Having more internalized diamonds, however, is advantageous for labeling.

Although the method to quantify uptake does not count the exact number of diamond particles, we received a relative measure for the uptake. The method is designed in a way that membrane associated aggregates are excluded from the samples. This may have resulted in higher variation of the particles and in an underestimation of the number of internalized particles.

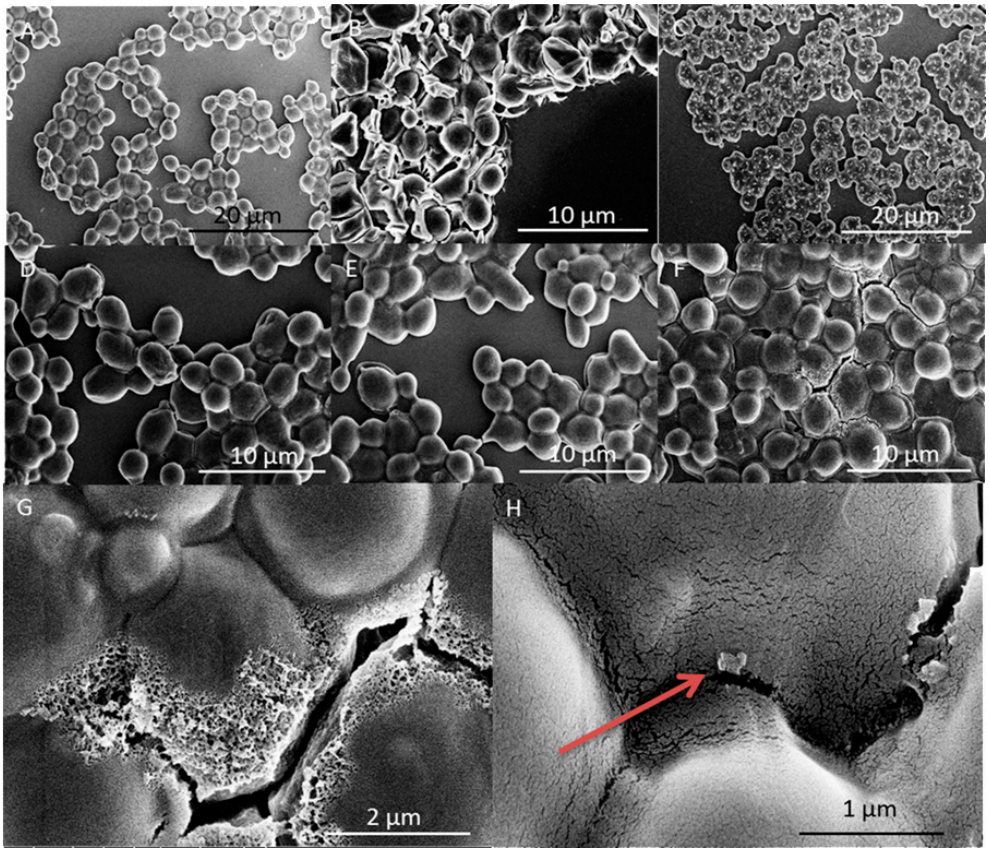

Figure 4. SEM visualizations of yeast cell topography and morphology. (**A**) Cells incubated with FNDs. (**B**) Cells after treatment with 2% DMSO and TMIX. Distorted cell morphology shows the side effects of this technique. (**C**) Cells treated with 0.1% Triton and FNDs: an accumulation of salts due to drying on the outside of the cells can be seen in white. (**D**) Cells treated with 0.1% Triton, TMIX and FNDs. (**E**) Cells electroporated with 1 pulse. Some light cellular damage can be observed. (**F**) Cells electroporated with 8 pulses. The cell wall of these cells is severely damaged as a result of the applied high electrical currents. (**G**) Disintegration of the cell wall results in puncturing and will lead to cell death (close up of F). (**H**) Close up of a diamond particle on the outside of a cell (indicated by the arrow, close up of A).

References

1. Mohan, N., Chen, C. S., Hsieh, H. H., Wu, Y. C. & Chang, H. C. In vivo imaging and toxicity assessments of fluorescent nanodiamonds in caenorhabditis elegans. *Nano Lett.* **10,** 3692–3699 (2010).
2. Schirhagl, R., Chang, K., Loretz, M. & Degen, C. L. Nitrogen-vacancy centers in diamond: nanoscale sensors for physics and biology. *Annu. Rev. Phys. Chem.* **65,** 83–105 (2014).
3. Neumann, P. *et al.* High-precision nanoscale temperature sensing using single defects in diamond. *Nano Lett.* **13,** 2738–2742 (2013).
4. Grinolds, M. S. *et al.* Nanoscale magnetic imaging of a single electron spin under ambient conditions. *Nat. Phys.* **9,** 215–219 (2013).
5. Hemelaar, S. R. *et al.* The interaction of fluorescent nanodiamond probes with cellular media. *Microchim. Acta* 1–9 (2017). doi:10.1007/s00604-017-2086-6
6. Perevedentseva, E. *et al.* Effect of surface adsorbed proteins on the photoluminescence of nanodiamond. *J. Appl. Phys.* **109,** (2011).
7. Krueger, A. New carbon materials: Biological applications of functionalized nanodiamond materials. *Chem. - A Eur. J.* **14,** 1382–1390 (2008).
8. Hemelaar, S. R. *et al.* Nanodiamonds as multi-purpose labels for microscopy. *Sci. Rep.* **7,** 720 (2017).
9. Faklaris, O. *et al.* Detection of single photoluminescent diamond nanoparticles in cells and study of the internalization pathway. *Small* **4,** 2236–2239 (2008).
10. Pope, I. *et al.* Coherent anti-Stokes Raman scattering microscopy of single nanodiamonds. *Nat. Nanotechnol.* **9,** 940–946 (2014).
11. McGuinness, L. P. *et al.* Quantum measurement and orientation tracking of fluorescent nanodiamonds inside living cells. *Nat. Nanotechnol.* **6,** 358–363 (2011).
12. Yu, S. J., Kang, M. W., Chang, H. C., Chen, K. M. & Yu, Y. C. Bright fluorescent nanodiamonds: No photobleaching and low cytotoxicity. *J. Am. Chem. Soc.* **127,** 17604–17605 (2005).
13. Fang, C. Y. *et al.* The exocytosis of fluorescent nanodiamond and its use as a long-term cell tracker. *Small* **7,** 3363–3370 (2011).
14. Chu, Z. *et al.* Unambiguous observation of shape effects on cellular fate of nanoparticles. *Sci. Rep.* **4,** 4495 (2014).
15. Kucsko, G. *et al.* Nanometre-scale thermometry in a living cell. *Nature* **500,** 54–8 (2013).
16. Tzeng, Y. K. *et al.* Superresolution imaging of albumin-conjugated fluorescent nanodiamonds in cells by stimulated emission depletion. *Angew. Chemie - Int. Ed.* **50,** 2262–2265 (2011).
17. Faklaris, O. *et al.* Photoluminescent diamond nanoparticles for cell labeling: Study of the uptake mechanism in mammalian cells. *ACS Nano* **3,** 3955–3962 (2009).
18. Perevedentseva, E. *et al.* Nanodiamond internalization in cells and the cell uptake mechanism. *J. Nanoparticle Res.* **15,** (2013).
19. Simpson, D. A. *et al.* In vivo imaging and tracking of individual nanodiamonds in drosophila melanogaster embryos. *Biomed. Opt. Express* **5,** 1250–1261 (2014).
20. Petranovic, D. & Ganley, A. THEMATIC ISSUE YEAST Yeast Cell Aging and Death Guest Editors : *FEMS Yeast Res.* **14,** 1–2 (2014).

21. Nielsen, J. Production of biopharmaceutical proteins by yeast: Advances through metabolic engineering. *Bioengineered* **4,** 207–211 (2013).
22. Kelly, D. & Kelly, S. Rewiring yeast for drug synthesi. *Nat. Biotechnol.* **21,** 133–134 (2003).
23. Ferrer-Miralles, N., Domingo-Espín, J., Corchero, J. L., Vázquez, E. & Villaverde, A. Microbial factories for recombinant pharmaceuticals. *Microb. Cell Fact.* **8,** 17 (2009).
24. Hjertstedt, J., Hahn, B. L., Kos, W. L. & Sohnle, P. G. Comparison of fungal viability assays using Candida albicans yeast cells undergoing prolonged incubation in the absence of nutrients. *Mycoses* **41,** 487–492 (1998).
25. Nikko, E. & Pelham, H. R. B. Arrestin-mediated endocytosis of yeast plasma membrane transporters. *Traffic* **10,** 1856–1867 (2009).
26. Balasubramanian, G. *et al.* Nanoscale imaging magnetometry with diamond spins under ambient conditions. *Nature* **455,** 648–651 (2008).
27. Nagl, A., Hemelaar, S. R. & Schirhagl, R. Improving Surface and Defect Center Chemistry of Fluorescent Nano-Diamonds for Imaging Purposes – A Review. *Anal. Bioanal. Chem.* (2015). doi:10.1007/s00216-015-8849-1
28. Pham, T. A., Kawai, S. & Murata, K. Visualization of the synergistic effect of lithium acetate and single-stranded carrier DNA on Saccharomyces cerevisiae transformation. *Curr. Genet.* **57,** 233–239 (2011).
29. Rech, E., Dobson, M., Davey, M. & Mulligan, B. Introduction of a yeast artificial chromosome vector into Saccharomyces cerevisiae cells by electroporation. *Nucleic Acids Res.* **18,** 1313 (1990).
30. Torrano, A. a *et al.* A fast analysis method to quantify nanoparticle uptake on a single cell level. *Nanomedicine* **8,** 1815–1828 (2013).
31. Kuipers, J., de Boer, P. & Giepmans, B. N. G. Scanning EM of non-heavy metal stained biosamples: Large-field of view, high contrast and highly efficient Supplemen

Supplementary Information

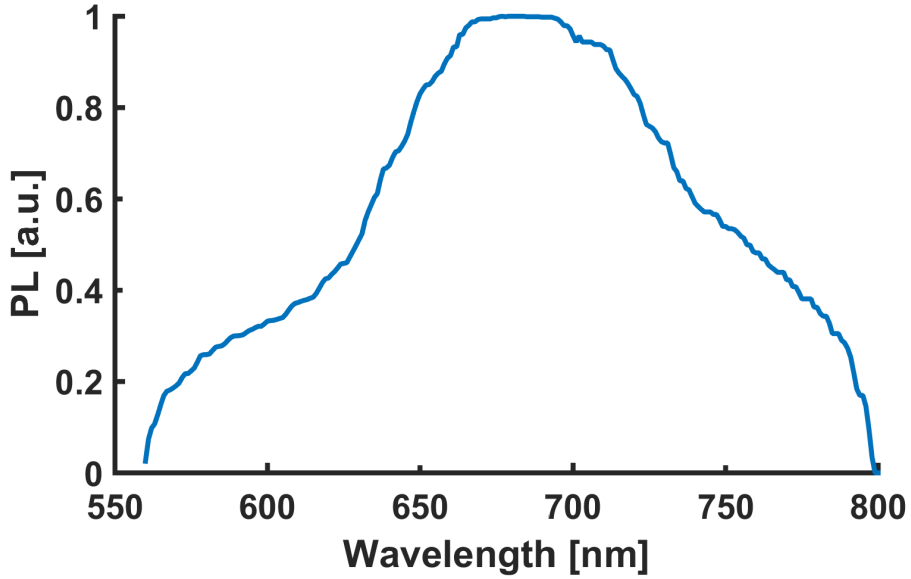

Supplementary Figure 1. Photoluminescent emission spectrum of 70nm FNDs measured at 532nm excitation (bandwidth 5nm) between 560 and 800nm. The spectrum was recorded using a Thermo Scientific Varioskan® Flash plate reader. Diamond emission was scanned with a wavelength step size of 1 nm and data was processed using the median filter function of MathLab software (http://www.mathlab.mtu.edu/mediawiki/index.php/Main_Page). The decrease of intensity at the lower and upper bounds are artefacts originating from the limits of the spectrophotometer and the median filter function.

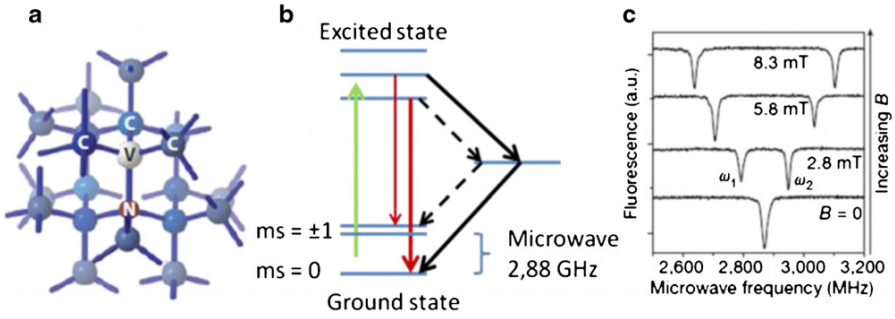

Supplementary figure 2. Optomagnetic properties of the NV-center. a One carbon atom is replaced by a nitrogen next to a vacancy in the diamond lattice. **b** Simplified energy diagram of an NV-center. After excitation with a green laser, the NV-center emits red photons. If the electron is in the ms=±1 state, there is also an alternative way to the ground state over a dark state. As a result, fewer red photons are emitted and decreased fluorescence is observed. If a microwave is applied whose energy equals the difference between the energies of the two states (2.88 GHz at zero field), the spins flip into the ms=±1 state. This effect can be observed as a drop in fluorescence (bottom curve in **c**). In presence of an external magnetic field the ms=±1 states are no longer equal in energy and thus split into two lines (top three curves in **c**). The difference is proportional to the field (Zeemann splitting), and the magnetic field can be determined. (**a** Reprinted with permission from [1]; **b** reprinted with permission from [2]; **c** reprinted with permission from [3]).

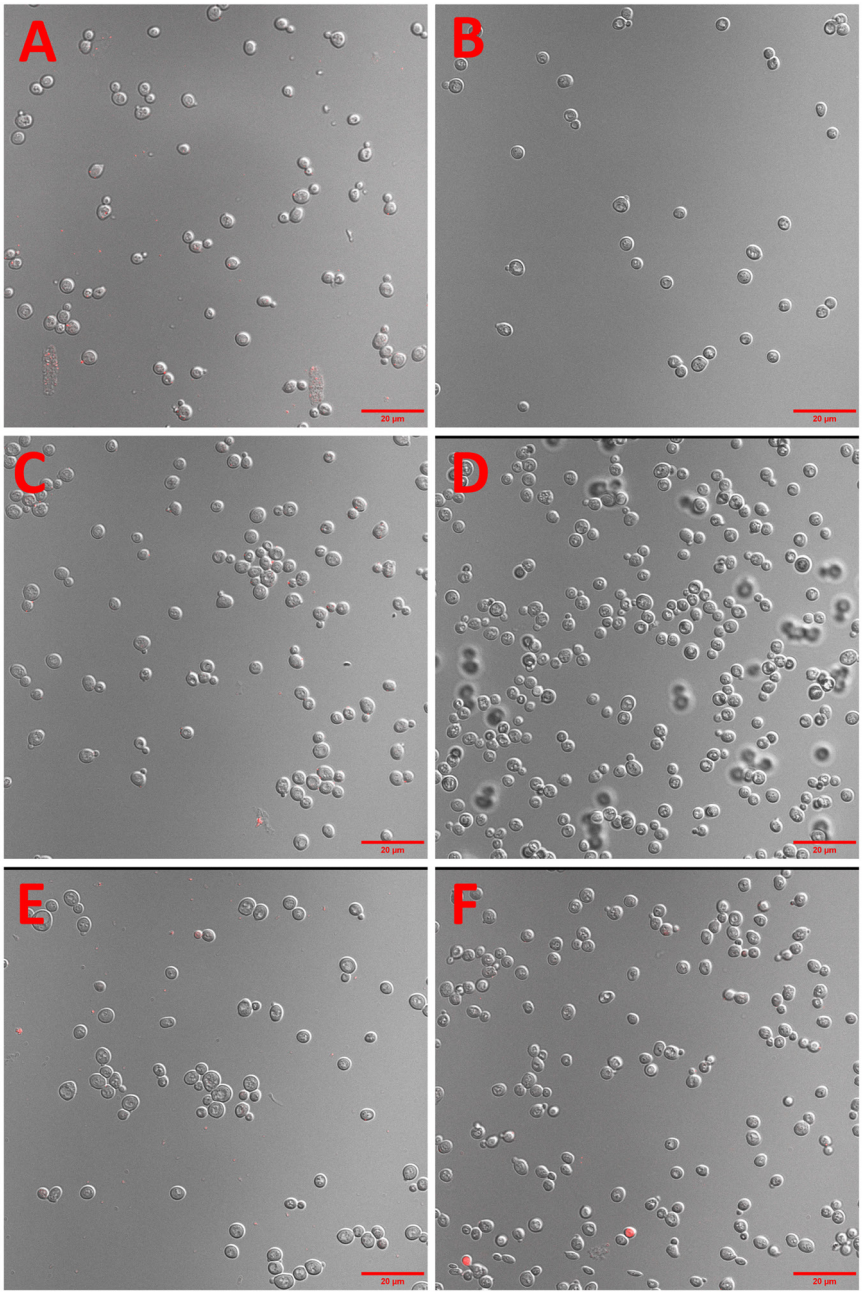

Supplementary Figure 3 Incubation conditions. Yeast cells were incubated with FNDs (2 µg/ml) in 1M sorbitol under different conditions for 2 hours at 30°C under different conditions without transformation, to show the non-uptake of yeast cells. **A.** The control sample. **B.** Instead of 1M sorbitol as a solvent for the FNDs, H2O was used. **C.** FNDs coated with Glucose. **D.** Cells were incubated in the dark instead of in the light. **E.** FNDs coated with FBS. **F.** FNDs incubated for 4 hours instead of 2. In none of the samples internalized FNDs can be found. In some cases cells appeared positive for diamond, however we confirmed that this was background or the FNDs were stuck to the exterior of the cells.

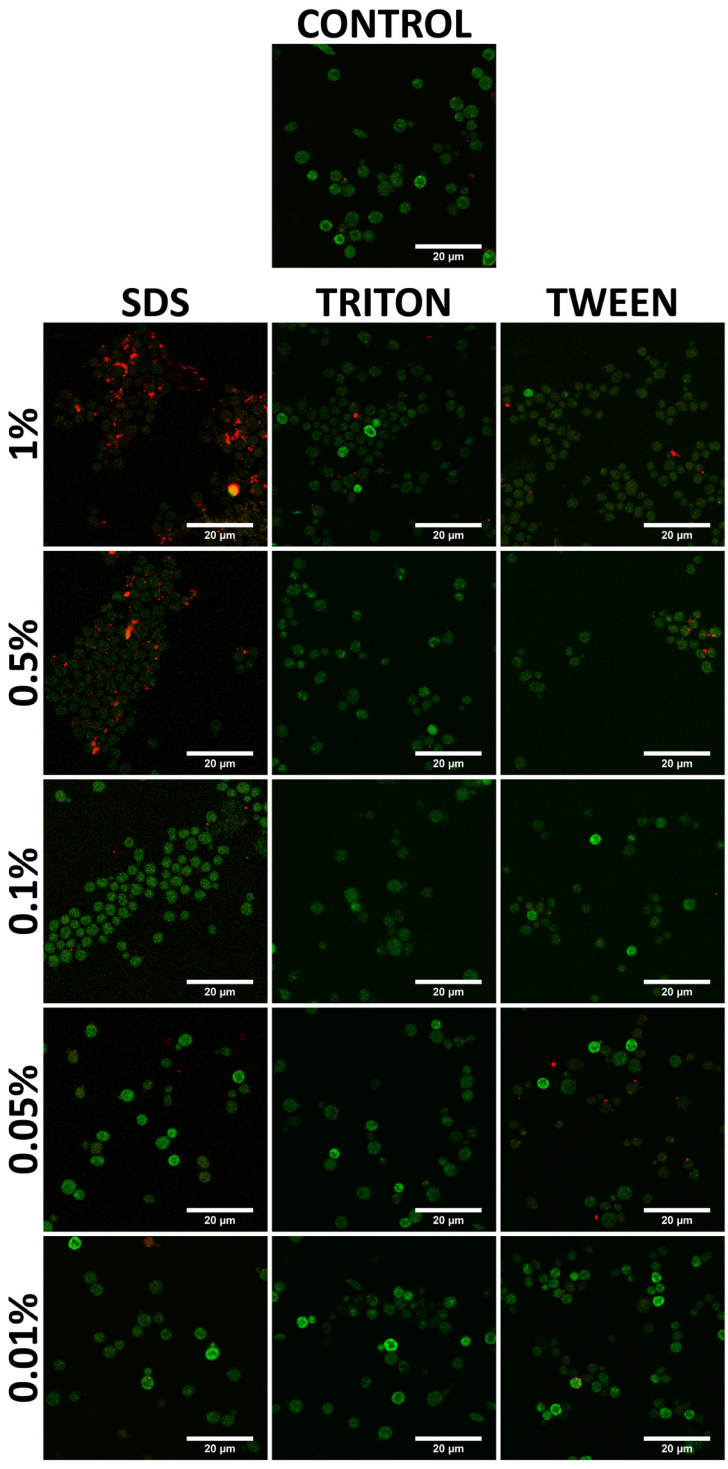

Supplementary Figure 4 Soap concentrations. We tested different soap concentrations of different soaps to see which would wash off externally bound FNDs the most efficiently. This appeared to be 0.01% Triton. Higher concentrations of SDS result in more extracellular bound FNDs. The SDS causes aggregation of the particles and at these high concentrations the cell wall is damaged, increasing the number of binding sites for diamond (aggregates) of the particles which were still present in the sample.

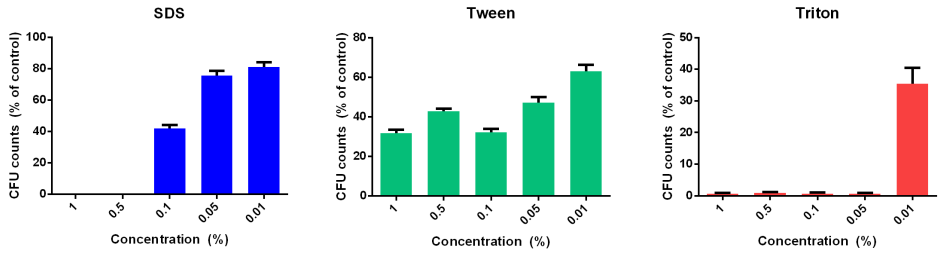

Supplementary Figure 5 Effect of detergents on viability. The different detergents used for removing particles from the cell surface, were tested for their effect on the viability of the cells. A concentration-dependent effect on the viability was found for all three soaps. SDS showed a strong negative influence on the cells at high concentrations. Tween had a minor effect on the cells even showing considerable amounts of viable cells at the highest soap concentration. Triton appeared to be the soap with the highest impact, decreasing the viability at all concentrations except the lowest (0.01%). To make sure that this low concentration was not an artifact, we also confirmed the viability to resemble normal values under even lower concentrations (0.001%, data not shown).

References

1. Schirhagl, R., Chang, K., Loretz, M. & Degen, C. L. Nitrogen-vacancy centers in diamond: nanoscale sensors for physics and biology. *Annu. Rev. Phys. Chem.* **65**, 83–105 (2014).
2. Nagl, A., Hemelaar, S. R. & Schirhagl, R. Improving Surface and Defect Center Chemistry of Fluorescent Nano-Diamonds for Imaging Purposes – A Review. *Anal. Bioanal. Chem.* (2015). doi:10.1007/s00216-015-8849-1
3. Balasubramanian, G. et al. Nanoscale imaging magnetometry with diamond spins under ambient conditions. *Nature* **455**, 648–651 (2008)

The response of HeLa cells to fluorescent nanodiamond uptake

Simon R. Hemelaar[1], Babujhi Saspaanithy[1], Severin R. M. L'Hommelet[1], Felipe P. Perona Martinez[1], Kiran J. van der Laan[1] & Romana Schirhagl

[1]Department of Biomedical Engineering, University Medical Center Groningen, The Netherlands.

Sensors **18:2** 355 (2018)

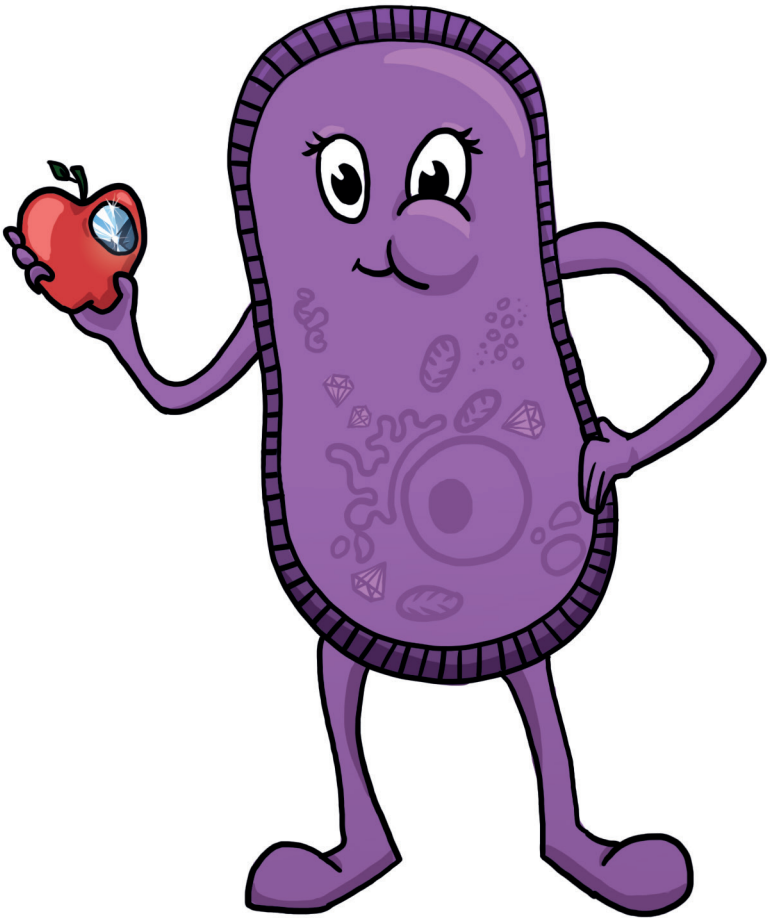

"An apple-diamond a day and the cell stays health-ay"

Abstract

Fluorescent nanodiamonds are promising probes for nanoscale magnetic resonance measurements. Their physical properties predict them to have particularly useful applications in intracellular analysis. Before using them in intracellular experiments however, it should be clear whether diamond particles influence cell biology. While cytotoxicity has already been ruled out in previous studies, we consider the non-fatal influence of fluorescent nanodiamonds on the formation of reactive oxygen species (an important stress indicator and potential target for intracellular sensing) for the first time. We investigated the influence of different sizes, shapes and concentrations of nanodiamonds on the genetic and protein level involved in oxidative stress-related pathways of the HeLa cell, an important model cell line in research. The changes in viability of the cells and the difference in intracellular levels of free radicals, after diamond uptake, are surprisingly small. At lower diamond concentrations, the cellular metabolism cannot be distinguished from that of untreated cells. This research supports the claims of non-toxicity and includes less obvious non-fatal responses. Finally, we give a handhold concerning the diamond concentration and size to use for non-toxic, intracellular measurements in favour of (cancer) research in HeLa cells.

Introduction

While nanodiamonds have been widely used as abrasives for decades, new applications have been discovered recently. In Fluorescent Nanodiamonds (FNDs), a nitrogen vacancy (NV) center is created which can be utilized as stable single photon emitter[1] or spin qubit in quantum information.[2] The spin properties of diamond defects are utilized in nanoscale sensors. These can detect magnetic resonances,[3,4] pressure,[5] temperature[6] or electric fields[7] with unprecedented spatial resolution.[8] In addition, nanodiamonds are under consideration for drug delivery[9,10] and photostable fluorescence labeling.[11,12] As a result, there is a broad interest in studying the (bio) compatibility of nanodiamonds. Their internalization into different cell types[13–18] and lack of cytotoxicity[19–21] have been confirmed in several studies in different cell models. We confirm this finding and see virtually no effect on cell viability. FND toxicity *in vivo* has been found to be very low or negligible repeatedly in different organisms.[22,23] However, Marcon et al. found a decrease in the rate of survival of frog embryos after administration of relatively high concentrations of 2 mg/mL of 4 nm detonation nanodiamonds. In most rodent studies (mouse or rats) no clinical symptoms can be found of either small or large nanodiamonds and the diamonds tend to accumulate in lung and liver tissues.[24–26] In cynomoglus monkeys, some abnormalities were seen in histological evaluations of the heart and liver, using detonation nanodiamonds at a high concentration of 25 mg/kg bodyweight.[27] Some more toxic effects have been found for detonation nanodiamonds,[28,29] while other studies report no cytotoxic effects depending on the surface treatment.[30,31] FNDs and detonation nanodiamonds have very different properties due to size, surface to volume ratio and surface termination. Detonation nanodiamonds are not the topic of this study. Non-toxic influences are very important since these might still alter the cell biology. Such influences have only been taken into account in very few studies. Thomas et al. for instance studied the expression of genes related to inflammatory responses and observe down regulation of these genes (at a relatively high diamond concentration of 50 µg/mL).[32] Moore et al. investigated genes involved in proliferation, inflammation and apoptosis and did not see any differences compared to the control sample.[33] Huang et al. found no indication of cell death but did see morphological changes in neurons after exposure to FNDs.[34] In malignant cell growth, free radical levels are an important determining factor.[35] Mohan et al. investigated overall reactive oxygen species (ROS) levels in *Caenorhabditis elegans*.[36] They did not find altered ROS levels, nor did they detect any genotoxic effects.

The goal of this study is to assess in detail if FNDs are suitable for intracellular sensing and what non-fatal impact the presence of diamond particles has on a cell. We chose to study HeLa cells since they are a very common cell model for various types of research. When the term biocompatible is used in this paper, this refers specifically to compatibility for HeLa cells. We provide a detailed analysis of non-fatal influences of diamond on the reactive oxygen species formation in cells for the first time. This is particularly relevant, for two reasons. First, they are an attractive analyte for sensing applications and second they indicate oxidative stress.

Materials and Methods

Cell Culturing

HeLa cells were cultured in Dulbecco's Modified Eagle Medium with 4500 mg/L glucose (DMEM-HG), supplemented with 10% Foetal Bovine Serum (FBS), 1% Penicillin/ streptomycin and 1% Glutamax (Gibco, ThermoFisher Scientific, Etten-Leur, The Netherlands) at 37 °C, 5% CO_2. HeLa cells are a favourable model in (cancer) research, as these are an extensively studied cancer cell line. Cells were seeded in gamma irradiated 35 mm glass bottom collagen coated dishes (MatTek corporation, Ashland, MA, USA) until clusters of at least 10 cells grew for confocal microscopy. For mRNA and protein analysis, cells were grown in 6-well plates (Greiner Bio-One, Frickenhausen, Germany). For the MTT (3-(4,5-dimethylthiazol-2-yl)-2,5-diphenyltetrazoliumbromid) viability assay and total free radical analysis, cells were grown in Greiner 96-wells flat-bottomed plate.

Diamond Uptake

From Petr Cígler, IOCB Prague, we received etched diamond particles[16] (with rounded edges). The other diamonds were obtained from Adámas Nanotechnologies (Raleigh, NC, USA), see also **Table 1**. Nanodiamonds were first suspended in 100 µL 100% FBS-HI (Heat-Inactivated Foetal Bovine Serum) to prevent aggregation, as shown previously.[13] Next, 900 µL DMEM-HG was added and the diamond suspensions were incubated with precultured cells for 5 hours at 37 °C, 5% CO_2. We used concentrations, which ensured that at least every cell had multiple intracellular diamonds. When performing Electron Spin Resonance (ESR) measurements, it is preferable to have one or a handful of nanodiamonds per cell, as too many diamonds will make it more difficult to obtain the spectra of a single particle or NV-center. Therefore, we chose to use 10 µg/mL of nanodiamonds as an upper limit, as this results in already more diamonds per cell than useful for quantum measurements. One sample was taken into account in which the particles were added directly to DMEM-HG supplemented with FBS and thus aggregation was not prevented. As a positive control for cellular damage, cells were incubated with 1 mM, 200 µM or 40 µM H_2O_2 (hydrogen peroxide) for 2 hours. Afterwards, the diamond or H_2O_2 containing medium was removed and the cells were used for microscopic visualization or different analysis methods, see below. To investigate the long-term influence of the diamonds as well as possible recovery from an impact, we also tested the cells after incubating them for 24 more hours (T = 24) in supplemented DMEM-HG medium without diamonds or H_2O_2 before further analysis.

Table 1. Diamond samples.

Name	NV-centers	Average Diameter	Concentration/ Condition Used	Surface Termination	Surface Potential
FND_{120}	>1000 NV/ particle	120 nm	1 µg/mL	Carboxylated-COOH	−20 mV
FND_{70}	>300 NV/ particle	70 nm	10 µg/mL, 1 µg/mL, 0.1 µg/mL, 1 µg/mL aggregated	Carboxylated-COOH	−40 mV
FND_{40}	10–15 NV/ particle	40 nm	1 µg/mL	Carboxylated-COOH	−45 mV
Rounded FNDs		25 nm		Carboxylated-COOH	−23 mV

Microscopic Analysis

We performed a microscopic analysis to identify and quantify ingested diamond particles. Cells were fixed in 3.7% PFA (Paraformaldehyde) and subsequently blocked in 5% PBSA (bovine serum albumin in phosphate buffered Saline). After blocking, we used 2 µg/mL phalloidin-FITC (Sigma-Aldrich, Zwijndrecht, The Netherlands) to label f-actin and 4 µg/mL DAPI to label the nucleus (Sigma-Aldrich, Zwijndrecht, The Netherlands) in 1% PBSA. The samples were imaged using a LSM780 confocal microscope (Zeiss, Sliedrecht, The Netherlands) using a 405, 488 and 561 nm laser. Images were analyzed using FIJI 2.0.0 software (https://fiji.sc). A visual inspection of the morphological changes was performed to estimate the effect of the diamond uptake on the cells cytoskeletal condition. Next, a specific, custom-made FND quantification plugin was used to approximate the amount of internalized FNDs. The analysis was divided into three phases: Cell Selection, Masking and Particle Analysis. During the first phase, the images were visually inspected and random cells were selected for the analysis. Cells with diamond aggregates associated with the cell membrane were rejected to prevent false positive results. The images were composed of several slices (Z-stacks) and the cellular region was defined in all the three dimensions. In the horizontal plane, the selection considered an area containing only the cell of interest. In the height, the first and last slices containing the cell were identified. As a result, the first phase defines a volume that holds only the cell of interest. In the Masking phase, that volume is moulded in order to resemble the shape of the cell. The phalloidin-FITC signal is converted to binary using the Isodata algorithm to calculate the threshold[37] and the cell's perimeter is detected in every slice. To find the inner volume of the cell, the program shrinks the cell's region in order to exclude the cell membrane from the analysis. The final step uses a special function of Fiji, which analyzes the particles found in a selected region. Applying this function to the masked image, it is possible to directly obtain the number of objects (connected positive pixels) in the specified region. A threshold is used to separate the background light from the signal emitted by the FNDs. Every pixel with intensity less than the threshold is assumed as background and set as black, while every pixel with an intensity greater than or equal to the threshold is assumed as part of a particle. To find an adequate value for this parameter, the image was visually inspected and different values were probed. Finally, we chose the lowest possible value, which gives zero for a negative control image. In the end, this method gives two important

values: the number of objects, which reflects the amount of adjacent FND positive pixels, where a single diamond or multiple diamonds can be counted as 1 and the number of particles, which reflects the actual number of particles by calculation from the intensity and size of the objects.

Cellular Viability

To test the viability after incubation with FNDs, HeLa cells were washed once with PBS (phosphate buffered saline). Next, 0.05% MTT (3-(4,5-dimethylthiazol-2-yl)-2,5-diphenyltetrazoliumbromid, Sigma Aldrich, Zwijndrecht, The Netherlands) and serum-free medium were added to the cells. After two hours of incubation at 37 °C, 5% CO_2, the cells were washed with PBS. Subsequently, the cells were dissolved using 2-propanol and the absorption of the purple solution was measured using a FLUOstar Omega Microplate Reader (BMG Labtech, De Meern, The Netherlands) at 560 nm. After correction and comparison to the background, this gives a ratio of the viability of the cell, where 0.8–1.2 is considered to be the normal range.[38] Results of MTT were validated using light microscopy.

Total ROS Activity

2′,7′-dichlorodihydrofluorescein diacetate (DCFDA) can be used as an indirect measure for the total ROS production inside a cell. After entering the cell, DCFDA is deacetylated and later oxidized by ROS to 2′,7′-dichlorodihydrofluorescein (DCF) which is highly fluorescent. First, 20 μM DCFDA in phenol red-free DMEM medium is added to the cells and incubated for 45 minutes. Then the cells were incubated with FNDs. Incubation with 50 μM tert-butyl hydroperoxide (TBHP) instead of FNDs is used as a positive control. HeLa cells without a stimulant were used as a negative control. In case of T = 24 hours measurements, TBHP was added 4 hours and DCFDA 45 minutes prior to the end of the incubation time. Fluorescence was measured directly after incubation using a FLUOstar Omega Microplate Reader, excitation 485 nm and emission 520 nm. All samples were related to the negative control after subtraction of the background (medium without cells) and shown as a fold increase. A separate negative control was made for cells after 24 hours. All samples were tested in triplicate. While the DCFDA analysis gives a good measure for the overall ROS production, quantitative polymerase chain reaction (qPCR) and western blotting measures the cell's response to these stress factors.

RNA Isolation and Real-Time PCR

qPCR was used to evaluate intracellular mRNA transcription levels of Catalase (CAT), Glutathion Reductase (GSR), SuperOxide Dismutase 1 (SOD1) and Caspase-3 (CASP). These are common enzymes, which are expressed as a response to oxidative stress. More precisely, superoxide dismutase 1 is involved in the conversion of singlet oxygen radicals to hydrogen peroxide. Catalase and glutathion reductase are both involved in metabolizing H_2O_2 into non-toxic compounds like water

or oxygen. Caspase-3 is a marker for apoptosis. Total RNA was isolated from cell cultures using the InVisorb Spin Cell RNA Mini Kit (InVitek, GmbH, Berlin, Germany), following the manufacturer's instructions. The quantity and purity of RNA were determined using a spectrophotometer (NanoDrop, Wilmington, DE, USA). RNA was reverse-transcribed using the I-script reverse transcription kit (Bio-Rad Inc., Hercules, CA, USA) while following the manufacturer's instructions. Real-time polymerase chain reaction (PCR) amplification of cDNA was performed using the Sybr green mix from Abgene (Westburg BV Leusden, The Netherlands) and specific oligonucleotide primers listed in **Table 2**. The real-time PCR parameters were as follows: 95 °C for 15 minutes, then 40 cycles at 95 °C for 15 s, 57 °C–60 °C for 15 s and 72 °C for 15 s. Data were analyzed using the $2^{-\Delta\Delta CT}$ method of Livak and Schmittgen,[39] using the housekeeping gene 18S (a gene which encodes for ribosomal RNA and is present in the same amount in every cell) to calculate the ΔCT and using the control at each measurement to calculate the ΔΔCT. This value gives a measure to quantify the genetic response in relation to the basic metabolism in the cell. All samples were tested in triplicate and measured in 3 independent qPCR runs.

Table 2. Primer sequences.

Target cDNA	Primer Sequence 5'->3'	Product Size, bp	Tm
Catalase	CGCAGAAAGCTGATGTCCTG	20	60.5 °C
Glutathion Reductase	TCAACGAGCTTTACCCCGAT	20	60.4 °C
SuperOxide Dismutase 1	ACAGCAGGCTGTACCAGTGC	20	59.9 °C
Caspase-3	GGGATCGTTGTAGAAGTCTAACTG	24	57.1 °C
18S	AAGGAGACTCTGGCATGCTAAC	22	58.5 °C

Western Blot

PCR shows the production of mRNA in response to an impact. This is a first, fast response of a cell and thus reflects the 'intentions' of the cell. However, the cell has also epigenetic self-correction mechanisms. As a result, not all mRNA is actually translated to proteins. The protein level, which we evaluated via western blot, gives a better measure of the current situation in the cell. Western blot analysis was used to evaluate intracellular protein levels of catalase, glutathion reductase, superoxide dismutase 1 and caspase-3. For this, HeLa cells were harvested in denaturation buffer (10 mM Tris-HCl pH 7, containing 1 mM EDTA, 2.5% SDS, 2% 2-mercaptoethanol and 10% glycerol) and proteins were analyzed by SDS-PAGE according to the method of Laemmli using a 11% running gel as previously described.[40] After separation, the gel was blotted to nitrocellulose and blocked for 1 hour with 3% BSA, 0.1% Tween in TBS (tris buffered saline). After incubation overnight at 4°C with the primary antibody, different secondary antibodies (listed in **Supplementary Table S1**) were added and allowed to incubate for 1 hour. Then, the blot was incubated with alkaline phosphatase(AP)-conjugated tertiary antibody diluted 1:1000 for another hour. After washing, the blot was developed with nitro blue tetrazolium and 5-bromo-4-chloro-3-indolyl phosphate in AP buffer. All incubation and washing steps were performed at room temperature, unless stated otherwise. The primary antibodies rabbit anti-caspase 3, anti-superoxide dismutase 1, anti-catalase and anti-gluthation

reductase (Supplementary Table S1) were further incubated with mouse anti rabbit IgG (Jackson ImmunoResearch Laboratories Inc., West Grove, PA, USA) first and then with goat anti-mouse AP (Bio-Rad Inc., Hercules, CA, USA). Mouse anti-tubulin and anti- glyceraldehyde-3-phosphate dehydrogenase, two housekeeping proteins, used as a loading control (Supplementary Table S1), were incubated with goat anti-mouse IgG (Jackson ImmunoResearch Laboratories Inc., West Grove, PA, USA) and then with rabbit anti-goat AP (Bio-Rad Inc., Hercules, CA, USA). The ratio between the protein of interest and the loading standard tubulin or GAPDH was calculated using FIJI software. All samples were performed in triplicate and measured in 3 independent Western Blots.

Results

Uptake of FNDs in HeLa Cells

The uptake of differently shaped and sized FNDs, as well as the uptake following incubation for 24 hours, was visualized using confocal microscopy. We used FIJI software with a homemade script to define objects and particles as an arbitrary measure to quantify the internalized particles. In **Figure 1**, examples of the confocal images are shown. We selected our 'standard' quantity of diamonds, 1 µg of FND_{70}, immediately after uptake and 24 hours after uptake. Also, FNDs of a different size (FND_{120}) and shape (rounded FNDs) are shown. The shape of the particles we used in this study have already been characterised elsewhere. To confirm the rounded and prickly shape we would like to refer the reader to SEM images in references.[16,41] We deliberately made a selection of incubation conditions as showing all of these overall gives the same idea. In these images sometimes multiple adjacent pixels are positive for FND. This can be explained by aggregation of particles, a limited resolution (the pixel size here is approximately 1 µm) or colocalization of the diamonds in for example endosomes. The variation of ingested objects/particles between the different incubation conditions is quantified in **Figure 2**, the original images from which this data was calculated can be seen in **Supplementary Figure S1**. As can be expected, the number of diamonds added to the samples also results in a corresponding increase or decrease of the number of objects inside a cell. 10 µg / mL of diamonds results in a significantly higher concentration of internalized objects. The different sizes and shapes of diamonds do not result in a rigorously altered ingestion. The difference between the immediate analysis and the analysis after 24 hours is not significant. An image of the cells without diamonds (data not shown) resulted in 0 particles/cell. It also has to be noted, that the time intervals for cell divisions for these cells is around 22 hours.[42] During the 24 hours further incubation time, some cell divisions will have taken place and hence there are more cells, which influences the results at T = 24. The diamonds seem to be distributed equally over all cells, indicating that there is no selection process for the diamonds during cell division. The number of FNDs inside the cells does not change significantly over 24 hours, indicating that there is no excretion of the particles. In **Supplementary Figure S5** and **Supplementary Table S3** we give an approximation of the

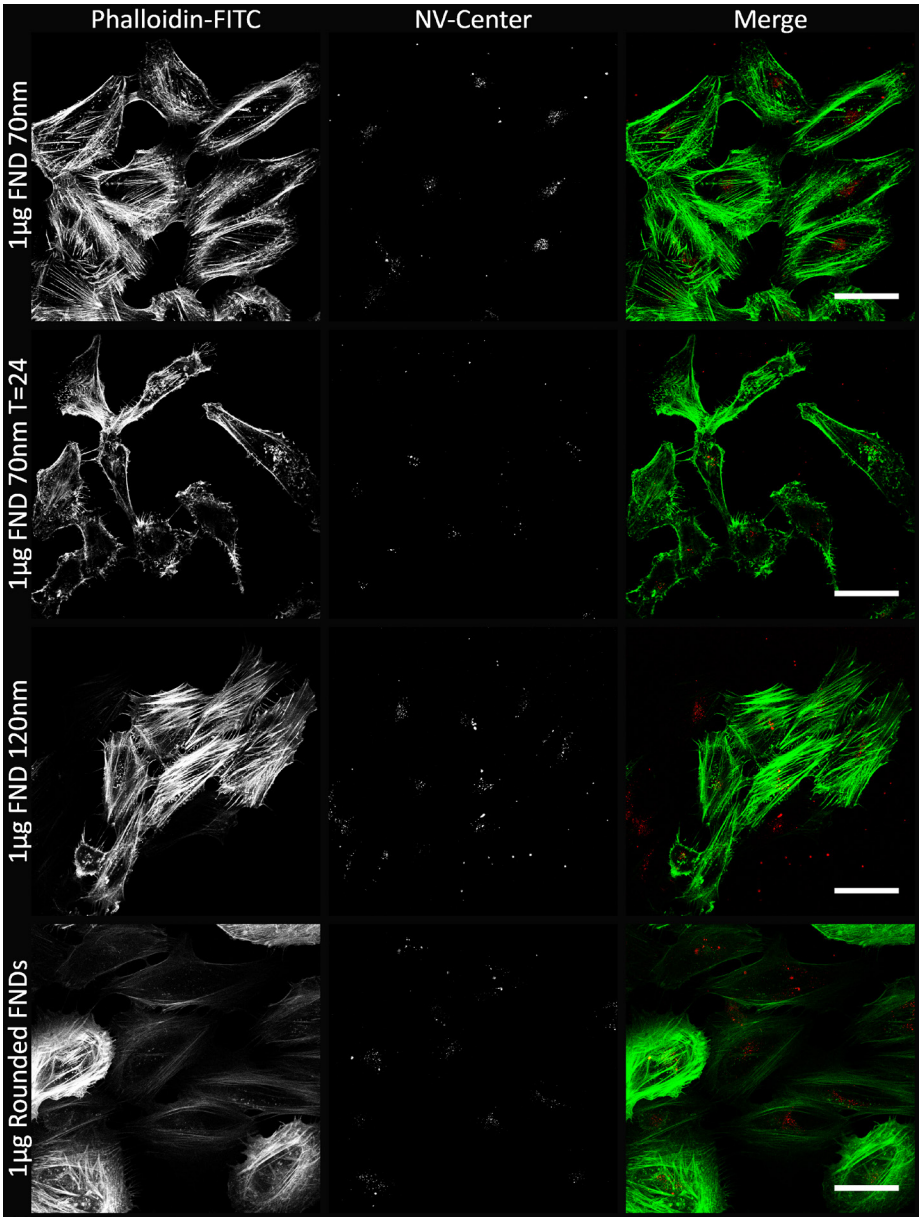

Figure 1. Confocal images of HeLa cells incubated with FNDs. To visualize internalized nanodiamond particles (in red), HeLa cells were fixed with 3.7% PFA and subsequently stained with Phalloidin-FITC and imaged using a LSM780 microscope. Phalloidin-FITC stains the actin cytoskeleton of the cells (in green). For visualization purposes, both signals are shown in white and merged. As examples, cellular uptake of the standard situation (1 µg FND_{70}), the uptake after 24 h, cells with 120 nm FNDs (1 µg FND_{120}) and cells with rounded FNDs are shown. The morphological differences between the cells in the images are a natural variation. As each cluster grows out of one mother cell, they resemble the closest sister cells but not by definition the cells of other clusters. The images were recorded in z-stacks and a focal plane was chosen to display here, approximately 2 µm above the cover glass, as these show the largest volume of the cells. The scale bars in these single optical section images represent 50 µm.

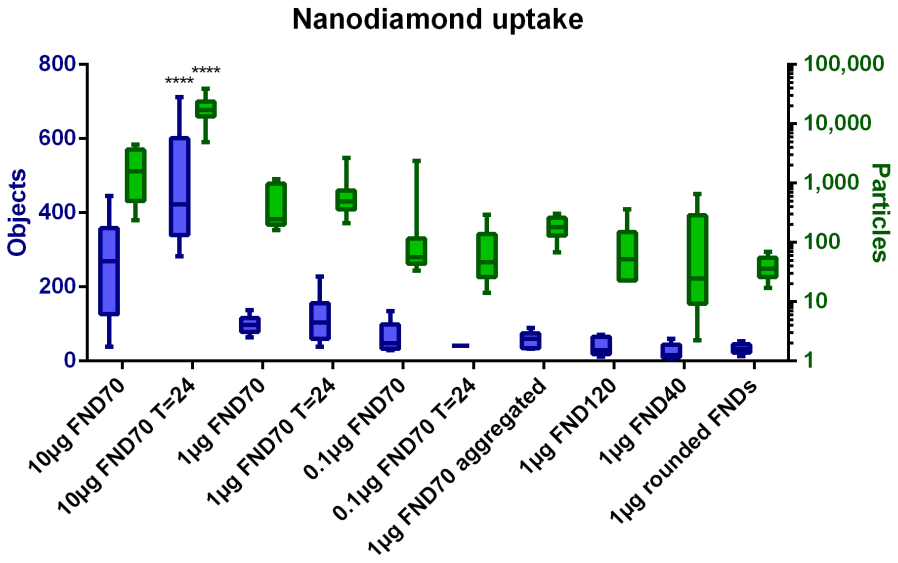

Figure 2. FND uptake in HeLa cells. After confocal imaging, cells are analyzed using FIJI software. Our analysis counts the objects (in purple) and particles (in green) inside cells, giving an arbitrary measure for the amount of diamonds taken up. Objects are adjacent FND positive pixels in cells, incorporating both single particles and aggregates or adjacent particles. Particles represent an estimation of the number of FNDs, calculated by the intensity and size of the objects. The sample incubated with more nanodiamonds, 10 µg of 70 nm FNDs T = 24, resulted in significantly more nanodiamonds per cell ($p < 0.001$) in comparison to most other samples with the exception of 10 µg of 70 nm FNDs T = 0.

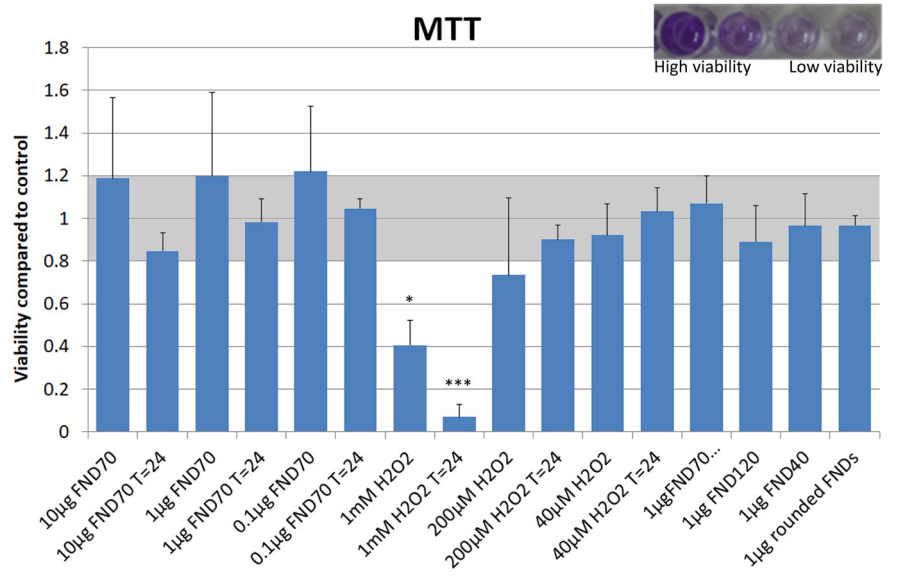

Figure 3. Viability of cells after FND uptake. If the viability compared to the control is between 0.8 and 1.2 it is considered to be unaffected. The samples in which 1 mM H_2O_2 was used differed significantly from the control (* $p < 0.05$, *** $p < 0.001$). Error bars show the standard deviation.

morphological changes at different time points after uptake of different concentrations of 70 nm FNDs, in comparison to a control (no diamonds).

Biocompatibility of Nanodiamonds

The viability of cells in all different conditions of nanodiamonds and H_2O_2 were tested using a MTT assay. MTT is converted by mitochondrial reductase enzymes to formazan, which has a purple colour. This process only happens if the cell is alive and metabolically active. The results of this analysis can be found in **Figure 3**. The inset in Figure 3 shows the dark purple solution resulting from viable cells, whereas the colourless solution indicates non-viability. It is important to note that the viability is generally considered equal to the control if it is between 0.8 and 1.2 times the control values. Thus, we can conclude that the viability of cells after diamond uptake is not changed in any of our experiments. Hydrogen peroxide was used as a positive control to directly be able to measure the effects of an increased concentration of oxidative products. We have also tested the production of free radicals and viability after administration of different concentrations of LPS (lipopolysaccharide), as this can increase cellular oxygen radical production.[43] This however did not lead to a sufficient overall free radical production to show the desired effects, see **Supplementary Figure S2** (Free radical production) and **Supplementary Figure S3** (Viability). Therefore, we chose a series of hydrogen peroxide concentrations to better evaluate the cellular response. The shape, size or concentration of the diamonds does not influence the viability of the cells. All samples after 24 hours are also in the normal viable state, with the exception of the positive control were high concentrations of hydrogen peroxide were added.

Total ROS Activity

To evaluate the total ROS production inside HeLa cells, we evaluated the free radical dependent conversion of DCFDA into its fluorescent metabolite DCF. The fluorescence of each sample was compared to the negative control (**Figure 4**). As could be expected, adding high concentrations of hydrogen peroxide to the cells increases the fluorescence drastically and significantly. After 24 hours we do not see this increase; by then all the free radicals have reacted to other compounds, damaging the cells. The FNDs do not alter the total ROS production significantly, however a slight, non-significant decrease in ROS activity was found in the samples after 24 hours and in the samples with 120 nm FNDs (see **Supplementary Figure S4**). This may suggest a free radical scavenging function of the diamonds.

Real-Time PCR

For a closer look at the cellular response to diamond uptake, we analyzed the changes in mRNA levels. mRNA indicates a cell's first response, as the nucleus transcribes those parts of the DNA that are needed at that time. In general, a downregulation of genes involved in the scavenging of free radicals can be seen (**Figure 5**). For diamond

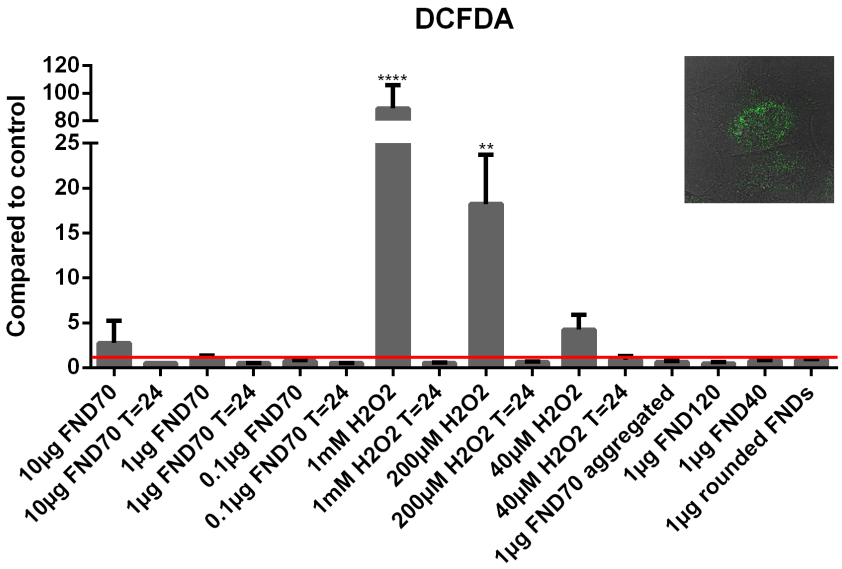

Figure 4. Mean free radical production. ROS production can be measured by the conversion of DCFDA to DCF. The more DCF there is, the higher the fluorescent signal a sample emits. As expected, adding a high concentration of hydrogen peroxide increases the signal drastically (up to 100-fold). No diamond samples alter the total free radical production inside cells. HeLa cells without a stimulant were used as a negative control to relate all values to. ** $p < 0.01$, **** $p < 0.0001$. Error bars show the standard deviation. The inset in this figure shows a cell in greyscale with the metabolized DCF in green.

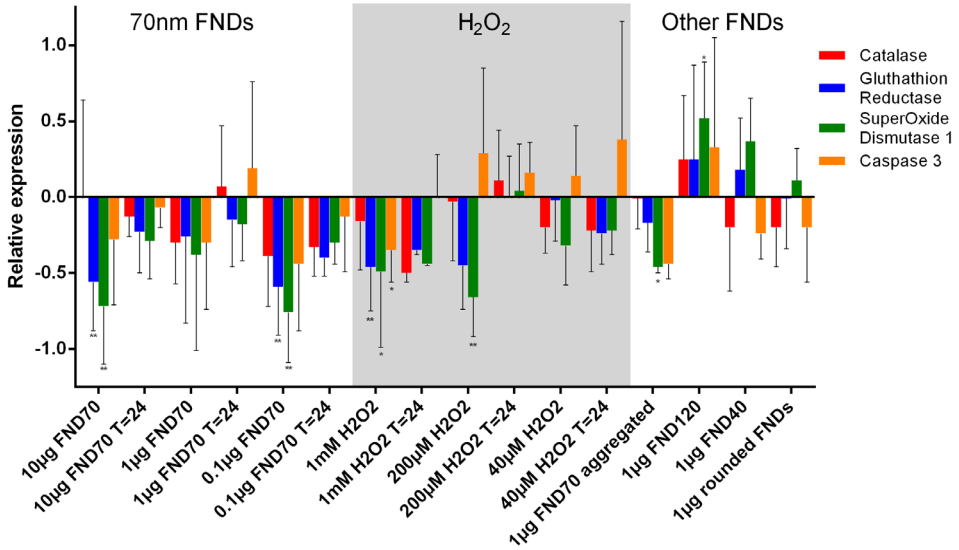

Figure 5. Relative expression of oxidative stress-related genes. The relative expression of four different genes as a response to the uptake of diamonds or the presence of H_2O_2 has been analyzed using quantitative PCR. The control is set as zero, the increase or decrease of the genetic expression is showed for all samples. Glutathion reductase and superoxide dismutase differed most often significantly from the control. * $p < 0.05$, ** $p < 0.01$. Error bars show standard deviation. Values are averages out of three independent qPCR runs that were performed in triplicate.

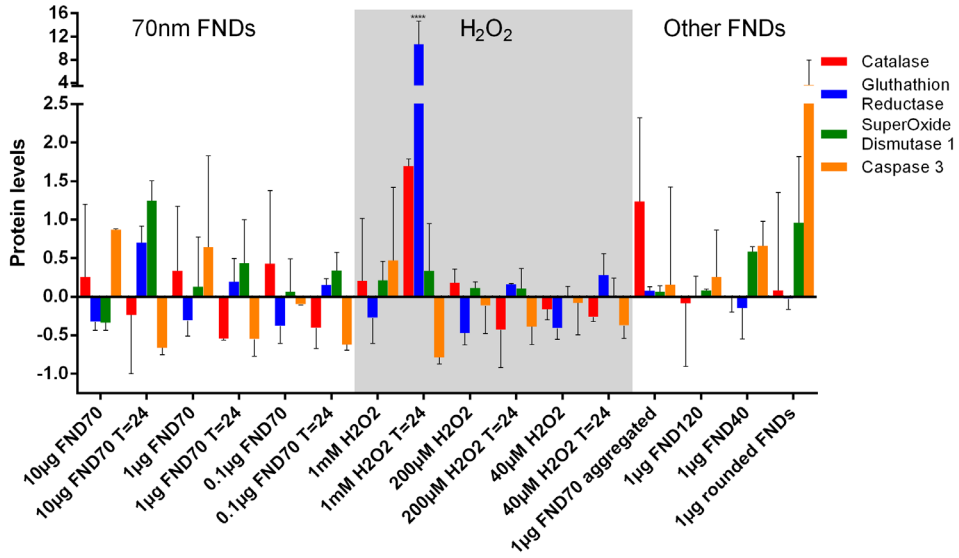

Figure 6. Levels of oxidative stress-related proteins. By quantitating Western Blots, protein levels as a response to the uptake of diamonds or the presence of H_2O_2 have been analyzed. The control is set as 1, the protein levels are shown as fold increase or decrease for all samples. The protein levels after uptake of 40, 70 and 120 nanometre FNDs did not differ significantly from the control situation. Note that although in cells with rounded FNDs the caspase-3 levels are increased, this is not significant. **** $p < 0.0001$. Error bars show the standard deviations. The values are averages out of 3 independent Western Blots of samples in triplicate.

particles, we see a larger down regulation for oxidative stress-related genes. When comparing aggregated to non-aggregated particles or different concentrations we do not see any significant changes. In the case of hydrogen peroxide, we see an upregulation of caspase-3 at lower concentrations (200 µM and 40 µM), which indicates the onset of apoptosis. At the highest hydrogen peroxide concentration (1 mM) we see a slight downregulation of caspase-3, which is probably due to a progression of apoptosis. As can be seen in the MTT assay, (Figure 3) many of the cells have already died at this point.

Protein Transcription

By analysing Western Blots the protein levels in cells can be measured. This reflects the current situation inside the cell, whereas the measurement of mRNA levels reflects the "intentions" of the cell. Western Blot proves a useful tool to observe if the altered mRNA levels also affect cellular protein levels. This is visualized in **Figure 6** and **Supplementary Table S2**, the latter correlating the (non-significant) changes of both the qPCR and the Western Blot. Generally, the differences in protein levels are less pronounced than in mRNA levels. This could be due to epigenetic changes of the mRNA or a feedback mechanism on the protein. We also see drastic changes in protein expression in the sample with 1 mM H_2O_2. Here the surviving cells clearly have produced a high abundance of GSR and catalase to deal with the peroxide. This

demonstrates that the protein response of the cells to oxidative stress requires some time to be fully effective. Catalase and glutathion reductase play a smaller role in the samples where diamond particles were internalized. In the control situation, no FND incubation or H_2O_2 treatment of the cells took place.

Discussion

Here we have for the first time studied the non-fatal response to nanodiamond uptake for diamonds with different sizes, shapes and concentrations. Although there are some changes to the cellular mRNA and protein levels, the overall data indicate that diamonds are biocompatible and do not negatively influence the total free radical level inside the cell. Furthermore, while we see slight changes immediately after the uptake, cells recover very well from the ingestion after 24 hours. HeLa cells respond especially well to concentrations of 1 µg/mL FND_{70} and lower, 24 hours after uptake. At this time point, the smallest genetic and protein differences are found. A normal viability level, as well as a conventional number of oxidative products in the cells, also argues for an ideal culturing condition. On the morphological level, the cytoskeleton of the cells seems to be mostly normal after 24 hours, although some indication of an early onset of apoptosis can be seen. This however happens also under control conditions. Another explanation can be found in the microscope setup, where a different focus or different light intensity can show a slightly altered picture. Typically, 24 hours is long enough for most FND related experiments but to rule out longer term viability difficulties, cells could be monitored after 48 hours. Using a concentration of 1 µg/mL FND_{70}, every cell has at least tens of internalized objects; for most magnetic resonance measurements 1 nanodiamond per cell is already sufficient. The internalized diamonds were calculated after excluding diamonds in the membrane region. It is possible that the diamonds attached to the membrane also influence the cellular behaviour. If some cells would have only a few diamond particles ingested the effect on the cell biology could be too low to measure, which is why we chose higher than necessary concentrations. Our results therefore overestimate the effects for the desired application.

Most stress-related genes are down-regulated after incubation with nanodiamonds. This could have three reasons: (1) the number of radicals is decreased by scavenging, so that the cells have less compensation needed for an excessive radical production, (2) the cells are going into apoptosis or (3) a temporary increase in stress at a prior point before FND incubation is completed results in an overshoot and down-regulation of scavenging related proteins. To differentiate the cases, we can compare the levels at 24 hours after uptake as well as the results from the MTT assay. The fact that the values generally decrease after 24 hours indicates that the cells are recovering (as opposed to the positive control). There are no signs of decreasing metabolic activity visible in the MTT assay, which underlines the suggestion that downregulation could be due to a scavenging effect. Diamonds of 120 nm in diameter do cause a significant up-regulation of superoxide dismutase-1. The up-regulated transcription does not result in a higher protein translation however, as can be deducted from Figure 6.

In a previous study, we have extensively studied the formation and prevention of FND aggregates for applications in cell culturing.[13] Confocal images revealed that even in samples where aggregation was prevented, diamonds seemed to cluster. It has to be noted that conventional confocal microscopy is diffraction limited. Multiple diamonds can be located in the same pixel, without being aggregated. Super resolution confocal microscopy or electron microscopy can be used to more accurately analyze this aggregation. Aggregated diamonds enter HeLa cells in a similar fashion to their single counterpart. This is true for HeLa cells which more easily take up particles but will not be true for cells which are less prone to take up larger particles, such as colon carcinoma cells.[44]

The exact localization of nanodiamonds is an interesting topic of research. Chu et al. showed that nanodiamonds escape to the cytoplasm[16] but did not give an indication to which organelle the diamonds are ultimately localized. Lake and Bouchard very thoroughly demonstrated that they were able to target nanodiamonds toward the nuclear pore complex[45] and Chan et al. directed the diamonds towards the mitochondria.[46] During our confocal analysis, we found that diamonds seem to localize near the nucleus. Future research should point out if and to what extent and distance the nanodiamonds colocalize with cellular organelles.

Next to advancements and opportunities for *in vitro* applications of nanodiamonds, like monitoring magnetic resonances and temperature, nanodiamonds have also shown potential for biomedical purposes by numerous *in vivo* studies (reviewed in [47]). Within the nanomedicine field, one of the applications that has attracted increasing attention is drug delivery. Using nanodiamonds in drug delivery systems aims to improve stability of drugs in physiological environment and to increase targeting efficiency and localized drug release.[48–50] Another purpose for nanotechnology in biomedical sciences can be found in imaging, where nanodiamonds are used as (carriers for) MRI contrast agents[51,52] or as stable, fluorescent labels in lifetime imaging.[36,53] Obviously, both these diagnostic and therapeutic applications could have great impact on clinical practice. Extensive pharmacokinetic analyses are required, as well as a thorough understanding of the behaviour of nanodiamonds in a physiological environment, to eventually make the translation of nanodiamond applications to the clinic.

Here we have performed an in-depth analysis of the biological impact of fluorescent nanodiamonds uptake on HeLa cells and the generation of ROS. For future intracellular magnetic resonance measurements, this is vital background knowledge, as free radicals can influence the readout of the quantum states of the nitrogen vacancy center. The relative safety of nanodiamonds paves the way for extensive cell experiments using FNDs and HeLa cells.

References

1. Aramesh, M. et al. Coupling of a single-photon emitter in nanodiamond to surface plasmons of a nanochannel-enclosed silver nanowire. *Opt. Express* **22**, 15530–41 (2014).
2. Weber, J. R. et al. Quantum computing with defects. *Proc. Natl. Acad. Sci. U. S. A.* **107**, 8513–8 (2010).
3. Grinolds, M. S. et al. Nanoscale magnetic imaging of a single electron spin under ambient conditions. *Nat. Phys.* **9**, 215–219 (2013).
4. Mamin, H. J. et al. Nanoscale nuclear magnetic resonance with a nitrogen-vacancy spin sensor. *Science* (80-.). **339**, 557–560 (2013).
5. Doherty, M. W. et al. Electronic properties and metrology applications of the diamond NV - Center under pressure. *Phys. Rev. Lett.* **112**, (2014).
6. Acosta, V. M. et al. Temperature dependence of the nitrogen-vacancy magnetic resonance in diamond. *Phys. Rev. Lett.* **104**, (2010).
7. Van Oort, E. & Glasbeek, M. Electric-field-induced modulation of spin echoes of N-V centers in diamond. *Chem. Phys. Lett.* **168**, 529–532 (1990).
8. Schirhagl, R., Chang, K., Loretz, M. & Degen, C. L. Nitrogen-vacancy centers in diamond: nanoscale sensors for physics and biology. *Annu. Rev. Phys. Chem.* **65**, 83–105 (2014).
9. Lam, R. & Ho, D. Nanodiamonds as vehicles for systemic and localized drug delivery. E*xpert Opin. Drug Deliv.* **6**, 883–895 (2009).
10. Alhaddad, A. et al. Influence of the Internalization Pathway on the Efficacy of siRNA Delivery by Cationic Fluorescent Nanodiamonds in the Ewing Sarcoma Cell Model. *PLoS One* **7**, (2012).
11. Fu, C.-C. et al. Characterization and application of single fluorescent nanodiamonds as cellular biomarkers. *Proc. Natl. Acad. Sci. U. S. A.* **104**, 727–732 (2007).
12. Hemelaar, S. R. et al. Nanodiamonds as multi-purpose labels for microscopy. *Sci. Rep.* **7**, 720 (2017).
13. Hemelaar, S. R. et al. The interaction of fluorescent nanodiamond probes with cellular media. *Microchim. Acta* 1–9 (2017). doi:10.1007/s00604-017-2086-6
14. Perevedentseva, E. et al. Nanodiamond internalization in cells and the cell uptake mechanism. *J. Nanoparticle Res.* **15**, (2013).
15. McGuinness, L. P. et al. Quantum measurement and orientation tracking of fluorescent nanodiamonds inside living cells. *Nat. Nanotechnol.* **6**, 358–363 (2011).
16. Chu, Z. et al. Unambiguous observation of shape effects on cellular fate of nanoparticles. *Sci. Rep.* **4**, 4495 (2014).
17. Wu, T.-J. et al. Tracking the engraftment and regenerative capabilities of transplanted lung stem cells using fluorescent nanodiamonds. *Nat. Nanotechnol.* **8**, 682–9 (2013).
18. Hemelaar, S. R. et al. Generally Applicable Transformation Protocols for Fluorescent Nanodiamond Internalization into Cells. *Sci. Rep.* **7**, (2017).
19. Yu, S. J., Kang, M. W., Chang, H. C., Chen, K. M. & Yu, Y. C. Bright fluorescent nanodiamonds: No photobleaching and low cytotoxicity. *J. Am. Chem. Soc.* **127**, 17604–17605 (2005).
20. Lien, Z.-Y. et al. Cancer cell labeling and tracking using fluorescent and magnetic nanodiamond. *Biomaterials* **33**, 6172–6185 (2012).

21. Paget, V. et al. Carboxylated nanodiamonds are neither cytotoxic nor genotoxic on liver, kidney, intestine and lung human cell lines. *Nanotoxicology* **8**, 46–56 (2014).
22. Vaijayanthimala, V. et al. The long-term stability and biocompatibility of fluorescent nanodiamond as an in vivo contrast agent. *Biomaterials* **33**, 7794–7802 (2012).
23. Yuan, Y. et al. Pulmonary toxicity and translocation of nanodiamonds in mice. *Diam. Relat. Mater.* **19**, 291–299 (2010).
24. Rojas, S. et al. Biodistribution of amino-functionalized diamond nanoparticles. in vivo studies based on 18F radionuclide emission. in *ACS Nano* **5**, 5552–5559 (2011).
25. Tsai, L. W. et al. Nanodiamonds for medical applications: Interaction with blood in vitro and in vivo. *Int. J. Mol. Sci.* **17**, (2016).
26. Zhang, X. et al. Biodistribution and toxicity of nanodiamonds in mice after intratracheal instillation. *Toxicol. Lett.* **198**, 237–243 (2010).
27. Moore, L. et al. Biocompatibility Assessment of Detonation Nanodiamond in Non-Human Primates and Rats Using Histological, Hematologic, and Urine Analysis. *ACS Nano* **10**, 7385–7400 (2016).
28. Solarska, K., Gajewska, A., Kaczorowski, W., Bartosz, G. & Mitura, K. Effect of nanodiamond powders on the viability and production of reactive oxygen and nitrogen species by human endothelial cells. *Diam. Relat. Mater.* **21**, 107–113 (2012).
29. Lim, D. G. et al. Comprehensive evaluation of carboxylated nanodiamond as a topical drug delivery system. *Int. J. Nanomedicine* **11**, 2381–2395 (2016).
30. Liu, K.-K. et al. Covalent linkage of nanodiamond-paclitaxel for drug delivery and cancer therapy. *Nanotechnology* **21**, 315106 (2010).
31. Chow, E. K. et al. Nanodiamond therapeutic delivery agents mediate enhanced chemoresistant tumor treatment. *Sci. Transl. Med.* **3**, 73ra21 (2011).
32. Thomas, V., Halloran, B. A., Ambalavanan, N., Catledge, S. A. & Vohra, Y. K. In vitro studies on the effect of particle size on macrophage responses to nanodiamond wear debris. *Acta Biomater.* **8**, 1939–1947 (2012).
33. Moore, L. et al. Comprehensive interrogation of the cellular response to fluorescent, detonation and functionalized nanodiamonds. *Nanoscale* **6**, 11712–21 (2014).
34. Huang, Y.-A. et al. The effect of fluorescent nanodiamonds on neuronal survival and morphogenesis. *Sci. Rep.* **4**, 6919 (2014).
35. Diplock, a T. et al. Functional food science and defence against reactive oxidative species. *Br. J. Nutr.* **80** Suppl 1, S77–S112 (1998).
36. Mohan, N., Chen, C. S., Hsieh, H. H., Wu, Y. C. & Chang, H. C. In vivo imaging and toxicity assessments of fluorescent nanodiamonds in caenorhabditis elegans. *Nano Lett.* **10**, 3692–3699 (2010).
37. Torrano, A. a et al. A fast analysis method to quantify nanoparticle uptake on a single cell level. *Nanomedicine* **8**, 1815–1828 (2013).
38. Nargi, F. E. & Yang, T. J. Optimization of the L-M cell bioassay for quantitating tumor necrosis factor in serum and plasma. *J. Immunol. Methods* **159**, 81–91 (1993).
39. Livak, K. J. & Schmittgen, T. D. Analysis of Relative Gene Expression Data Using Real-Time Quantitative PCR and the 2−ΔΔCT Method. *Methods* **25**, 402–408 (2001).
40. Laemmli, U. K. Cleavage of structural proteins during the assembly of the head of bacteriophage T4. *Nature* **227**, 680–685 (1970).
41. Ong, S. Y., Chipaux, M., Nagl, A. & Schirhagl, R. Shape and crystallographic orientation

of nanodiamonds for quantum sensing. *Phys. Chem. Chem. Phys.* (2017). doi:10.1039/C6CP07431F

42. Posakony, J. W., England, J. M. & Attardi, G. Mitochondrial growth and division during the cell cycle in HeLa cells. *J. Cell Biol.* **74**, 468–91 (1977).
43. Jersmann, H. P., Rathjen, D. A. & Ferrante, A. Enhancement of lipopolysaccharide-induced neutrophil oxygen radical production by tumor necrosis factor alpha. *Infect. Immun.* **66**, 1744–1747 (1998).
44. Pelka, J. et al. Cellular uptake of platinum nanoparticles in human colon carcinoma cells and their impact on cellular redox systems and DNA integrity. *Chem. Res. Toxicol.* **22**, 649–659 (2009).
45. Lake, M. P. & Bouchard, L. S. Targeted nanodiamonds for identification of subcellular protein assemblies in mammalian cells. *PLoS One* **12**, (2017).
46. Chan, M. S., Liu, L. S., Leung, H. M. & Lo, P. K. Cancer-Cell-Specific Mitochondria-Targeted Drug Delivery by Dual-Ligand-Functionalized Nanodiamonds Circumvent Drug Resistance. *ACS Appl. Mater. Interfaces* **9**, 11780–11789 (2017).
47. Van der Laan, K., Hasani, M., Zheng, T. & Schirhagl, R. Nanodiamonds for In Vivo Applications. *Small* (2018). doi:10.1002/smll.201703838
48. Gupta, C., Prakash, D. & Gupta, S. Cancer treatment with nano-diamonds. *Front. Biosci. Sch.* **9**, 62–70 (2017).
49. Ho, D., Wang, C.-H. K. & Chow, E. K.-H. Nanodiamonds: The intersection of nanotechnology, drug development, and personalized medicine. *Sci. Adv.* **1**, e1500439 (2015).
50. Augustine, S. et al. Recent advances in carbon based nanosystems for cancer theranostics. *Biomater. Sci.* **5**, 901–952 (2017).
51. Hou, W. et al. Nanodiamond–Manganese dual mode MRI contrast agents for enhanced liver tumor detection. *Nanomedicine Nanotechnology, Biol. Med.* **13**, 783–793 (2017).
52. Manus, L. M. et al. Gd(III)-nanodiamond conjugates for MRI contrast enhancement. *Nano Lett.* **10**, 484–489 (2010).
53. Kuo, Y., Hsu, T. Y., Wu, Y. C. & Chang, H. C. Fluorescent nanodiamond as a probe for the intercellular transport ofproteins invivo. *Biomaterials* **34**, 8352–8360 (2013).

Supplementary information

Supplementary Table 1. Antibodies

Antibody	Abbreviation	Dilution	Manufacturer + *reference*	Size	Blot
Primary					
αCatalase	CAT	1:1000	Abcam ab16731	60 kDa	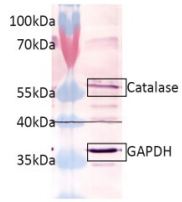
αGlutathion Reductase	GSR	1:1000	Abcam ab16801	58 kDa	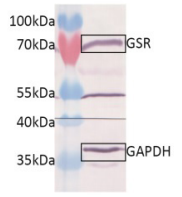
αSuperOxide Dismutase 1	SOD1	1:1000	Santa Cruz Biotechnology *sc-11407*	23 kDa	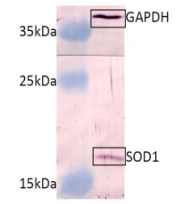
αCaspase-3	CASP	1:1000	Cell Signaling *#9662*	35 kDa	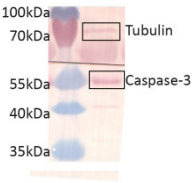
αTubulin	TUB	1:1000	Sigma-Aldrich *T4026*	55 kDa	
αGlyceraldehyde-3-Phosphate DeHydrogenase	GAPDH	1:1000	Abcam *ab9484*	36 kDa	
Secondary					
Mouse αRabbit	MαRb	1:1000	Jackson ImmunoResearch 211-005-109		
Goat αMouse	GαM	1:1000	Jackson ImmunoResearch *115-005-071*		
Tertiary					
Goat αMouse-AP	GαM-AP	1:1000	Bio-Rad *#1706520*		
Rabbit αGoat-AP	RbαG-AP	1:1000	Jackson ImmunoResearch 305-055-046		

Supplementary Table 2. Simplified comparison of Western Blot and qPCR results.

Sample	Catalse		GSR		SOD1		Caspase 3	
	qPCR	Western Blot	qPCR	Western Blot	qPCR	Western Blot	qPCR	Western Blot
10 ug FND_{70}	≈	↑	↓	↓	↓	↓	↓	↑↑
10 µg FND_{70} T=24	≈	≈	≈	↑	↓	↑↑	≈	↓
1 µg FND_{70}	↓	↑	↓	↓	↓	≈	↓	↑
1 µg FND_{70} T=24	≈	↓	≈	≈	≈	↑	≈	↓
0.1 µg FND_{70}	↓	↑	↓	↓	↓↓	≈	↓	≈
0.1 µg FND_{70} T=24	↓	↓	↓	≈	↓	↑	≈	↓
1mM H_2O_2	≈	≈	↓	↓	↓	≈	↓	↑
1mM H_2O_2 T=24	↓	↑↑	↓	↑↑	↓	↑	≈	↓↓
200µM H_2O_2	≈	≈	↓	↓	↓	≈	↑	≈
200µM H_2O_2 T=24	≈	↓	≈	≈	≈	≈	≈	↓
40µM H_2O_2	≈	≈	≈	↓	↓	≈	≈	≈
40µM H_2O_2 T=24	≈	↓	≈	↑	≈	≈	↑	↓
1 µg FND_{120}	≈	↑↑	≈	≈	↓	≈	↓	≈
1 µg FND_{40}	≈	≈	↑	≈	↑	≈	↑	↑
1 µg FND_{70} aggregated	≈	≈	≈	≈	↑	↑	≈	↑
1 µg rounded FNDs	≈	≈	≈	≈	≈	↑↑	≈	↑↑

↑↑ reflects a higher than 0.75% increase, ↑ reflects a 0.25 to 0.75 % increase, ≈ reflects a similar comparison 0.25% to -0.25%, ↓ reflects a -0.25% to -0.75% decrease, ↓↓ reflects a bigger than -0.75% decrease.

0.1 µg FND 70nm

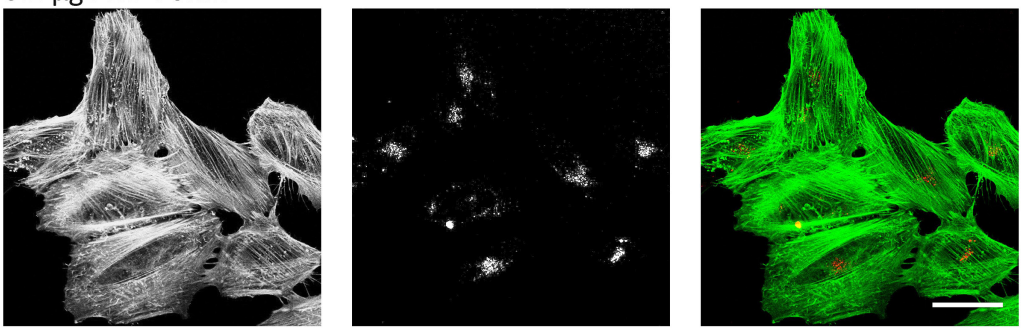

0.1 µg FND 70nm T=24

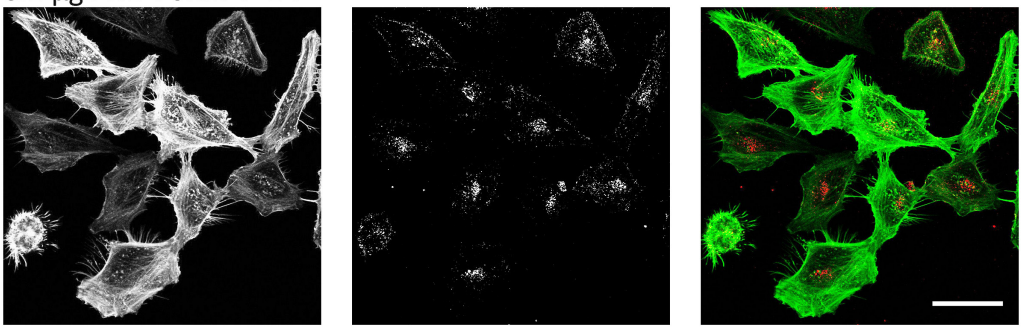

1 µg FND 70nm

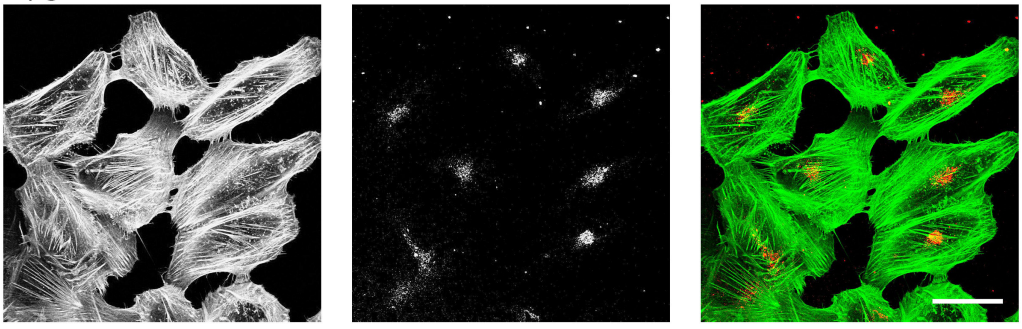

1 µg FND 70nm T=24

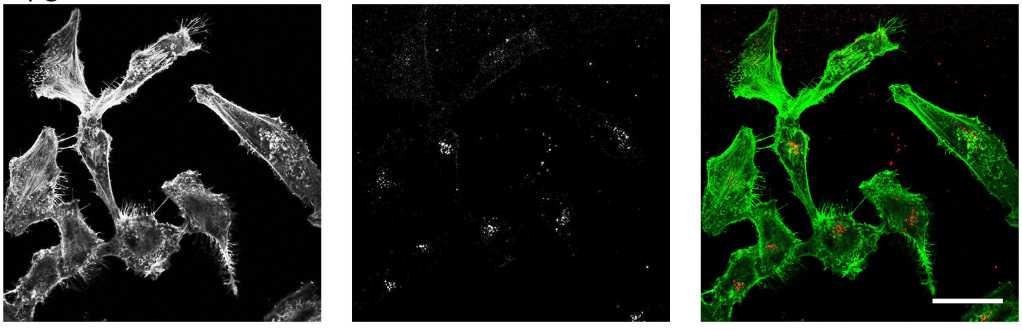

10 µg FND 70nm

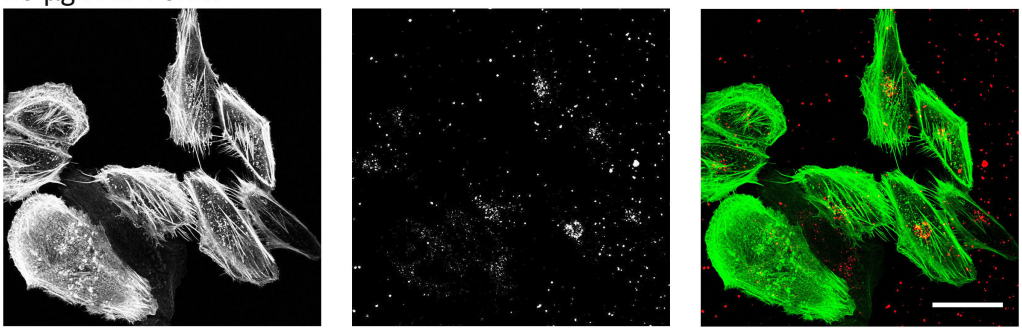

10 µg FND 70nm T=24

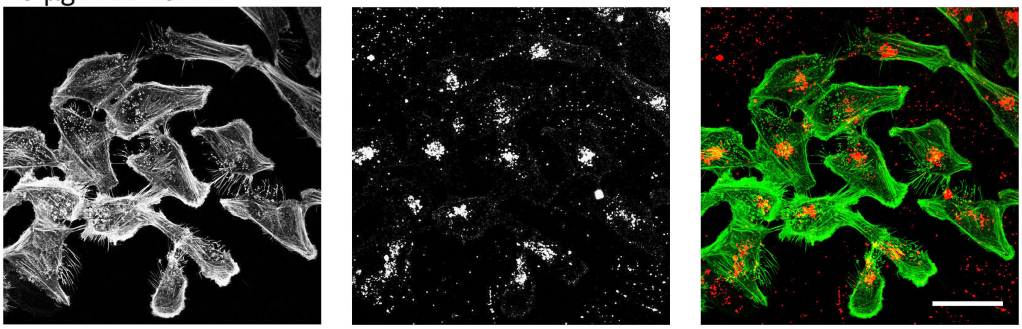

1 µg aggregated FND 70nm

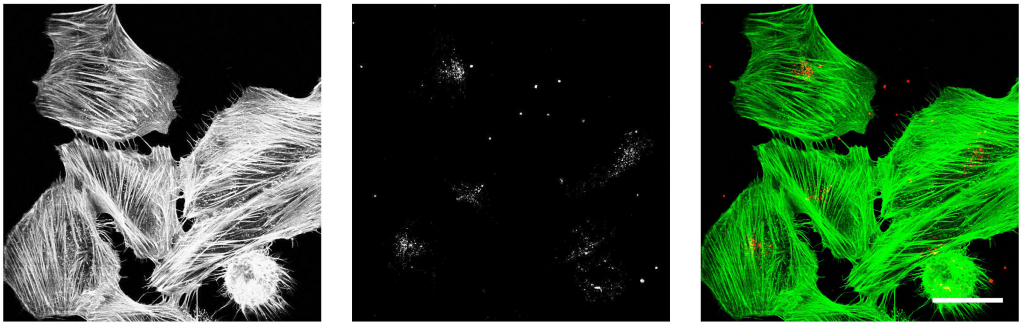

1 µg rounded FNDs

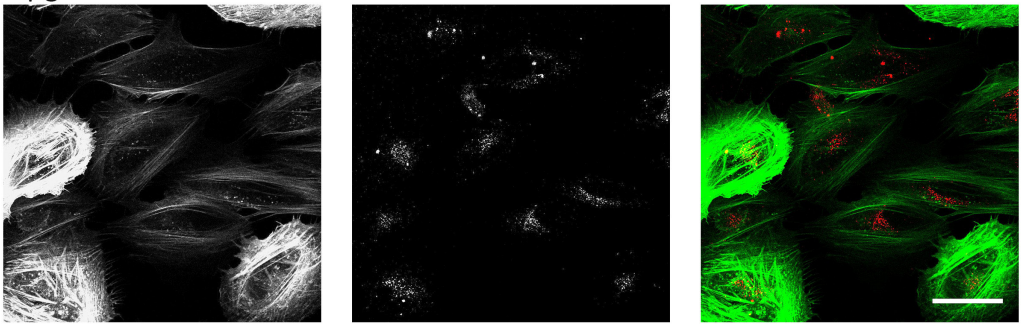

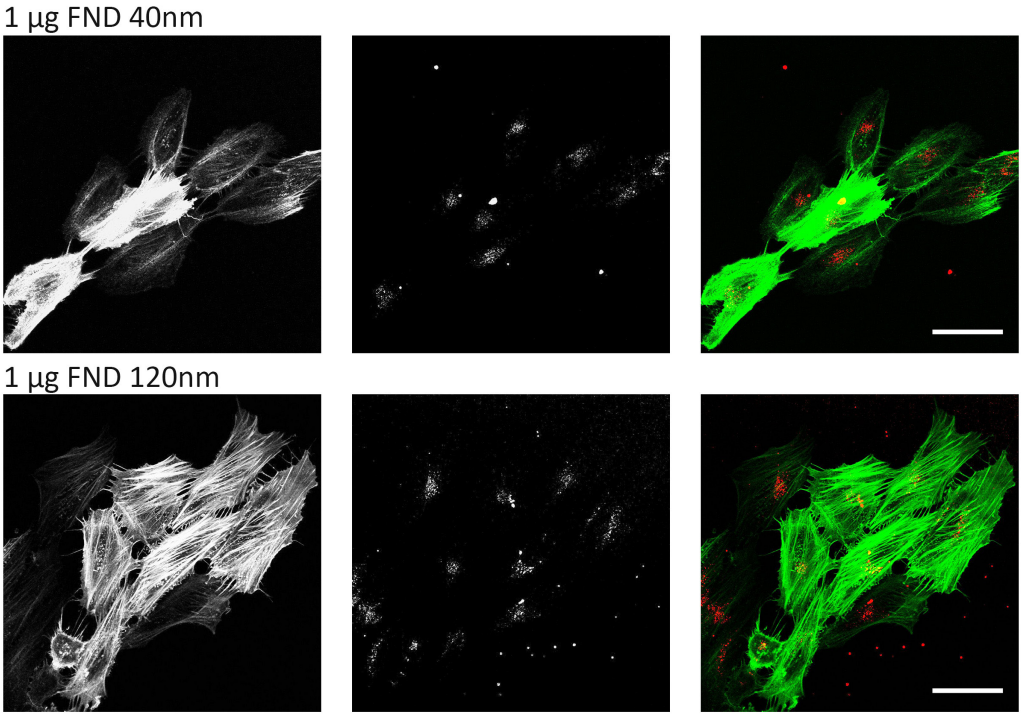

Supplementary Figure 1. Confocal images of HeLa cells used for particle and object counting. Each horizontal line of panels represents one condition, the condition is listed on top of the left image. All images are cross sections at the base of the HeLa cells. Left images are a greyscale of the signal coming from FITC-Phalloidin, which labels the actin cytoskeleton. The center images present the signal of FNDs, also in grey scale. In the right images, an overlay is made from both the FITC signal (in green) and the FND signal in red. The scale bar represents 50µm.

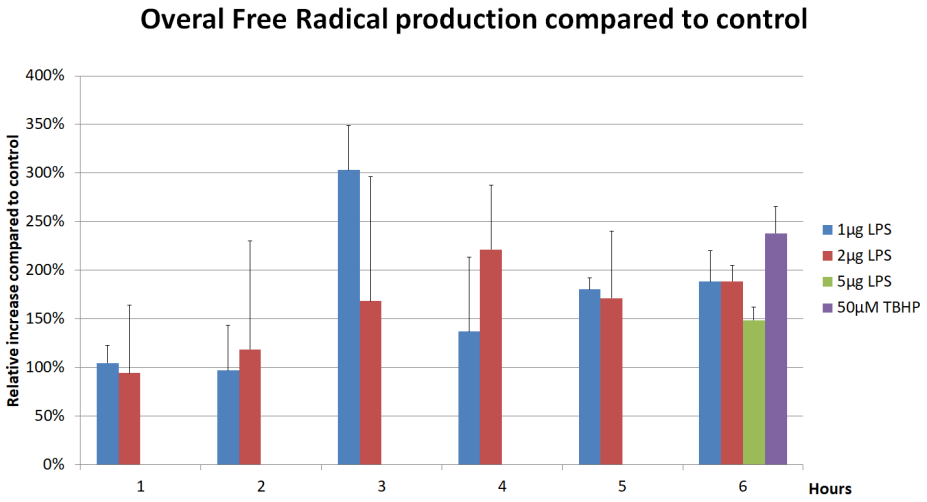

Supplementary Figure 2. Overall free radical production after stimulation using LPS. In order to test how big the increase of free radical production after stimulation with LPS was, we incubated HeLa cells with DCFDA and stimulated them with different concentrations of LPS for different amounts of time. Then we measured the generated fluorescent signal with an FLUOstar Omega Microplate Reader and related the signal to a non-stimulated control. This gave values of fold increase, which are expressed in percentages. As a positive control we used 50 µM TBHP, provided by the manufacturer of the DCFDA kit. Although the free radical production was increased after LPS stimulation, this difference was not nearly as big as when we stimulated the cells using hydrogen peroxide. Because of this the genetic and protein differences will be smaller to see and more difficult to relate. Therefore we chose to stick with H_2O_2 as a stimulant. Error bars show the standard deviation.

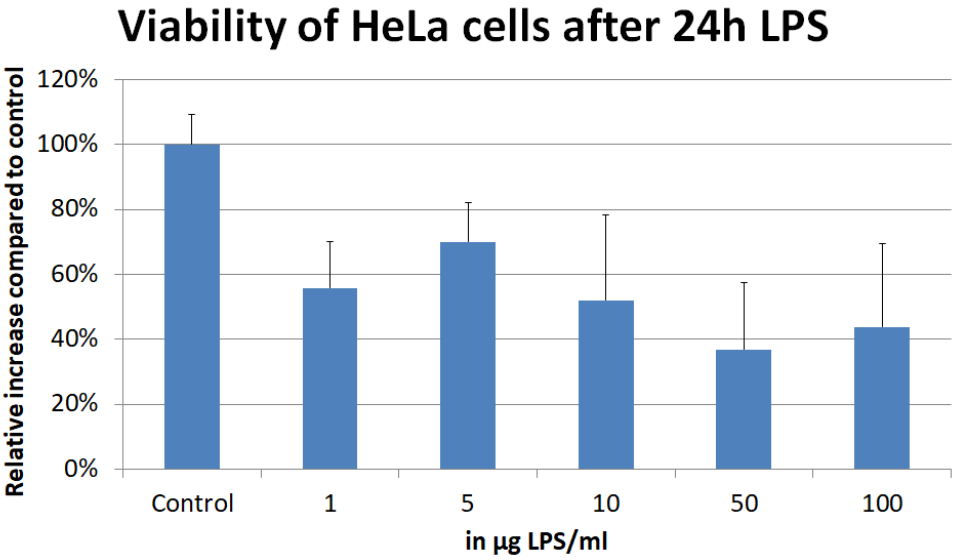

Supplementary Figure 3. Viability of HeLa cells after 24h stimulation using different concentrations of LPS. We stimulated HeLa cells for 24 hours using LPS to see what was the effect on the viability of HeLa cells. Even at low concentrations of 1µg LPS / ml the cellular viability was reduced by half. This rendered a time as long as 24 hours not viable for LPS experiments. Error bars show the standard deviation.

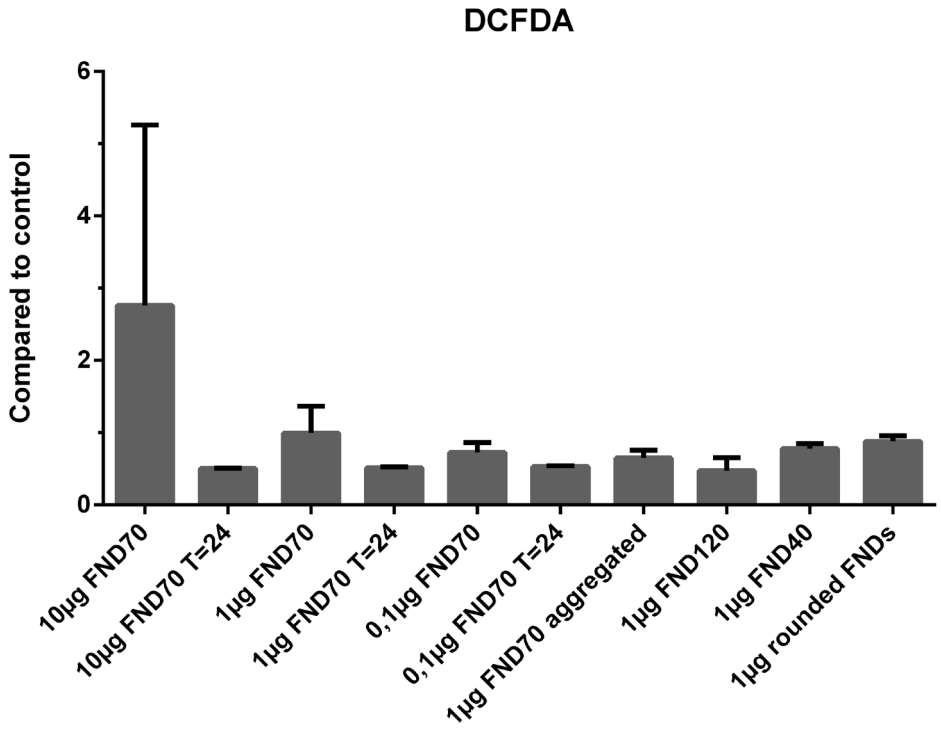

Supplementary Figure 4. Mean free radical production of nanodiamonds. A close up of Figure 4 shows a more detailed overview of the (non-significant) changes to total free radical production in HeLa cells. Error bars show the standard deviation.

Supplementary Table 3. Summary of morphological differences.

	Protrusions	Uneven filament distribution	Rounding of cells	Blebbing	Other
Control T=0	1%	0%	2%	0%	7%
Control T=24	2%	7%	2%	0%	1%
Control T=48	2%	1%	3%	0%	1%
0.1µg FND_{70} T=0	0%	0%	0%	0%	5%
0.1µg FND_{70} T=24	0%	0%	0%	0%	2%
0.1µg FND_{70} T=48	2%	0%	1%	0%	3%
1µg FND_{70} T=0	0%	0%	0%	0%	3%
1µg FND_{70} T=24	1%	1%	1%	0%	2%
1µg FND_{70} T=48	0%	2%	2%	0%	1%
10µg FND_{70} T=0	0%	4%	4%	0%	9%
10µg FND_{70} T=24	0%	0%	0%	0%	1%
10µg FND_{70} T=48	2%	2%	0%	0%	0%

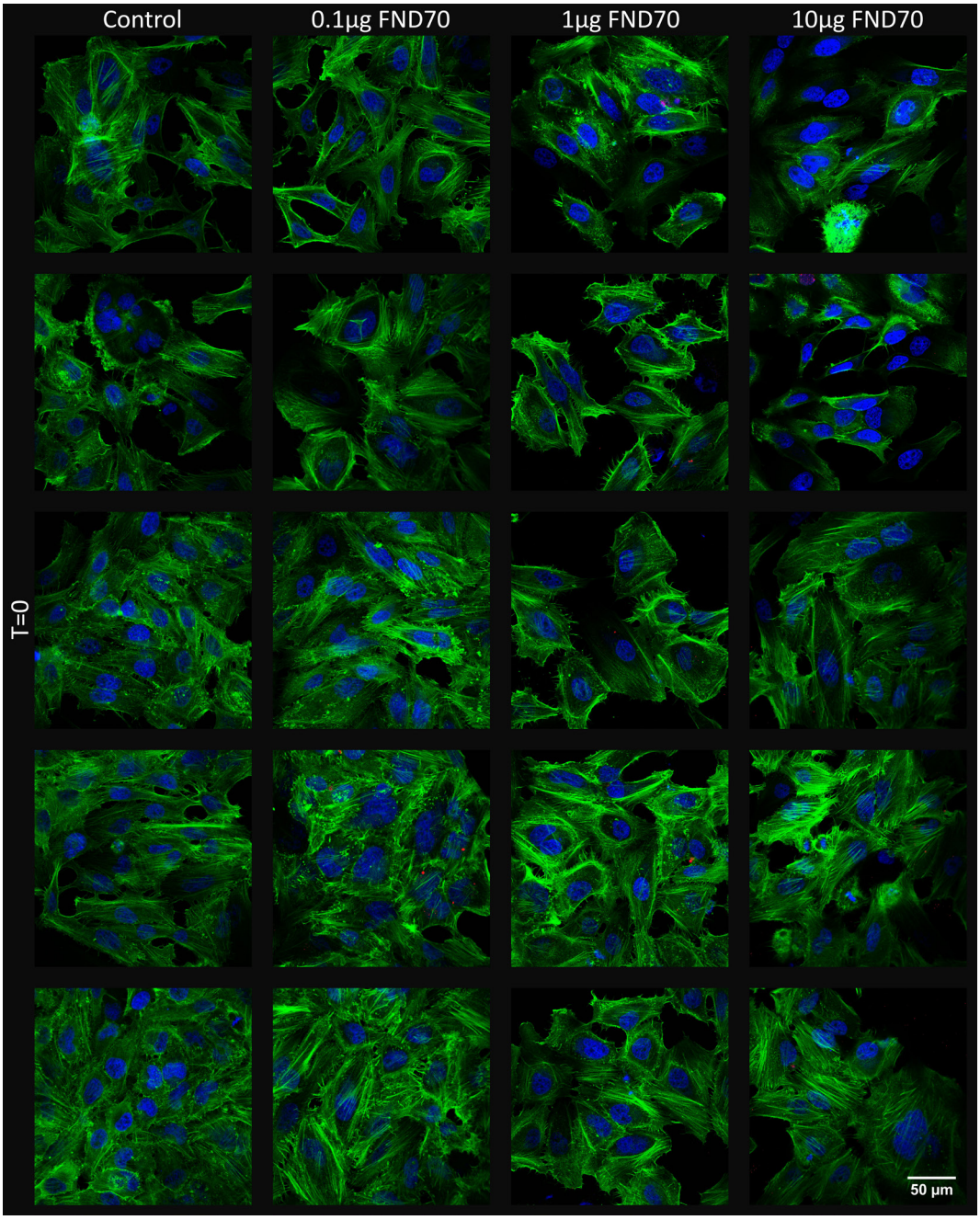
Control
0.1µg FND70
1µg FND70
10µg FND70
T=0
50 µm

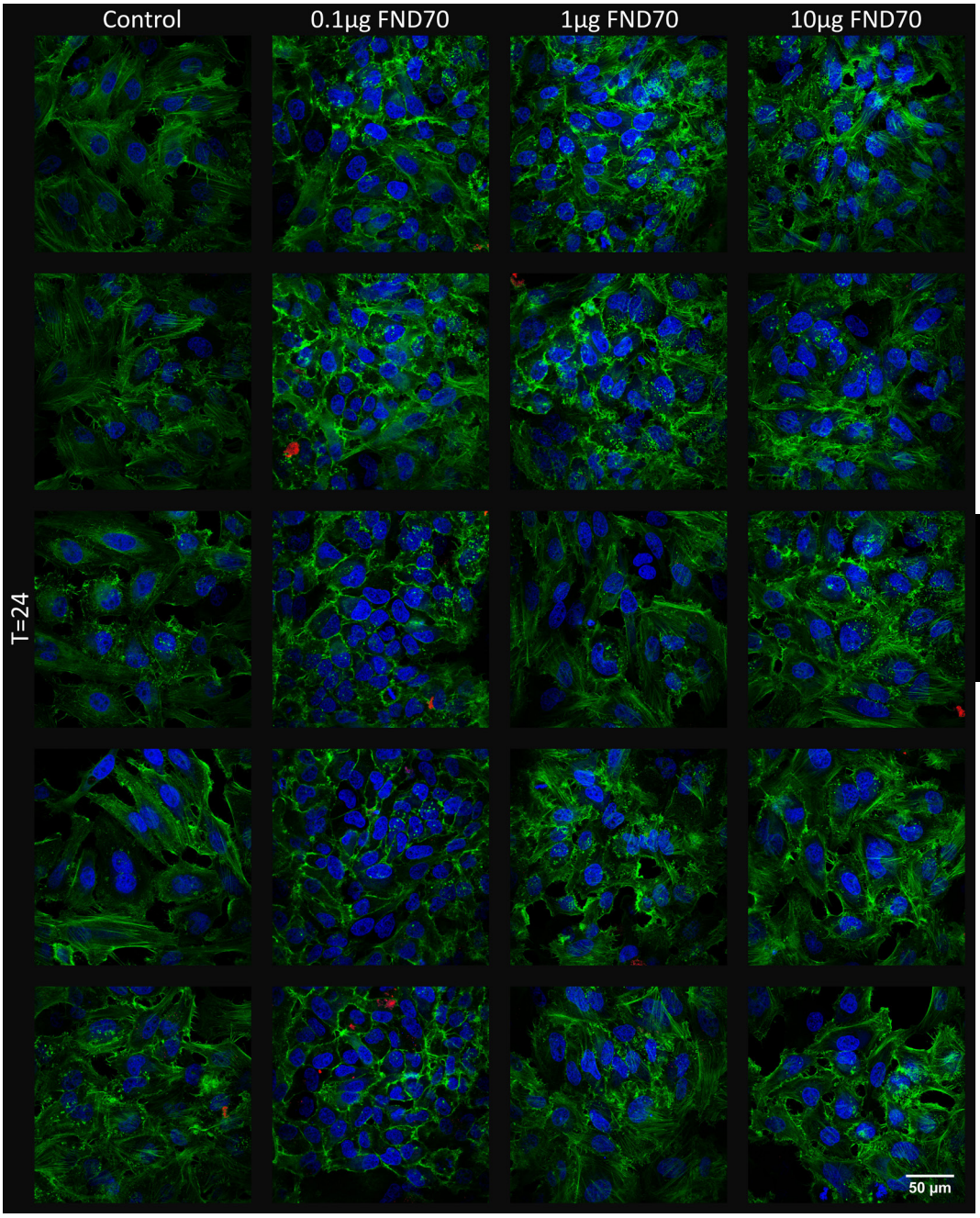
Control
0.1µg FND70
1µg FND70
10µg FND70
T=24
50 µm

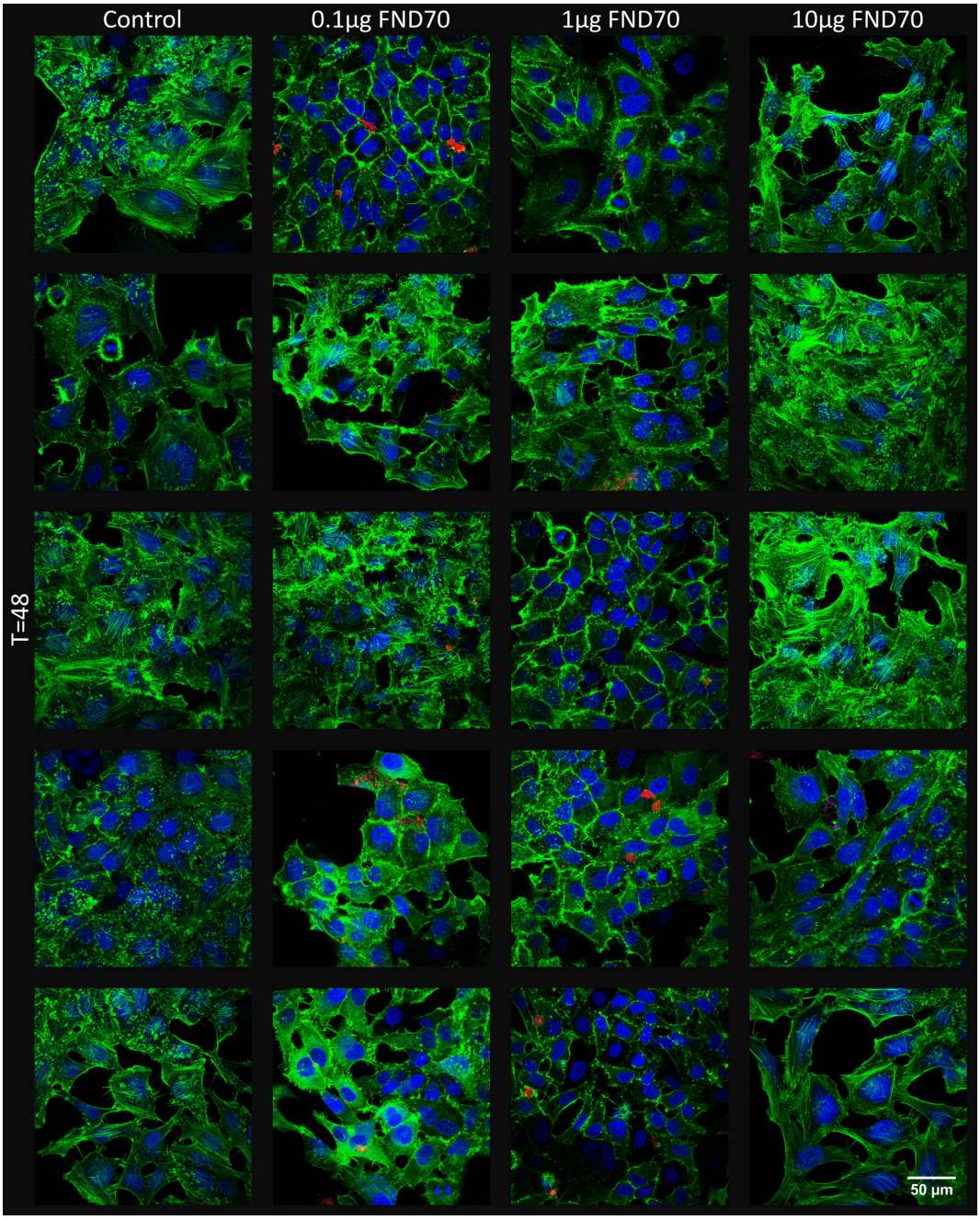
Control
0.1µg FND70
1µg FND70
10µg FND70
T=48
50 µm

Supplementary Figure 5 (previous pages). Morphological comparison between different concentrations of FND_{70} directly after uptake, 24 hours after uptake and 48 hours after uptake. After incubation of HeLa cells with different concentrations of FND_{70}, we either immediately fixed the cells in 3.7% PFA or we incubated them for 24 or 48 hours more with supplemented DMEM medium and then fixed them. The resulting samples were stained with phalloidin-FITC and DAPI and imaged using a ZEIS LSM780 microscope. Of each sample 5 pictures were made to obtain enough cells to count. If available, samples from Supplementary Figure 1 were also taken into account. The scale bar represents 50µm and is the same for all images. The results are summarized in Supplementary Table 3 and can be seen as an estimation of the effect of nanodiamonds on the cytoskeletal morphology of the cells. The term 'other' refers to cells which don't look normal but are not specified further. Sometimes this might also refer to cells in mitosis. The other morphological changes are indicators of an early onset of apoptosis.[1] Although some samples show early signs of apoptosis, this can also be found in the control sample, therefore we attribute this to a natural variation.

References

1. Taylor, R. C., Cullen, S. P. & Martin, S. J. Apoptosis: Controlled demolition at the cellular level. *Nature Reviews Molecular Cell Biology* **9,** 231–241 (2008).

Intracellular targeting and tracking of fluorescent nanodiamonds

Simon R. Hemelaar[1], Alina Sigaeva[1], Linyan Nie[1], Thamir Hamoh[1], Anggrek C. Nusantara[1], Felipe P. Perona Martinez[1], Mayeul Chipaux[1], Charles A. Mignon[1] & Romana Schirhagl[1]

[1]Department of Biomedical Engineering, University Medical Center Groningen, The Netherlands.

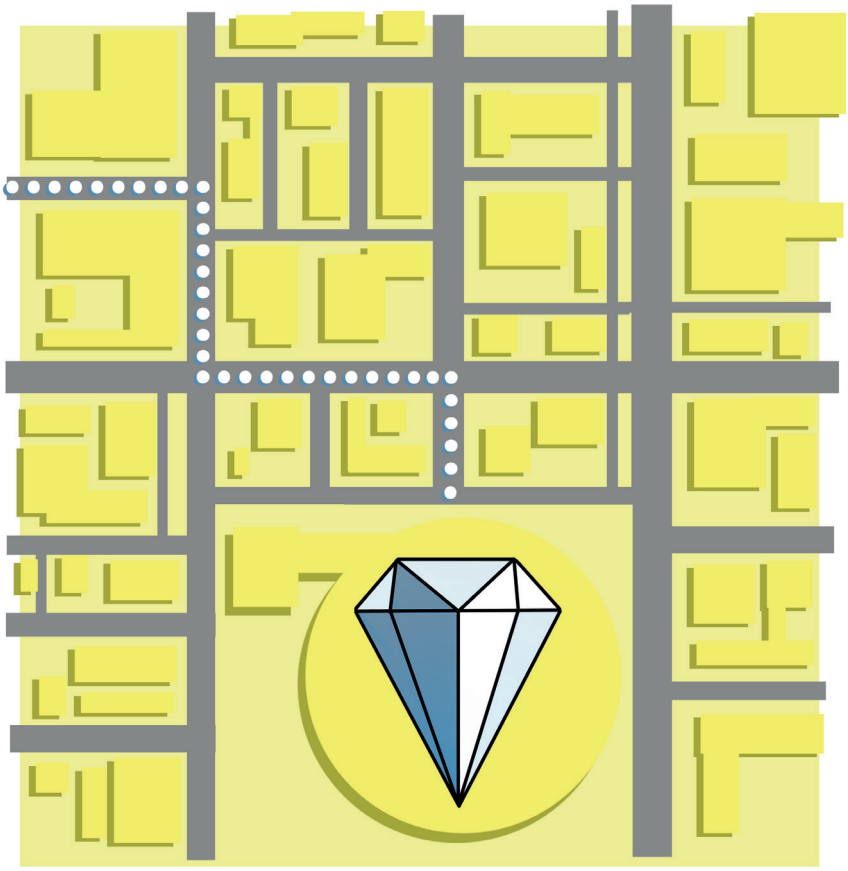

"Navigating the route to the center with Diamond Maps"

Abstract

Fluorescent nanodiamonds are versatile tools, which can be employed as perfectly photostable labels as well as for intracellular sensing of a wide array of forces and chemical products due to their fluorescent nitrogen vacancy center. Since these sensors only probe their environment within a few nanometers it is absolutely essential to control their location. To achieve this goal we have analyzed both adsorption and covalent attachment of antibodies on the surface of fluorescent nanodiamonds as modification for targeting the particle toward the nucleus of HeLa cells. We measured the efficiency of targeting between traditional immunostaining techniques and diamond-antibody conjugates by comparing the distance between the particle and the nucleus of the cell. We also compared targeting between living and fixed cells, using the measured distances. In addition, we tracked nanodiamonds inside living HeLa cells and were able to produce 3D trajectories. From these trajectories, we extracted the mean square displacement, the mode of diffusion of a particle and segment specific parameters. We show that in fixed HeLa cells, covalent attachment of antibodies to the nanodiamond surface is the most promising approach for nuclear targeting. In living HeLa cells, we see that even after long times of incubation primary antibodies can still be identified and show no signs of degradation in the cytoplasm. We are also able to successfully target the nucleus using diamonds with adsorbed antibodies in 24-hour incubation experiments. Finally, we discuss the relevance of our findings, the importance of the tracking method and give suggestions for future experiments.

Introduction

In the field of nanosensing, fluorescent nanodiamonds (FNDs) have attracted attention owing of their outstanding fluorescent and magnetosensitive properties.[1] The internal Nitrogen Vancancy (NV) center is sensitive to changes of the environment in strain,[2] temperature[3] and magnetic or electric fields.[4,5] In addition, the fluorescence of the NV center does not bleach or blink, making it ideal for long term labelling and imaging.[6] Diamond particles themselves are biocompatible[8] and non-genotoxic.[9] They have been tested extensively in cells[10] and in organisms[11] and only very high concentrations of diamonds can have a toxic influence. Ultimately these properties make the fluorescent nanodiamond particle extremely suitable for the intracellular sensing of chemical products or physical parameters. Pristine FNDs enter cells via the endosomal pathway and eventually escape the endosomes.[12] However, this means that if the location is not controlled, sensing and labelling is limited to these locations.

To use fluorescent nanodiamonds for the above mentioned applications the diamond probe has to be close to the molecule or cellular structure of interest. This requires the targeting of diamond particles to specific regions inside the cell. To control the location of diamonds, Chan et al. conjugated diamonds to a Mitochondria Leader Sequence (MLS) peptide and to folic acid to target the diamond towards mitochondria and cancer cells, respectively.[13] Lake and Bouchard used detonation nanodiamonds conjugated to an antibody against Nup98, a component of the nuclear pore.[14] Using TEM images they were able to quantify the number of diamonds and also analyze the distance between the nuclear pore and the diamond as an indicator of successful targeting. However, these detonation nanodiamonds do not have the desired optical properties of FNDs, are much smaller and chemically different. Recently, Bray and colleagues qualitatively showed that they were able to target FNDs toward the nucleus using trans-activating transcriptional activator peptides, which gives the molecule a positive charge. They have elegantly shown the targeting of different diamonds with different fluorescent defects but have not quantitatively assessed these approaches yet.[15]

A big dispute in the field concerns the best way of attaching molecules to diamonds. Some groups conjugate nanodiamonds covalently, which includes several chemical steps to bind the targeting molecules on the surface of the nanodiamond particle. This is time consuming, expensive and often requires an elaborate fine-tuning process. Other groups utilise simple adsorption of molecules on the surface. This has already proven to prevent aggregation[16] and allow for extracellular targeting.[17,18] So an important question we want to answer is, if or when the more elaborate covalent binding is indeed necessary and beneficial or if simple adsorption is enough? In the intracellular environment other forces and proteolytic enzymes play a role. The stability of a nanodiamond-antibody conjugate may differ between the inside and outside of a cell. And even if the conjugate resists the destructive forces of the cell, will it still be able to target its structure of interest?

In this research we have for the first time compared the targeting efficiency of adsorbed antibodies on fluorescent nanodiamonds with that of covalently bound antibody-nanodiamond conjugates in targeting the cellular nucleus (**Figure 1**). By using conventional confocal microscopy we could quantify the relative amount of nanodiamonds, targeted toward the nucleus of the cell. We produced a software protocol to extract displacement and velocity data of moving particles inside HeLa cells and relate these to the quality of the targeting. Ultimately we show successful targeting using adsorbed antibodies on diamonds in living HeLa cells and we give suggestions for future experiments, which involve targeting using adsorbed and covalently bound antibodies on fluorescent nanodiamonds.

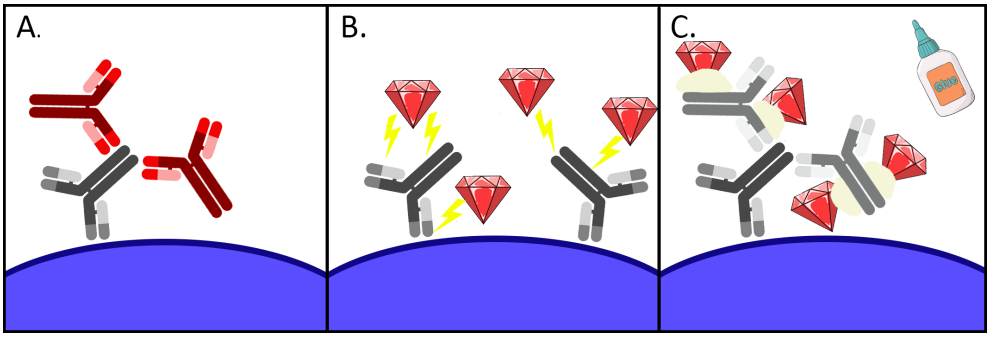

Figure 1. Representation of immunochemical staining of cell structures. A. Traditional immunological staining in which a primary antibody is used to identify a structure of interest, the blue membrane, representing the nucleus of the cell. Then a secondary antibody, raised against the species of the first antibody, is used to visualize the primary target with a fluorescent label. **B.** Successful adsorption of fluorescent nanodiamonds on primary antibodies will also lead to identification of the structure of interest. **C.** Fluorescent nanodiamonds covalently bound to secondary antibodies lead to the identification of the primary antibody and hence can visualize the structure of interest. In this research covalent attachment was done by using EDC and NHS linkers.

Materials and Methods

Materials

For our adsorption assays, we used 70nm FNDs from Adámas Nanotechnologies (ND-NV-70, NC, USA). These diamonds are produced by the grinding down of larger HPHT diamonds and contain approximately 300 nitrogen vacancies per particle. They have a carboxylated surface due to cleaning with oxidizing acids. Anti-Nuclear Pore Complex Proteins (αNPC) antibody was purchased from from Abcam (Cambridge, UK). As a positive control for the αNPC we used Rhodamine Red™-X (RRX) AffiniPure Goat Anti-Mouse IgG (Jackson ImmunoResearch, PA, USA). Goat Anti-Mouse IgG FND (abbreviated as FNDαM) was obtained from FND BIOTECH (Taipei City, Taiwan) which were conjugated following the method as previously described.[18] To summarize, they activated the carboxyl groups on the surface of the FND with EDC and NHS, which generates amine-reactive terminus groups. It is further activated using carboxyl PEG amines which ultimately results in covalent coupling between the PEG carboxyl groups and the amine groups on the secondary antibody. For transfection of cells

we used branched polyethylenimine, 25kDa (PEI, Sigma-Aldrich, Zwijndrecht, the Netherlands).

Cell culture

HeLa cells were cultured under standard culturing conditions until the moment of the experiment in DMEM complete medium, consisting of Dulbecco's Modified Eagle Medium with 4500 mg/L glucose (DMEM-HG), supplemented with 10% Foetal Bovine Serum (FBS), 1% Penicillin/ streptomycin and 1% Glutamax (Gibco, ThermoFisher Scientific, Etten-Leur, The Netherlands) at 37°C, 5% CO_2. For experimental conditions, cells were grown in glass bottom CELLview™ cell culture dishes (Greiner Bio-One B.V., Alpen aan den Rijn, the Netherlands) until approximately 60-90% confluency on the day of the experiment.

Selection of primary antibody

To analyze the success rate of targeting using antibodies, we chose to direct the fluorescent nanodiamonds towards the nucleus. The cellular nucleus is easily recognizable using bright field or differential interference contrast (DIC) microscopy, without the need of secondary staining. In addition, potential targets have their mechanism of action in or near the nucleus. These products, such as free radical species, lead to DNA damage and thus play a crucial role in cancer and could be detected using the nitrogen vacancy center. Therefore we chose to use an antibody called αNPC against a nucleoporin protein of the Nup84/Nup107 family, which is located on the cytoplasmic side of the nucleus and hence should therefore be accessible by cytoplasmic diamond particles.

Fixed cell staining

In order to evaluate the correct binding of the αNPC antibody to the nuclear pore proteins, we evaluated different concentrations of the antibody followed by visualization using a Red-X labeled anti-mouse antibody. In parallel we tested the efficiency of adsorbed antibodies on FNDs and covalently bound anti-mouse FNDs. After the HeLa cells have reached the desired confluency, cells were fixed using 3.7% PFA for 15 minutes. The cells were then permeabilized using 0.5% Triton in PBS (Phosphate Buffered Saline) and consequently blocked with 5% Bovine Serum Albumin in Phosphate Buffered Saline (PBSA). The cells which were incubated with adsorbed αNPC on diamonds were not blocked to maximize the chance of successful labeling. After blocking, the cells were incubated with either αNPC for 1 hour in 1% PBSA or for various times with the adsorbed αNPC-FNDs and afterwards washed according to the final washing steps. Next the cells were washed three times in 1% PBSA and incubated with either Goat anti-Mouse Red-X for 1 hour or FNDαM for various times. Then the samples were finally washed twice in 1% PBSA and once in PBS. Afterwards they were stored in 1% PFA to optimally preserve the cellular ultrastructure until microscopic analysis. These protocols are summarized in **Table 1**.

Table 1. Summarized fixed cell protocol

Sample	Blocking?	1st step	Time	2nd step	Time
Reference	Yes	αNPC	1 hour	Goat anti-mouse Red-X	1 hour
αNPC adsorbed FNDs	No	αNPC-FNDs	Various	N/A	N/A
Anti-mouse covalent FNDs	Yes	αNPC	1 hour	FNDαM	Various

Nuclear targeting in living cells

αNPC-FNDs incubation
HeLa cells were grown in DMEM complete medium in quartered glass bottom CELLview™ cell culture dishes. We first optimized the time and concentration for incubation with αNPC antibodies by fixation and staining with Goat anti-Mouse Red-X (following the protocol as described above) after various conditions. Next we incubated the cells with adsorbed αNPC-FNDs, the theory behind this being that the adsorption could be strong enough to keep the antibody diamond coagulate together in the cell, while the sharp shape of the diamond may even help it to escape the endosome and thereby achieve successful targeting. This experiment was performed for different durations and ratios between the amount of diamond and antibody.

αNPC-FND transfection using polyethylenimine
Branched polyethylenimine was used to increase the amount of the adsorbed αNPC-FNDs, as PEI is known to increase the uptake of nanoparticles.[19] Therefore, the diamond (2 µg) and / or antibody (1.6 µg) was mixed with PEI (0.5 µg) and allowed to interact for 15 minutes. Then, serum free DMEM was added and the resulting mixture was added to the HeLa cells and incubated for 5 hours. Afterwards the sample was fixed in 3.7% PFA for 15 minutes. The sample with only αNPC was stained with Goat anti-Mouse Red-X (as described for fixed cell staining) as a positive control for the functionality of αNPC. Samples were stored in 1% PFA until microscopic analysis.

αNPC and FNDαM incubation
To analyze if we could build a secondary antibody tree inside living cells, we incubated HeLa cells for 6 hours with αNPC (1.6 µg) and added 2 µg FNDαM in 5 µl FBS simultaneously or after the start of αNPC for 5 or 2.5 hours. Then the samples were fixed as described before and stored in 1% PFA until microscopic analysis.

Microscopic analysis

Cells were imaged in a LSM780 Zeiss microscope (Zeiss, Sliedrecht the Netherlands), using a 405 nm laser for a DIC image and a 561 nm laser to detect the signal of the FNDs or the Red-X dye. From all samples DIC and confocal images were produced and Z-stacks were made to get depth information. All samples were produced in the same way and for each sample an image with 4-14 cells could be made. When necessary, new images were taken to avoid images with debris or large aggregates.

Image processing

All confocal images were processed in FIJI 2.0.0 software (https://fiji.sc) using specific plugins. First the images were deconvolved to get more reliable particle locations and a lower background using the 'Diffraction PSF 3D' and 'Iterative Deconvolve 3D' plugins.[20] Next the Z-slice with the largest nuclei surface per cell was identified and an outline of the nuclei and corresponding cells were manually drawn. Of this image a threshold was set to discriminate between background and particles. Within each cell the corresponding particles were identified by the software, and its corresponding area value (the amount of pixels positive after setting the threshold), were calculated. Then a Euclidean Distance Map was made of each nucleus, giving each pixel a value corresponding to the distance in pixels from the nucleus of the cell. If the minimal distance between the internalized particle and the cell nucleus is shorter than 5 pixels or 1.32 µm, the targeting is considered successful. This value was chosen to safely correct for the manual drawing of the nucleus without including particles, which are too far from the nucleus. See also **Figure 2** for an illustration of the process.

Tracking

Tracking the movement of the particles gives us further information on the fate of the diamond particle. If a particle reaches its target, we expect it to be locked in place and show less movement. In our homebuilt confocal setup we use a 532 nm laser together with a bright field image to determine if an FND has entered a cell. After the particle has been manually selected, the software takes a 2×2 µm image of a single optical plane. Based on the Gaussian fitting of the XY intensity profiles of the resulting image, the software calculates the position of the particle's center. Then a 5-µm Z-stack of the center is acquired to determine the Z-axis position of the nanodiamond center. The calculated XYZ coordinates of the center are recorded, and the procedure is repeated continuously for 45 minutes, with each repetition taking approximately 1.8 seconds (total 1500 repetitions). Each individual trajectory is then divided into subtracks, using a "rolling window" of 200 repetitions (approximately 7 minutes).

An MSD curve is calculated for every subtrack, as described by Levi and Gratton.[21] Briefly, the XYZ coordinates of two points on the trajectory, separated by a certain time interval τ, are used to calculate the squared distance between these two points (i.e., the squared displacement of the particle that occurred after τ seconds). Squared displacements are calculated for each possible pair of points that belong to the trajectory and are separated by the same time interval τ. The average of these displacements is called Mean Squared Displacement for a given τ (MSD(τ)). It is a measure of the distance that the particle travels on average during this period of time. By calculating MSD values for the whole possible range of τ, we can obtain a curve that provides an integrated description of the particle's movement both at short-term (~2 seconds) and long-term (up to 45 minutes) time scales. MSD curves are typically calculated for the whole trajectory[22] to get a better statistical estimate

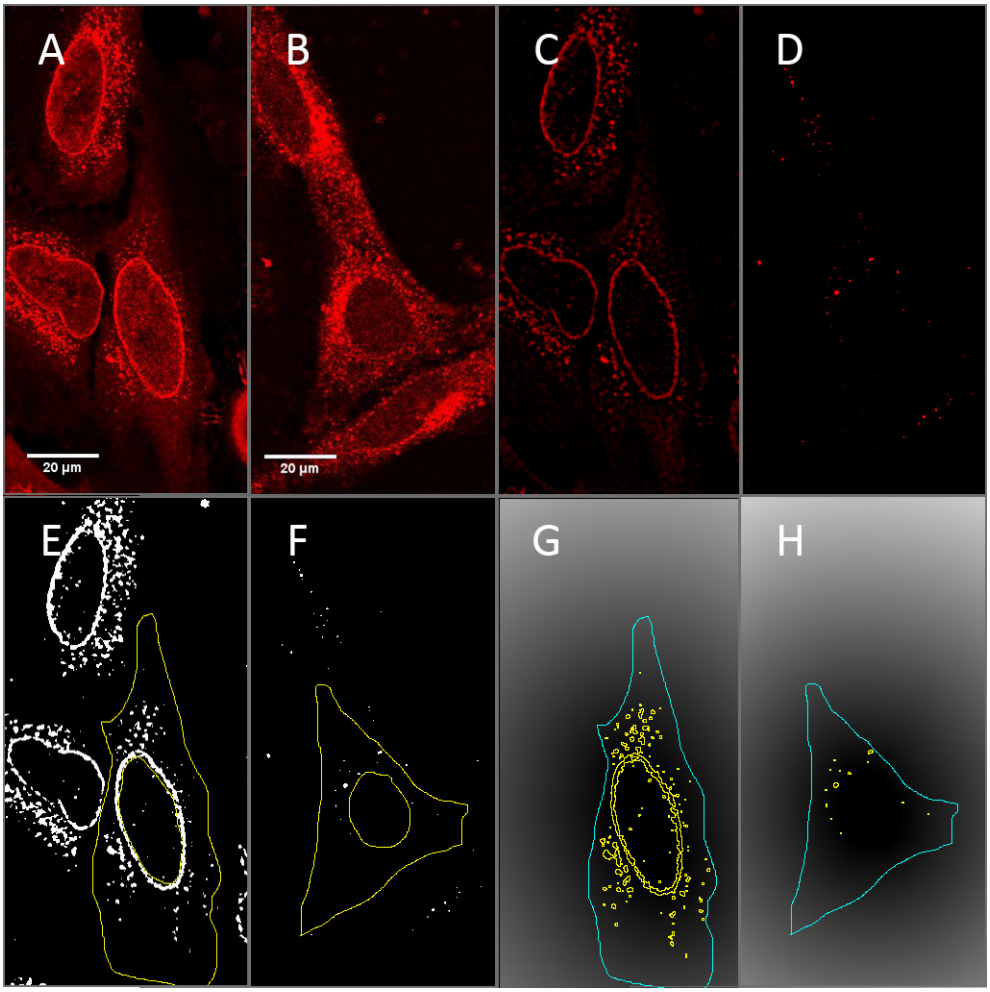

Figure 2. Measuring targeting efficiency through Euclidean Distance Maps. A. Fixed HeLa cells incubated with 320 ng of αNPC antibody, followed by incubation of 2.5 µl Goat Anti-Mouse Red-X. **B.** Living HeLa cells incubated with 1.6 µg αNPC adsorbed on 2 µg FND for 24 hours. From these samples **A** and **B** a Z-stack is made using a confocal Zeiss LSM 780 microscope. The signal from the secondary antibody and the FND can be seen in red. **C** & **D.** The stack is then deconvolved using FIJI software. This improves the contrast and reduces the noise, allowing one to better detect FNDs in the images. **E** & **F.** Next a threshold is set to discriminate between background and particles. The outline of the nucleus and its corresponding cell are drawn and the particles within the cell are identified by the software. **G** & **H.** From the outline of the nucleus a Euclidean Distance Map is generated which gives every pixel a value corresponding to the distance to the nucleus. The distance for each particle is measured. If the distance is below 5 pixels or 1.32 µm from the nucleus, the targeting is considered successful. Scale bars are 20 µm and the same for each image.

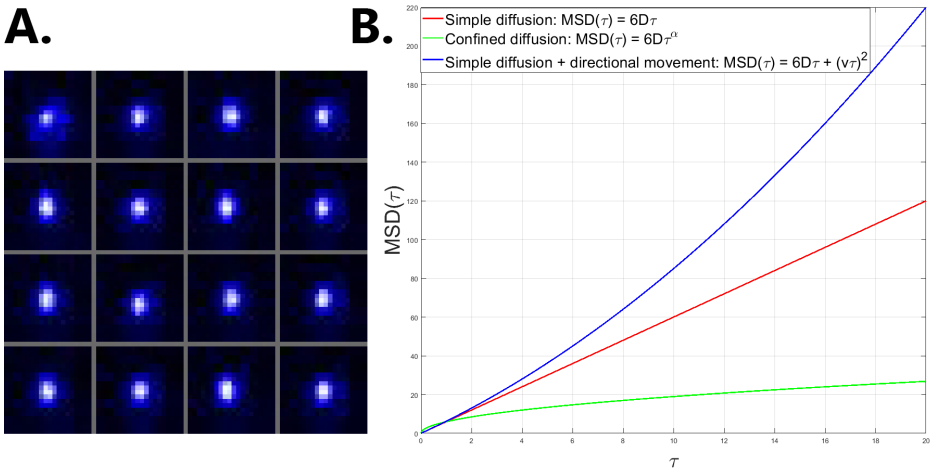

Figure 3. Tracking of intracellular nanodiamonds movement. We have explored the possibilities to employ nanodiamond movement in cells as an indicator of efficient targeting. **A.** A nanodiamond particle is identified in a cell and 2x2x5 μm images are made in which the center of brightness is each time calculated and followed and the XYZ coordinates are stored for each image. This process is repeated 1500 times, here we show the first 16 images of a typical FND. **B.** The resulting set of coordinates can then be used to calculate Mean Squared Displacements (MSD) for different time intervals τ. By fitting the experimental MSD(τ) curve with one of three possible equations, we are able to extract quantitative information on the particle's movement: D, coefficient of simple diffusion; α, the power law exponent, reflecting the confined nature of the diffusion; v, the speed of directional movement. The plot shows 3 theoretical MSD(τ) curves for D = 1, α = 0.5, v = 0.5.

of the particle displacement. However, this approach results in "averaged" curves that are not able to reflect the transitions between different modes of motion, which might occur as the particle travels in the cytoplasm, possibly moving from one compartment to another. Thus, we calculate MSD curves separately for every possible 200-repetitions-long segment of the entire trajectory. To extract the information on the particles' modes of movement, the resulting curves are then fitted with one of the three possible equations (see **Figure 3b)**:

1. Simple diffusion: $MSD(\tau) = 6D\tau$, where D – Einstein-Stokes diffusion coefficient, $\mu m^2/s$
2. Confined diffusion: $MSD(\tau) = 6D\tau^{\alpha}$, with $0<\alpha<1$
3. Simple diffusion + directional movement: $MSD(\tau) = 6D\tau + (v\tau)^2$, where v is the speed of directional movement, μm/s

Due to the nature of MSD, its values at high τ have larger statistical uncertainty.[23] Therefore, we have used the first 75% of the resulting curves for fitting. Goodness of resulting fits is estimated with the adjusted R-squared. The best fit is then used to determine the mode of the particle's motion throughout this segment, as well as the parameters of this motion (D, α, v). We have performed this measurement for three different conditions: bare 70 nm FNDs, αNPC-FNDs and FNDαM all after 5 hours of uptake. From each condition at least 5 different tracks were made.

Statistical analysis

All statistical analyzes were performed using GraphPad Prism 6 software. Where applicable, averages and standard deviations were calculated and compared by one-way ANOVA with a Tukey post-hoc test to correct for multiple comparisons.

Results

Nucleus targeting by adsorbed and covalent antibodies on FNDs in fixed cells

Immunostaining using fixed cells, primary and secondary antibodies is the current gold-standard in the biological field. Adding a versatile probe such as Fluorescent Nanodiamonds to this broad application will yield some very interesting benefits such as long term imaging. Additionally, nanodiamonds remain fluorescent after embedding and staining for electron microscopy, which is interesting for correlative microscopy. We optimize the success rate of targeting by testing different concentrations and staining times using either adsorbed primary antibody on diamonds (αNPC-FNDs) or using covalently bound secondary antibodies on diamond (FNDαM). The success rate of immunostaining was assessed by measuring the distance of the particle within a cell towards its nucleus through Euclidian Distance Maps. An example of this analysis is shown in Figure 2. HeLa cells were fixed, extracted and blocked (if applicable) and subjected to different combinations, concentrations and incubation times of αNPC and FND or FNDαM. Unconjugated diamonds and diamonds in the absence of a primary antibody were used as a negative control and a secondary anti-mouse antibody with a Rhodamine Red-X label as a positive control, to assess the functionality of αNPC. Targeting of the nucleus was considered successful if the particle was within the 1.32 μm range from the border of the nucleus, see **Figure 4.** Covalently bound secondary anti mouse antibodies on FNDs showed a promising rate of nuclear localization, although not statistically significant compared to the other samples. For the αMouse Red-X samples, the area of the particles (positive pixels) per cells was typically between 5000 and 10000, for diamond samples it was not higher than 1-20 positive pixels per cell. When only diamonds are added to fixed cells, no nuclear targeting can be observed, showing that the targeting is not an artefact.

Immunostaining in living cells

To analyze potential degradation of the primary antibody αNPC, we have incubated HeLa cells with this antibody for multiple durations: 6, 7 and 8 hours. Then we fixed, extracted and blocked the cells and incubated them with αMouse Red-X and compared the distance to the nucleus with a traditionally immunostained sample, see **Figure 5a**. We found no statistical difference in staining between the living and fixed cells, demonstrating that we can use living cells to direct nanodiamond conjugates toward the nucleus without having account for degradation.

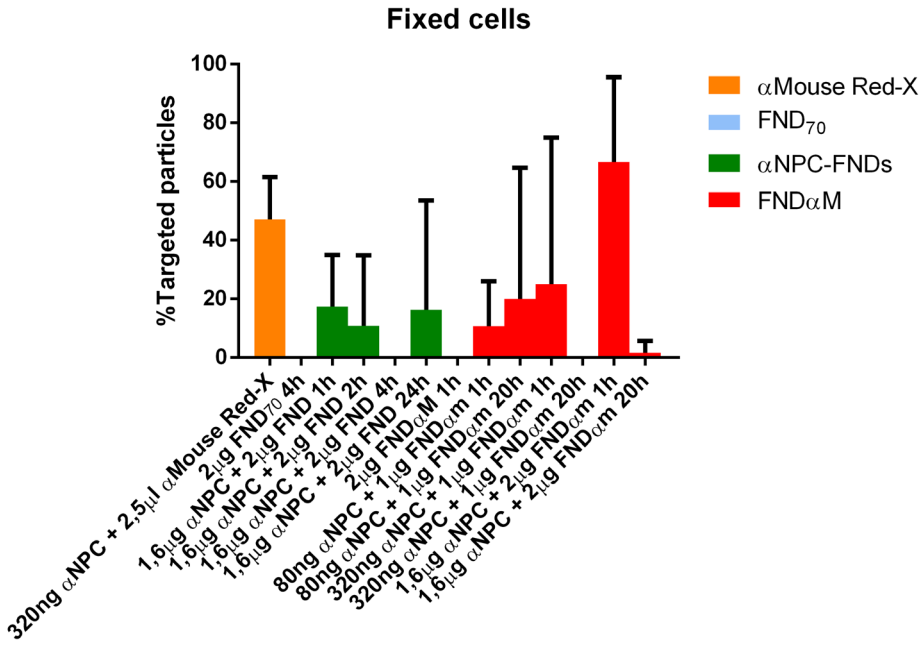

Figure 4. Efficiency of targeting in fixed HeLa cells to the nucleus. HeLa cells were fixed and immunostained according to a traditional staining protocol. First the cells are extracted and blocked (in case of αMouse Red-X and FNDαM). Then the cells are incubated with the αNPC antibody or with αNPC-FNDs. Next (if applicable) the cells are incubated with a secondary antibody, goat anti-mouse Red-X or FNDαM. After confocal analysis, the distances to the nucleus are calculated. For each cell the amount of targeted particles is calculated and compared to the total amount of particles. FNDs without the primary αNPC antibody were used as a negative control. Although no statistically significant effects are found, fixed staining using anti-mouse FNDs seems to be efficient at a high concentration and incubation for 1 hour. It has to be noted that the area with positive pixels, after setting the threshold, per cell in the anti-mouse Red-X samples is ordinarily between 5000-10000 pixels per cell, for FNDs this is typically between 1-20 positive pixels.

Adsorbed and covalently bound antibodies on FNDs in living HeLa cells

We used the positive control, which was also used in the previous section, as a reference to different concentration ratios of antibody and diamond, and different incubation times. We used non-conjugated diamonds and the absence of a primary antibody as a negative control. We also adapted a technique from the molecular biology domain: transfection using polyethylenimine. Polyethylenimine can form a positively charged shell around molecules such as DNA. This facilitates endocytosis and leads to release of the product in the cytoplasm by lowering of the osmotic pressure.[24] Here we used this technique to find out if we also could increase the diamond-antibody uptake in HeLa cells. Incubation of anti-mouse FNDs was performed either simultaneously with or right after incubation of the cells with αNPC for 6 hours (see **Figure 5b**). In living HeLa cells, FNDs are taken up under normal cell culturing conditions and we show that typically around 10-15% ends up near

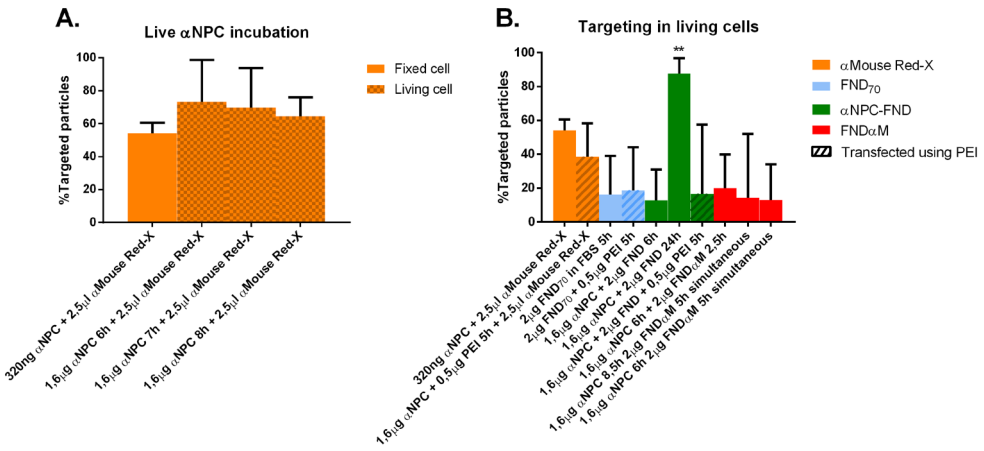

Figure 5. Efficiency of targeting in living HeLa cells. A. First we have analyzed if αNPC is degraded in cells or if it remains able to target the nucleus. The chequered bars show the living cells, the whole fill shows a fixed sample as a positive control. In the living cells, the αNPC antibody was incubated for 6, 7 or 8 hours and then the cells were fixed, extracted and incubated with goat anti-mouse Red-X. No significant differences can be identified between samples, indicating that the staining works to the same extent as in traditional immunostaining. **B.** In living HeLa cells we have incubated the cells with different concentration ratios and durations of antibody and fluorescent nanodiamonds. The same sample as in A. was used as a reference; 320ng αNPC + 2.5 µl αMouse Red-X. We have also adopted a technique from the transfection field, the use of PEI to increase uptake of particles in cells. Under conditions where there is no primary antibody present, there always are approximately 10-15% of the nanodiamonds located close to the nucleus. The addition of the transfection reagent PEI does not seem to influence the targeting efficiency. The most successful mode of targeting appears to use adsorbed αNPC on the surface of FNDs; there is statistically significant increase in targeting compared to the negative control sample, but not compared to the reference sample, indicating that incubating for a longer time with adsorbed antibodies has a high chance of successfully targeting the nucleus. It is important to note that the area of positive pixels per cell in the anti-mouse Red-X samples is ordinarily between 3000-8000 pixels per cell, for FNDs this is typically between 1-250 pixels.

the nucleus regardless of its modification or conjugation. Transfection using PEI did not result in a higher percentage of targeted diamonds and also not in a different uptake of particles per cell. The uptake was comparable to the other diamond samples (data not shown). Simultaneous or consequent incubation with FNDαM did not result in increased targeting. 24 hour incubation using adsorbed αNPC-FNDs was highly successful in targeting the nucleus. In the analyzed cells on average 87% of particles localized within 1.32 µm of the nucleus. This was statistically significant when compared to the negative control, showing that there is a definite difference of the particle localization.

Tracking of fluorescent nanodiamonds in living HeLa cells

Over the tracking period, the particles from each of the groups have on average moved approximately 3 µm away from the original locations (**Figure 6a**). MSD curves for entire trajectories (~45 minutes) in most cases show the complex nature of motion (**Figure 6b**), that cannot be approximated with either of the simple equations

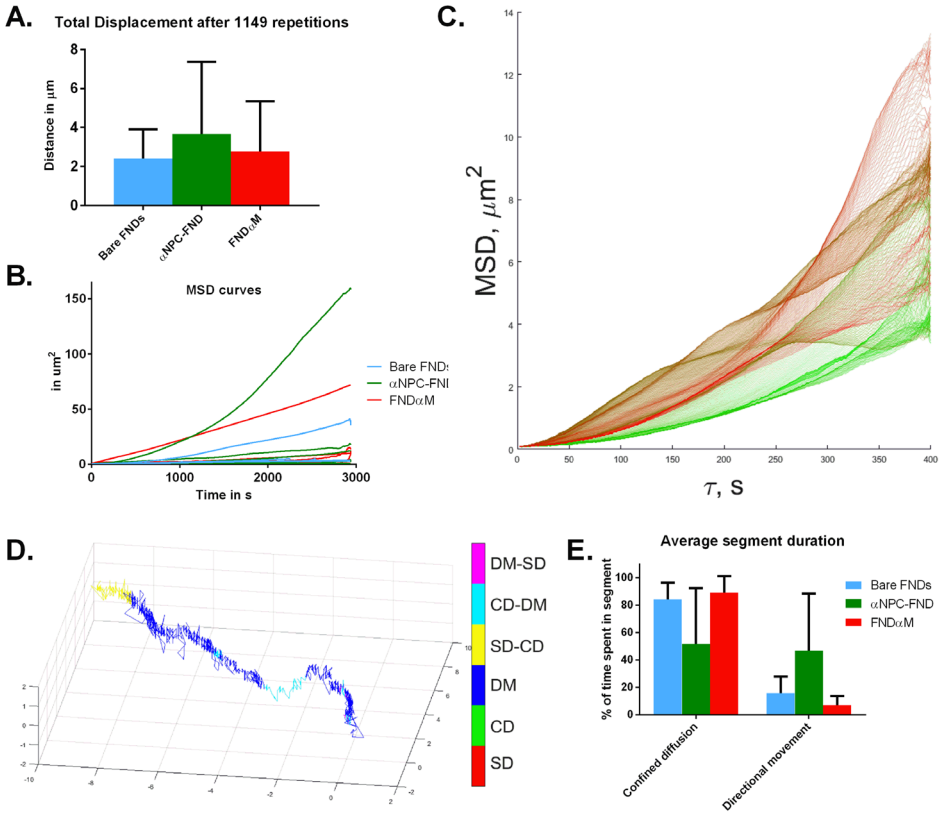

Figure 6. Analysis of the FND trajectories in living HeLa cells. For the first part of the analysis, we used full-length tracks. **A.** Over the tracking period, the particles from each group have on average moved approximately 3 µm away from the original locations. **B.** Mean Squared Displacement curves calculated for each particle show the total distance from the starting point and reveal the complex nature of the particles' movement in the cytoplasm. **C.** Separate MSD curves, plotted for each of the 400 second-long subtrajectories of a single track, show that particles can indeed switch between different types of motion. Color transition from green to yellow and red reflects the position of the subtrack in the original trajectory, with green curves corresponding to the beginning of the trajectory. **D.** Based on the results of the fitting, we can split the whole 3D-trajectory of the particle into the segments with distinct modes of motion. Here we show the trajectory of a single nanodiamond in the cytoplasm of a HeLa cell, with different colors corresponding to different modes of motion: simple diffusion (SD), confined diffusion (CD), or directional movement (DM), as well as the periods of transition between these phases. **E.** We compared the percentage of time spent in confined diffusion and in directional movement for the different particles. No significant differences were observed. The total percentages will not always add up to 100%, because the particles sometimes also move through simple diffusion. This is however rarely the case, and these events are relatively short, most likely representing transition from confined diffusion to directional movement and vice versa, so we do not show the data here.

(1)-(3) (Figure 3b). We did not observe statistically significant differences in the total distance travelled by the particles or in the overall mode of motion between bare FNDs and FNDs with adsorbed or covalently bound antibodies.

Separate MSD curves, plotted for each of the 400 second-long subtrajectories, reveal that particles can indeed switch between different types of motion, as they move inside the cells (**Figure 6c**). This approach allows one to divide the entire 3D trajectory of the particle into the segments with distinct modes of motion, as well as the periods of transition (**Figure 6d**). The most common mode of motion for all particles was confined diffusion (**Figure 6e**). We also observed phases of directional movement and occasional simple diffusion. However, detected periods of simple diffusion were very rare and relatively short, most likely corresponding to the transition from confined diffusion to directional movement and vice versa. We did not observe statistically significant differences in the relative duration of different phases between the particles from different groups.

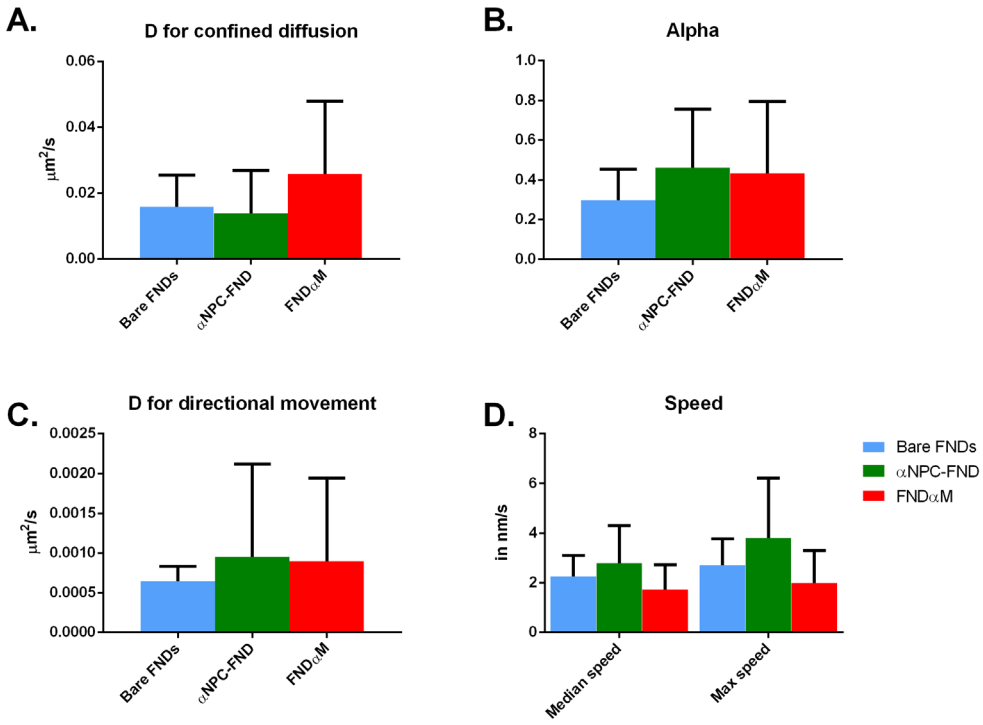

Figure 7. Quantitative parameters of the FND movements in living cells. Fitting of the MSD curves results in the estimates of the values of D, α and v, providing the basis for quantitative description of the particles' movement. **A.** During the periods of confined diffusion, the average value of D was approximately 0.02 $\mu m^2/s$, with no statistically significant differences between the experimental groups. **B.** The average value of α was in the range of 0.26-0.46, reflecting a high degree of confinement, experienced by the observed nanodiamonds. No significant differences were observed between the samples. **C.** During the periods of directional movement, the average value of D was approximately 0.0008 $\mu m^2/s$, with no statistically significant differences between the groups. **D.** The median and maximum speed of directional movement can then be calculated, which reflect the rate, at which the particle is transported in a specific direction, rather than randomly diffusing with no particular destination. Although some differences seem to occur, none are significantly relevant.

From the results of MSD curves fitting for the subtrajectories, we were able to estimate the coefficients D, α and v, in order to obtain a quantitative description of the particles' movements. During the periods of confined diffusion, the average value of D was 0.02 $\mu m^2/s$ (**Figure 7a**), and the value of α ranges from 0.26 to 0.46 (**Figure 7b**), showing high degree of confinement, experienced by the observed nanodiamonds. During the periods of directional movement, the average value of D was 0.0008 $\mu m^2/s$ (**Figure 7c**), while the highest speed reached by the particles was, on average, 3.0 nm/s (**Figure 7d**). We did not observe any statistically significant differences in the motion of tracked FNDs between different experimental groups.

Discussion

The localisation of fluorescent nanodiamonds towards organelles is an extremely relevant topic in the field of intracellular quantum measurements. Chemical composition of the FND environment and thus the magnetic field which will be measured by the NV center, are heavily influenced by the particles' location in the cell. Localization of FNDs without the need of organelle-identifying dyes leads to a higher sensitivity in reading out the NV center signal, because there is less background. A high targeting efficiency is therefore beneficial to be increasingly certain about the diamond location.

The more straightforward and simple a targeting protocol, the higher is its usefulness and the lower the chances for measurement errors. This is why we have made a comparison between an adsorbed primary antibody on the surface of nanodiamonds with covalently attached secondary antibodies on nanodiamond particles. It is hard to measure the simplicity of a protocol, but in case of the adsorbed nanodiamonds, no special reactions have to be performed on the surface of the nanodiamonds, although they can also be produced to order by companies such as FND BIOTECH. In addition, in the samples with covalently bound diamond-antibodies, we found a lot of micron-sized aggregated clusters when imaging in the confocal microscope. Analysis of these aggregates falls out of the scope of this study, but we assume that an interaction between the antibodies, diamonds and salts present in the medium results in large aggregate formation, similarly to what was shown before.[16] It is also interesting to note that different targeting protocols seem to favour different diamond conjugates. When targeting the nucleus in living cells, adsorbed αNPC-FNDs show very promising results, whereas in the samples with fixed cells, FNDαM displayed better results.

The analysis of our microscopic images has been extremely careful, to prevent having difficult to interpret results, as has been seen earlier in the targeting of nanodiamonds toward mitochondria.[13] This involved deconvolution of our images, a step which improves the contrast and reduces the noise, allowing one to detect FNDs in the images with higher certainty. At the same time, deconvolution can also lead to exclusion of particles which are too small to measure using confocal microscopy. In combination with the fact that we used a conventional confocal microscope,

which is limited in its sensitivity, this leads to an underestimation of the number of intracellular particles, as is identified before the calculation of the distance to the nucleus. Although this leads to an underestimation of the number of internalized particles, it will not influence the percentage of the targeted particles, as the limit of sensitivity is equal over the whole imaged sample. Addition of Electron Microscopy information will confirm if the size of a particle influences its fate.

The combination of our extremely sensitive homebuilt microscope with the mathematical equations for the analysis of the tracks of intracellular particles provides a large amount of useful data. More information can be extracted from the mean square displacement information:

- Diffusion coefficient D, which can provide further insight into the nanoscale environment of the particles and how easy it is for a nanoparticle to move in this environment;
- Coefficient of confined diffusion α, reflecting the size of the nanoscale "cage", in which a particle can be trapped;
- Speed of directional movement v, which can, for instance, imply the participation of the molecular motors in the nanoparticle motion and even provide a hint for the exact type of motors involved.

Our experimental data are in reasonable agreement with the results of nanoscale object tracking in live cells, obtained in other model systems, considering the difference in size of the particles. For instance, supposedly freely diffusing 70S ribosomes (26 nm in diameter, as determined by cryoelectron microscopy)[25] in a live *E. coli* cell show the diffusion coefficients of approximately 0.04 $\mu m^2/s$.[26] Quantum dots with the hydrodynamic radius of approximately 10 nm show confined diffusion in fibroblasts and fibrosarcoma cells, with the values of D and α being 0.04-0.09 $\mu m^2/s$ and 0.6-0.75, respectively.[27] MSD analysis of the trajectory of a 35-nm FND, moving in a directional way in the cytoplasm of a HeLa cell, resulted in the values of D and v being 0.002 $\mu m^2/s$ and 8 nm/s, respectively.[28] However, most of the studies focus on either obtaining large numbers of short trajectories from different particles, moving within the same system, or analysing the MSD curves for whole, relatively long (usually in the range of several minutes) trajectories of individual particles. Our approach allows one to observe the dynamic changes in the behaviour of a particular FND, as it moves in the cytoplasm of the living cell for much longer periods of time (up to an hour), in much finer detail than can be provided by the analysis of conventional MSD curves.

Although a very versatile tool, the use of the MSD has also shown it to be very complex and misuse can lead to misinterpretation of the experimental results. Performing of standardized tracking experiments could potentially yield specific alpha and speed scales for endosomal capture and escape, movement with cell motors or untargeted motion, which could be very useful in a large array of biological studies. This could also be combined with tracking in neurons or cellular vesicles to obtain more specific data of segmented movement.[290]

Our most successful approach to target the nucleus in living cells was by using adsorbed antibodies on the surface of fluorescent nanodiamonds and incubating these with cells for 24 hours. This protocol resulted in a high percentage of diamonds close to the nucleus. However it was not compared to bare nanodiamonds, which are incubated for 24 hours with cells or by only incubating a cell for 24 hours with the primary antibody, followed by identification using a secondary antibody. This information will improve the final conclusion and give irrefutable proof of the success of the targeting approach.
Future studies should focus on improving the targeting even more, increasing the sensitivity of the approach. In addition, the method shown here can be combined with antibodies against other organelles and cell structures, under the condition that there is enough space for the nanodiamond to manoeuvre in. This would greatly improve the versatility of the technique. In addition, other molecules could be used for adsorption on the surface of diamonds in a targeting approach. For example, positively charged particles have been shown to move toward the mitochondria.[31] Here, nanodiamonds coated with polypeptide chains could have an added benefit.[32]

Conclusion

Here we have for the first time shown nuclear targeting of fluorescent nanodiamonds using adsorbed or covalently bound antibodies. In both living HeLa cells and fixated cells we were able to get targets close to the nucleus. Adsorbed antibodies perform well in targeting under the right duration in living cells whereas covalently bound nanodiamonds show more promising results in fixated cells. The calculation of the success rate of targeting by deconvolution and using Euclidean Distance Maps is a very elegant and specific approach. Tracking of nanodiamonds inside cells and consequently performing an in-depth analysis on the different parameters of a diamond track result in accessible parameters, which can be used to explain the intracellular behaviour of the diamond particle.

References

1. Schirhagl, R., Chang, K., Loretz, M. & Degen, C. L. Nitrogen-vacancy centers in diamond: nanoscale sensors for physics and biology. *Annu. Rev. Phys. Chem.* **65,** 83–105 (2014).
2. Müller, T. *et al.* Wide-range electrical tunability of single-photon emission from chromium-based colour centres in diamond. *New J. Phys.* **13,** (2011).
3. Doherty, M. W. *et al.* Temperature shifts of the resonances of the NV-center in diamond. *Phys. Rev. B - Condens. Matter Mater. Phys.* **90,** (2014).
4. Balasubramanian, G. *et al.* Nanoscale imaging magnetometry with diamond spins under ambient conditions. *Nature* **455,** 648–651 (2008).
5. Van Oort, E. & Glasbeek, M. Electric-field-induced modulation of spin echoes of N-V centers in diamond. *Chem. Phys. Lett.* **168,** 529–532 (1990).
6. Ofori-Okai, B. K. *et al.* Spin properties of very shallow nitrogen vacancy defects in diamond. *Phys. Rev. B - Condens. Matter Mater. Phys.* **86,** (2012).
7. Haziza, S. *et al.* Fluorescent nanodiamond tracking reveals intraneuronal transport abnormalities induced by brain-disease-related genetic risk factors. *Nat. Nanotechnol.* **12,** 322–328 (2016).
8. Hemelaar, S. R. *et al.* The Response of HeLa Cells to Fluorescent NanoDiamond Uptake. *Sensors* **18,** 355 (2018).
9. Mohan, N., Chen, C. S., Hsieh, H. H., Wu, Y. C. & Chang, H. C. In vivo imaging and toxicity assessments of fluorescent nanodiamonds in caenorhabditis elegans. *Nano Lett.* **10,** 3692–3699 (2010).
10. Chipaux, M. *et al.* Nanodiamonds and Their Applications in Cells. *Small* 1704263 (2018). doi:10.1002/smll.201704263
11. van der Laan, K., Hasani, M., Zheng, T. & Schirhagl, R. Nanodiamonds for In Vivo Applications. *Small* (2018). doi:10.1002/smll.201703838
12. Chu, Z. *et al.* Unambiguous observation of shape effects on cellular fate of nanoparticles. *Sci. Rep.* **4,** 4495 (2014).
13. Chan, M. S., Liu, L. S., Leung, H. M. & Lo, P. K. Cancer-Cell-Specific Mitochondria-Targeted Drug Delivery by Dual-Ligand-Functionalized Nanodiamonds Circumvent Drug Resistance. *ACS Appl. Mater. Interfaces* **9,** 11780–11789 (2017).
14. Lake, M. P. & Bouchard, L. S. Targeted nanodiamonds for identification of subcellular protein assemblies in mammalian cells. *PLoS One* **12,** (2017).
15. Shimoni, O., Bray, K., Cheung, L., Aharanovich, I. & Valenzuela, S. Versatile Multicolor Nanodiamond Probes for Intracellular Imaging and Targeted Labeling. *bioRxiv* (2017).
16. Hemelaar, S. R. *et al.* The interaction of fluorescent nanodiamond probes with cellular media. *Microchim. Acta* 1–9 (2017). doi:10.1007/s00604-017-2086-6
17. Hemelaar, S. R. *et al.* Nanodiamonds as multi-purpose labels for microscopy. *Sci. Rep.* **7,** 720 (2017).
18. Chang, B. M. *et al.* Highly fluorescent nanodiamonds protein-functionalized for cell labeling and targeting. *Adv. Funct. Mater.* **23,** 5737–5745 (2013).
19. Xia, T. *et al.* Polyethyleneimine coating enhances the cellular uptake of mesoporous silica nanoparticles and allows safe delivery of siRNA and DNA constructs. *ACS Nano* **3,** 3273–3286 (2009).
20. Dougherty, R. Extensions of DAMAS and Benefits and Limitations of Deconvolution in

Beamforming. in *11th AIAA/CEAS Aeroacoustics Conference* (2005). doi:10.2514/6.2005-2961

21. Levi, V. & Gratton, E. Exploring dynamics in living cells by tracking single particles. *Cell Biochemistry and Biophysics* **48,** 1–15 (2007).
22. Zhang, Y. *et al.* A surface-charge study on cellular-uptake behavior of F3-peptide-conjugated iron oxide nanoparticles. *Small* **5,** 1990–6 (2009).
23. Qian, H., Sheetz, M. P. & Elson, E. L. Single particle tracking. Analysis of diffusion and flow in two-dimensional systems. *Biophys. J.* **60,** 910–921 (1991).
24. Akinc, A., Thomas, M., Klibanov, A. M. & Langer, R. Exploring polyethylenimine-mediated DNA transfection and the proton sponge hypothesis. *J. Gene Med.* **7,** 657–663 (2005).
25. Zhu, J., Penczek, P. A., Schröder, R. & Frank, J. Three-dimensional reconstruction with contrast transfer function correction from energy-filtered cryoelectron micrographs: Procedure and application to the 70S Escherichia coli ribosome. *J. Struct. Biol.* **118,** 197–219 (1997).
26. Bakshi, S., Siryaporn, A., Goulian, M. & Weisshaar, J. C. Superresolution imaging of ribosomes and RNA polymerase in live Escherichia coli cells. *Mol. Microbiol.* **85,** 21–38 (2012).
27. Grady, M. E. *et al.* Intracellular nanoparticle dynamics affected by cytoskeletal integrity. *Soft Matter* **13,** 1873–1880 (2017).
28. Zhang, B. *et al.* Receptor-mediated cellular uptake of folate-conjugated fluorescent nanodiamonds: A combined ensemble and single-particle study. *Small* **5,** 2716–2721 (2009).
29. Nagarajan, S. *et al.* Simultaneous cathodoluminescence and electron microscopy cytometry of cellular vesicles labeled with fluorescent nanodiamonds. *Nanoscale* **8,** 11588–11594 (2016).
30. Simpson, D. A. *et al.* Non-Neurotoxic Nanodiamond Probes for Intraneuronal Temperature Mapping. *ACS Nano* **11,** 12077–12086 (2017).
31. Wongrakpanich, A., Geary, S. M., Joiner, M. A., Anderson, M. E. & Salem, A. K. Mitochondria-targeting particles. *Nanomedicine* **9,** 2531–2543 (2014).
32. Zheng, T. *et al.* Recombinant Protein Polymers for Colloidal Stabilization and Improvement of Cellular Uptake of Diamond Nanosensors. *Anal. Chem.* **89,** 12812–12820 (2017).

Nanodiamonds as multi-purpose labels for microscopy

Simon R. Hemelaar[1#], Pascal de Boer[2#], Mayeul Chipaux[1], Wilco Zuidema[3], Thamir Hamoh[1], Felipe P. Perona Martinez[1], Andreas Nagl[1], Jacob P. Hoogenboom[3], Ben N. G. Giepmans[2] & Romana Schirhagl[1]

[1]Department of Biomedical Engineering, University Medical Center Groningen, The Netherlands. [2]Department of Cell Biology, University Medical Center Groningen, The Netherlands. [3]Department of Imaging Pysics, University of Delft, The Netherlands

[#]These authors contributed equally

Scientific Reports **7:1** 720-729 (2017)

"*Fluorescent diamond brings color to a black and white TV*"

Abstract

Nanodiamonds containing fluorescent nitrogen-vacancy centers are increasingly attracting interest for use as a probe in biological microscopy. This interest stems from (i) strong resistance to photobleaching allowing prolonged fluorescence observation times; (ii) the possibility to excite fluorescence using a focused electron beam (cathodoluminescence; CL) for high-resolution localization; and (iii) the potential use for nanoscale sensing. For all these schemes, the development of versatile molecular labeling using relatively small diamonds is essential. Here, we show the direct targeting of a biological molecule with nanodiamonds as small as 70 nm using a streptavidin conjugation and standard antibody labeling approach. We also show internalization of 40 nm sized nanodiamonds. The fluorescence from the nanodiamonds survives osmium-fixation and plastic embedding making them suited for correlative light and electron microscopy. We show that CL can be observed from Epon-embedded nanodiamonds, while surface-exposed nanoparticles also stand out in secondary electron (SE) signal due to the exceptionally high diamond SE yield. Finally, we demonstrate the magnetic read-out using fluorescence from diamonds prior to embedding. Thus, our results firmly establish nanodiamonds containing nitrogen-vacancy centers as unique, versatile probes for combining and correlating different types of microscopy, from fluorescence imaging and magnetometry to ultrastructural investigation using electron microscopy.

Introduction

In correlative microscopy, a comprehensive view on a specimen is acquired by combining information obtained with different modalities of microscopy. Arguably, correlative light and electron microscopy (CLEM)[1] constitutes the most widespread form of correlative microscopy. In CLEM, fluorescence microscopy (FM) prior to EM acquisition is used, e.g., to visualize fluorescently labeled molecules within the nanostructural environment imaged with EM. Alternatively one can pinpoint a region of interest for high-resolution EM investigation using live-cell or *in vivo* FM. However, the intrinsic resolution gap between FM and EM limits the degree to which molecules can be localized within the structural EM images. Preferably, this localization would be at the level of EM resolution. A major challenge in CLEM is thus to find approaches and labels that allow live-cell or *in vivo* observation, maintain their fluorescence during EM sample preparation, and can be localized with near-EM resolution.

Direct electron-beam fluorescence excitation, or cathodoluminescence (CL), provides a solution that allows EM localization, but standard organic or biological fluorophores are unstable under electron beam exposure.[2] In addition, most fluorescent labels do not survive the sample preparation needed for EM. Colloidal quantum dots are fluorescent, can be used in live cell experiments, and they can be precisely located in EM thanks to their electron dense core.[3,4] However, CL from bio-conjugated quantum dots, which would allow distinguishing multiple quantum dot labels in color, has not yet been shown. This is probably due to bleaching of quantum dot fluorescence under electron exposure. With phosphor nanoparticles, CL from particles with <50 nm diameter has been observed,[5–7] but application in an EM-prepared sample has to our knowledge not yet been demonstrated. Larger phosphor particles doped with rare-earth atoms have also been explored for upconversion luminescence,[8] which may be attractive in combination with *in vivo* imaging. CL from such particles after cellular uptake and sectioning for EM has been shown.[9,10] However, so far only particles of >100 nm have been reported, which precludes their use as a molecular label, and conjugation schemes for these particles have not yet been reported.

In recent years diamond nanoparticles containing defect centers have attracted increasing interest[11] for use as a molecular label because of their excellent photostability. These fluorescent nanodiamonds (FNDs) are also bio-compatible[12,13] and can be internalized in cells.[14–18] Further interest in the FNDs stems from the fact that they can be used as local sensors of magnetic[19] or electric fields,[20] temperature,[21] or strain,[22] which could enable multi-parameter correlative microscopy. Moreover, stable CL from FNDs containing nitrogen-vacancy (NV) centers,[5] as well as silicon-vacancy centers[23] has been demonstrated, for the NV-FNDs even after cellular uptake and embedding and sectioning for scanning transmission EM[24] or in live-cell EM studies.[25] However, in these studies the FNDs are large (100–150 nm), limiting the use to cell uptake studies only.

Here, we take the step towards FNDs that are 40 nm and 70 nm in size on average.

We show that fluorescence, optically detected magnetic resonance (ODMR), and CL can be recorded from these particles after internalization. Moreover, we present antibody-targeted labeling using the 70 nm FNDs, and demonstrate that these FNDs, targeted to a specific protein can be detected in tissue sections fixed and stained for EM using a standard protocol that allows ultrastructural preservation. Combined with live-cell fluorescence and optical recording of magnetic resonance spectra, our results demonstrate the unique potential of FNDs as biomolecular targets for multi-parameter correlative microscopy.

Material and Methods

Nanodiamonds

Fluorescent nanodiamonds of 40 nm (FND_{40}) and 70 nm (FND_{70}) contain 10–15 and >300 NV-centers, respectively as stated by the supplier (Adámas Nanotechnologies, NC, USA). FNDs were drop-casted on ITO-coated cover glasses (Optics Balzers, Liechtenstein) and subsequently air-dried. FNDs were analyzed with EM using secondary electron (SE) detection for size and dispersity on a FEI Verios scanning EM. The optimal excitation wavelength was assessed using a scanning confocal system (Zeiss LSM 780, Plan-Apochromat 63x/1.40 lens). Using lambda mode, emission spectra were recorded creating intensity profiles between 571 and 687 nm with 9 nm intervals upon excitation with 405, 440, 488, 514, 561 and 594 nm lasers with appropriate beam splitters. Intensities were measured by comparing grey values of the individual images at the 9 nm intervals using Matlab and plotted in arbitrary units. For the size measurements, images were analyzed using ImageJ. In total 5051 particles were analyzed for FND_{70} and 1141 for FND_{40}. As the particles were markedly non-spherical,[26] we defined the size as the square root of the surface area of FNDs as detected with secondary electrons. We note that this is an over-estimation as the shortest particle axis will mostly be perpendicular to the surface because of the drop-casting and drying. For the analysis of particle size versus CL intensity, the secondary electron images were used as a mask for the CL signal and the CL intensity of the FND was taken to be the mean signal in the mask areas. To find FNDs with zero CL intensity, the background signal plus one standard deviation was subtracted from the mean CL intensity of each ND, which was normalized afterwards.

FND_{40} uptake by J774 macrophages

J774A.1 macrophages (LGC Standards, Germany) which play an important role in the immune system, were cultured in Dulbecco's Modified Eagle Medium (DMEM) with high glucose, supplemented with 10% FBS, 1% Penicillin/streptomycin and 1% Glutamax (Gibco, ThermoFisher Scientific, The Netherlands). Cells were incubated with 1 µg/ml FND_{40} in cell culture medium for 5 hours at 37 °C and 5% CO_2 (**Figure 1a**). After removal of culture medium with FNDs, cells were fixed with 4% paraformaldehyde/0.1% glutaraldehyde in 0.1 M cacodylate buffer, pH 7.4 (CaCO) for 30 minutes at room temperature (RT). Nuclei were counterstained with

4',6-diamidino-2-phenylindole (DAPI). Before optically detected magnetic resonance (ODMR) measurements we used phalloidin-FITC (Sigma-Aldrich, The Netherlands) to label f-actin to visualize the cells. Samples were analyzed using a Zeiss LSM780 confocal microscope using 405 nm and 561 nm excitation. The amount of particles taken up by the cells was estimated using a home written script for the image analysis software FIJI (Fiji Is Just ImageJ, see **supplementary text S1** for a detailed explanation). Next the same samples were prepared for EM (see below).

FND immunolabeling of HT29-EpCAM-GFP cells

HT29 is a human epithelial colon carcinoma cell line, and HT29-EpCAM-GFP stable cells were engineered that overexpress the epithelial cell adhesion molecule (EpCAM) fused to GFP.[27] These were also cultured in DMEM complete medium. Cells were seeded in gamma irradiated 35 mm glass bottom collagen coated dishes (MatTek corporation, MA, USA) until clusters of at least 10 cells grew. Cells were fixed in 4% paraformaldehyde/0.1% glutaraldehyde in 0.1 M cacodylate (15 minutes, RT) and subsequently blocked in PBS with 5% BSA (PBSA). Then cells were incubated (1 hr RT) with an antibody against the extracellular domain of EpCAM, namely MOC31.[27,28] After washing in 1% PBSA, samples were incubated with rabbit-anti-mouse-biotin (Dako Netherlands) in 1% PBSA. Cells were washed in 0.1 M cacodylate and incubated with a premixed solution of FNDs and Streptavidin (Sigma-Aldrich, Zwijndrecht, the Netherlands) on a 1:20 weight ratio in 0.1 M cacodylate. As a positive control, cells were incubated with streptavidin-conjugated quantum dots (QD655, Life Technologies, The Netherlands). After washing, cells were imaged using a Zeiss LSM780 confocal microscope using a 488 nm and 561 nm laser. For every sample at least 3 different cell clusters were imaged at 3 different times. Confocal images were analyzed and processed (brightness and contrast) using Fiji.[29] EpCAM and FND signal overlap was calculated by manually removing GFP signal coming from membranes inside the cluster using FIJI software. Next the signals were subjected to a threshold and converted into binary values. Finally the percentage of FND positive EpCAM pixels was calculated and related to the total of EpCAM positive pixels.

Sample preparation for integrated light and electron microscopy

We proceeded with the J774 and HT29 EpCAM-GFP cells described above. After washing with 0.1 M cacodylate buffer, cells were incubated with 1% osmiumtetroxide/1.5% potassiumferrocyanide in 0.1 M cacodylate buffer (30 minutes on ice), followed by washing with water. Next, the cells were dehydrated through an increasing graded ethanol series and left overnight in 1:1 ethanol and Epon (Serva) mixture at room temperature, which was replaced by pure Epon (4 times) and finally polymerized overnight at 58 °C. The cover glass of the imaging dish was removed using hydrogen fluoride. Areas containing cells were selected using a stereo microscope and sawn from the Epon block. Subsequently, 300 nm sections were cut with an ultramicrotome (Leica EM UC7) using a glass knife and put on an ITO coated cover glass. Finally, sections were counterstained with Hoechst.

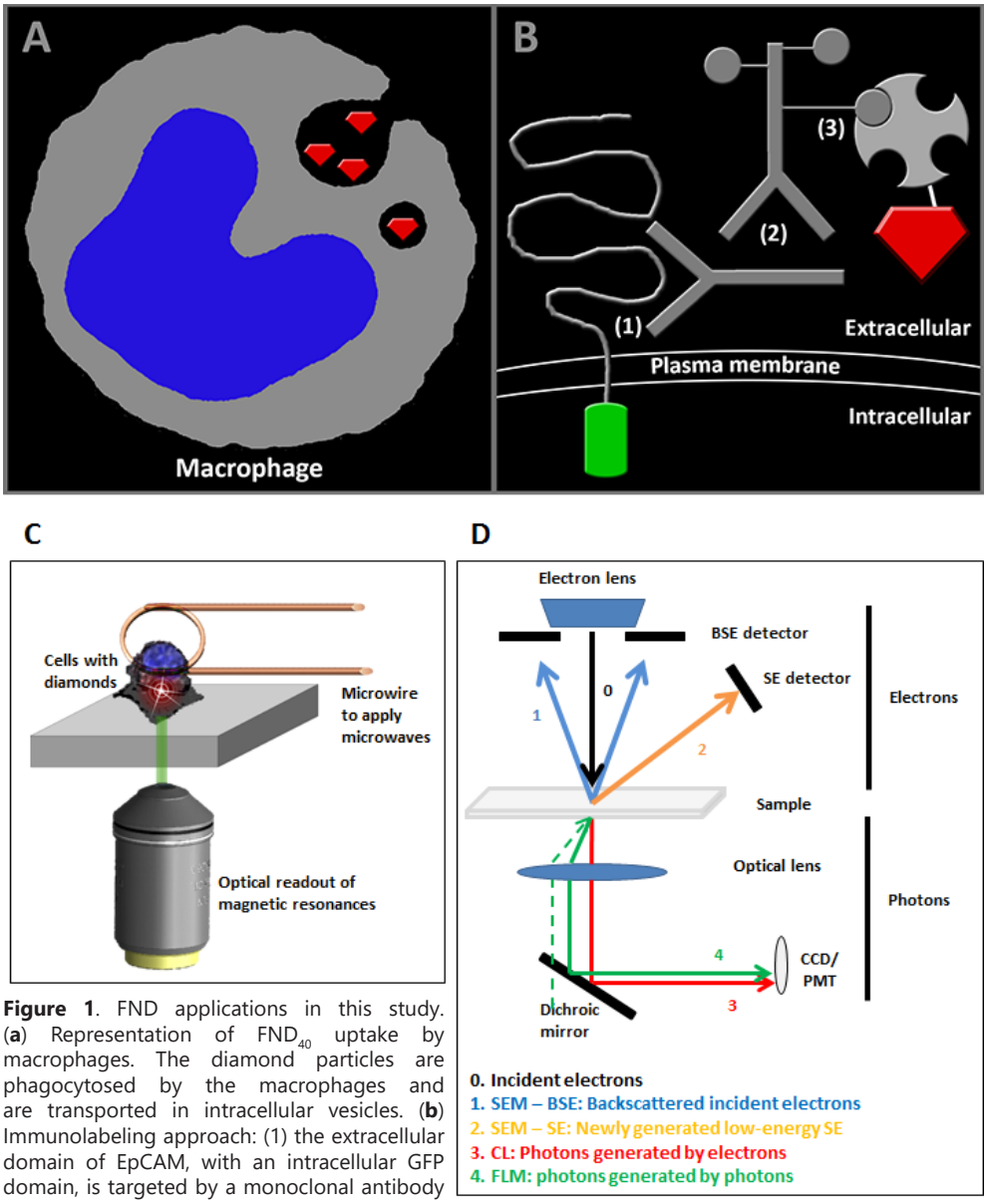

Figure 1. FND applications in this study. (**a**) Representation of FND_{40} uptake by macrophages. The diamond particles are phagocytosed by the macrophages and are transported in intracellular vesicles. (**b**) Immunolabeling approach: (1) the extracellular domain of EpCAM, with an intracellular GFP domain, is targeted by a monoclonal antibody (MOC-31); (2) biotinylated rabbit anti mouse IgG is used as a linker for labeling with (3) streptavidin-conjugated FND_{70} particles. (**c**) Schematic overview of the sample area of a diamond magnetometer for intracellular sensing. The cells, which contain diamond nanoparticles, are in a glass bottom petri dish. A microwire in close proximity is used to excite in the microwave regime. Simultaneously, fluorescence is collected through a microscope objective and a subsequent confocal microscope. (**d**) Schematic overview of integrated light and scanning EM and cathodoluminescence. (0) Primary incident electrons generate (1) backscattered electrons (BSE) and (2) secondary electrons (SE) which can be imaged in a SEM with the respective detectors. Also photons can be generated upon electron beam excitation called (3) cathodoluminescence (CL). Via an optical lens, these photons can be detected with for example a CCD camera or photo multiplier tube (PMT). Furthermore, with an integrated light and electron microscope (4) regular fluorescence imaging can be performed with photon excitation.

Integrated light and electron microscopy

Fluorescence preservation was checked using the Zeiss LSM780. Next, the same sections were imaged under high vacuum using a SECOM integrated microscope (Delmic, The Netherlands) in a Zeiss Supra55 scanning EM. The SECOM is equipped with a four color LED, a dichroic mirror (Di01-R405/488/561/635, Semrock, NY, USA), a filter wheel and a CCD camera. Fluorescence of both Hoechst and FNDs was recorded using a 20x/0.75 vacuum compatible objective. EM of the same ROI was acquired using a back scattered electron detector at 10 kV with 60 µm aperture at 9.7 mm working distance. Overlays were created using the SECOM software (Odemis). CL was recorded using a SECOM platform, only equipped with a vacuum compatible plan APO 40x/0.95 light objective and a photomultiplier tube (PMT), retrofitted to a Verios scanning EM (FEI, Eindhoven, The Netherlands). Simultaneously, CL, using the PMT, backscattered electrons, using a circular backscattered electron detector, and secondary electrons, using a through-lens detector, were recorded at 3 keV and 0.8 nA at a 7 mm working distance. Images were processed and analyzed using Fiji and overlays were created using Adobe Photoshop.

Optically detected magnetic resonance (ODMR) measurements

These measurements allow using the FND to read out their magnetic surrounding. Additionally, they offer a way to conclusively identify bright spots as FND defects. For magnetic resonance measurements a home built diamond magnetometer (similar to what is used in the community,[30,31] see **Figure 1c** for a schematic representation), which is a confocal microscope with built-in microwave electronics, has been used. As described previously macrophage cells where stained to identify cell borders. Borders of HT29 cells where identified via their intrinsic GFP signal. To separate the FNDs signal from the other fluorescent staining a 550 nm long pass filter was used. Signal above 550 nm was attributed to the FNDs. A laser power of 1 mW was used. After scanning an area with cells and identifying FND particles we focussed on the FND spots and recorded an optically detected magnetic resonance. The frequency was swept around the expected resonance frequency of the NV-center at 2,87 GHz. This microwave signal was produced with a microwave synthesizer (Hittite HMC-T2100) sending to a homemade antenna (short circuit of a copper wire at the end of a coaxial cable,[32] a few micrometer from the sample). Simultaneously, light intensity was collected using an Olympus UPLSAP40x2 NA = 1.3 objective and an Avalanche photodiode (SPCM-AQRF-15-FC) in single photon counting mode. The microwave power was 27 dBm the acquisition time was 13 minutes (averaging 300 individual runs).

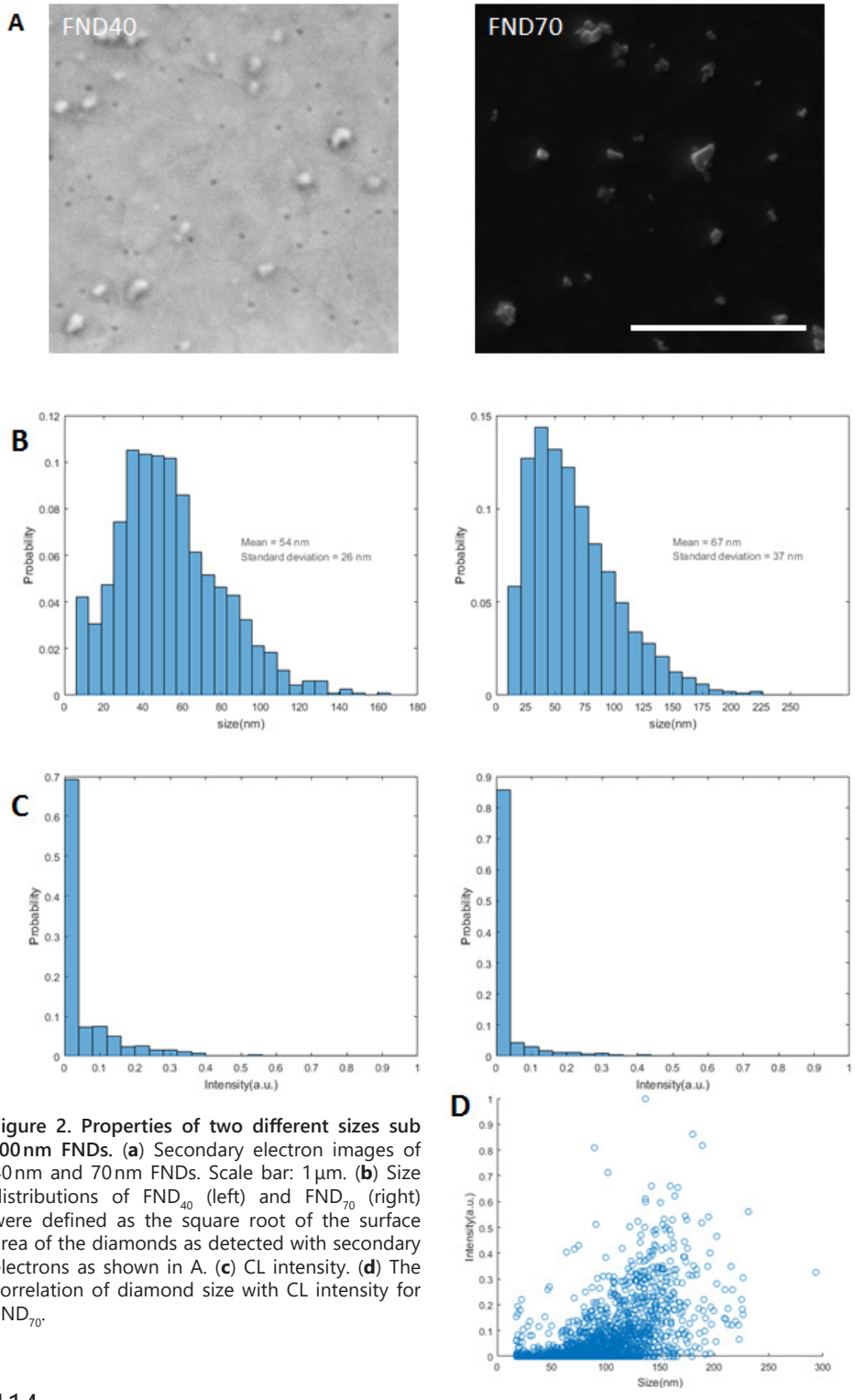

Figure 2. Properties of two different sizes sub 100 nm FNDs. (**a**) Secondary electron images of 40 nm and 70 nm FNDs. Scale bar: 1 µm. (**b**) Size distributions of FND_{40} (left) and FND_{70} (right) were defined as the square root of the surface area of the diamonds as detected with secondary electrons as shown in A. (**c**) CL intensity. (**d**) The correlation of diamond size with CL intensity for FND_{70}.

Results and Discussions

Properties of sub-100 nm FNDs

Recently, attention has gone to relatively large FNDs[33,34] which show high fluorescent and CL signals.[24] However, for bio-applications small FNDs, approaching the size of biomolecules, are preferred. First, we set out to characterize the FND_{40} and FND_{70} dispersions. When imaged with EM using secondary electron (SE) detection, the different FND types indeed show different sizes when spotted on ITO glass. However, both samples also show a substantial size variation, as can be seen for the FND_{70} in **Figure 2a**. **Figure 2b** shows the size distributions measured over 5051 and 1141 particles for FND_{70} and FND_{40} respectively, which confirm the observed size polydispersity. Distributions are markedly non-Gaussian with average sizes of 54 ± 26 nm and 67 ± 37, respectively. Next, fluorescence characteristics were assessed. Excitation with 561 nm laser gave the highest emission intensity, within the red spectrum with a maximum around 660 nm. Furthermore, emission intensity increases with FND size, which can be explained by the higher amount of NV-centers in FND_{70} (>300) compared to FND_{40} (10–15). Besides light-excited fluorescence, also electron-excited CL is observed from the FNDs. CL intensity measurements (**Figure 2c**) were performed simultaneously with the size measurements. These also displayed strong variations, with a few very bright FNDs and a majority of weak to dim FNDs. Note that fluorescence originates from both neutral (NV°) and negatively charged (NV^-) vacancy centers, while CL has been reported to only originate from NV° centers. Spectral measurements (see **Supplementary Figure 1**) confirmed NV°-only CL. FND size to CL intensity correlation (**Figure 2d**) shows that brightest CL originates from the relatively larger FNDs, as may be expected from a larger number of NV-centers in bigger particles together with reduced surface quenching of excitations. However, it is also observed that through the entire size range strong particle-to-particle variations in CL intensity occur. Thus, there are relatively CL-bright small FNDs together with relatively CL-dim larger FNDs. Factors accounting for this may be the unknown out-of-plane diameter of the non-spherical FNDs (although we note that we did not observe correlation between CL and SE intensity), variation in the number of vacancy centers per particle and/or different interparticle ratios of NV° vs NV^-. Despite the relatively low fluorescence of FND_{40}, the signal/noise measurements as performed on spotted FNDs directed us to evaluate the benefits of smaller size for bio-applications.

FND_{40} uptake by macrophages visible with EM and CL

Recently, FND ingested by different cell types have been shown.[9,10] We used macrophages for their uptake efficiency as a proof of principle set up for our different imaging approaches (Figure 1). Indeed, FND_{40} are taken up by macrophages as assessed by their fluorescence from within the cells (**Figure 3a**). Using our home written script for the FIJI software we estimated an average of 210 internalized particles per cell. The identity of the 40 nm diamonds was further confirmed by ODMR

measurements revealing the presence of FND_{40} particles inside the cells (**Figure 3b**). The characteristic NV-spectrum (a double dip at the resonance frequency of 2.87 GHz) uniquely identifies diamond particles. Next, these macrophages were embedded for subsequent EM. The fluorescence of the FNDs was preserved after conventional Epon embedding, including post fixation using 1% osmiumtetroxide (**Figure 3c**). The

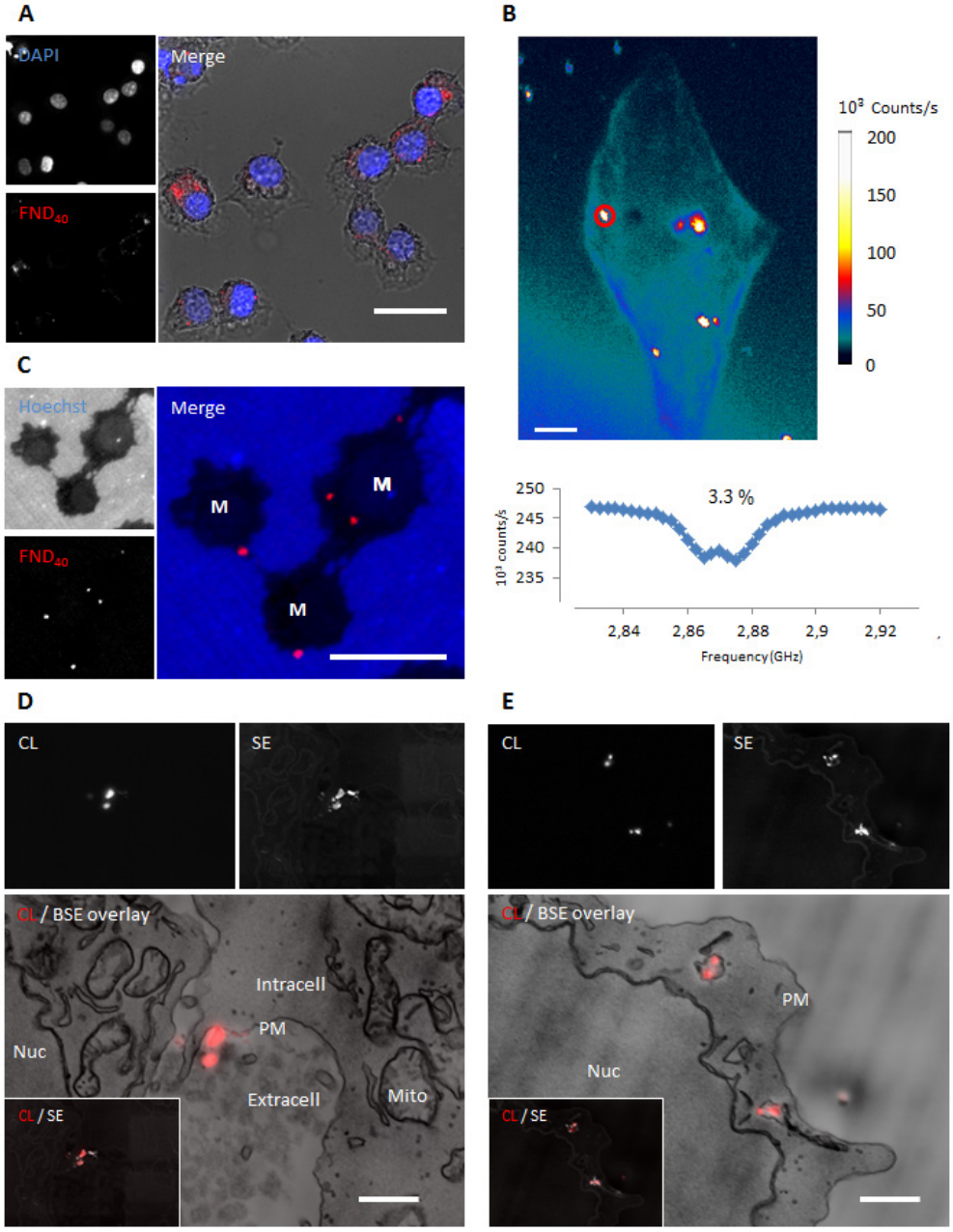

retention of fluorescence could be explained since their NV-centers are embedded in the diamond structure and therefore not accessible for osmium quenching. Loss of fluorescence is often a hurdle in CLEM and maintenance is highly desired especially when an integrated light and electron microscopy approach is used (reviewed in de Boer *et al.*[1]). Although engineered osmium-resistant fluorescent proteins and dedicated embedding protocols for fluorescence preservation exist[35–38] this may come at the expense of the ultrastructure preservation. Here however, ultrastructure is preserved, since we used conventional osmium post-fixation and Epon embedding (**Figure 3d,e**). Fluorescence from the EM samples is however still diffraction limited, precluding precise localization when overlaid with EM data. In order to achieve high resolution localization we utilized the CL properties of the FNDs which have been shown before with single nanodiamonds and for larger 150nm FNDs in cells.[5,24,25] Clearly, FND_{40} show up in CL on a dark background (Figure 3d,e). Variations in CL intensity between different FND_{40} are observed, e.g., in Figure 3d where two diamonds stand out and others appear dimmer, likely due to variations in size and number of NV^- centers contained in the particles. An advantage of SEM is that low energy SEs can be detected simultaneously. As diamond has an exceptionally high SE yield at few keV electron energy, which may even be more pronounced for defected diamond,[39] and SEs can readily escape from the small particles, the FND_{40} stand out particularly well in the SE image (Figure 3d). This confirms that the higher CL originates from the relatively larger particles. Compared to the SE image, a halo around the diamonds appears in CL, which we attribute to proximity excitation due to BSE or SE excited in the tissue. When overlaid with backscattered electron (BSE) data we find localisation of FND_{40} particles within the ultrastructure context of macrophages. This approach reveals different stages of phagocytosis including engulfment as the plasma membrane extrudes around the particles, which are still extracellular (Figure 3d), and FNDs in phagosomes shown by the presence of a membrane around the particles (Figure 3e).

Figure 3 FND_{40} uptake by macrophages assessed by fluorescence microscopy, EM, magnetic resonance and CL. (**a**) Pre-embedding fluorescence of FND_{40} internalized by macrophages as seen in the diffraction interference contrast (DIC) merged picture. Nuclei are counterstained with DAPI. (**b**) Magnetic resonance spectra where taken at the bright spots identified as diamonds. The graph shows the spectrum taken at the red circle. 3.3% is the contrast between the resonance line and the background for a single run. (**c**) Fluorescence from FND_{40} in a 300 nm semi-thin Epon section from macrophages (M). Nuclei are counterstained with Hoechst; blue outside the cells is autofluorescence caused by Epon. (**d**,**e**) CL, SE and the CL overlaid with BSE images of FND_{40} particles. (**d**) FNDs extracellular of the plasma membrane during engulfing. The lower left corner shows an overlay of CL and SE of the same image. Some particles are clearly observed with SE and not with CL. (**e**) FND_{40} particles internalized by the macrophage as they are inside vesicles. The lower left corner shows an overlay of CL and SE of the same image. Some particles are observed with SE and not with CL, but also particles observed with CL are not visible with SE. Note that single FND_{40} particles within one vesicle can be resolved by CL. M: macrophage; Nuc: nucleus; Intra: intracellular; Extra: extracellular; PM: plasma membrane; Mito: mitochondria; CL: cathodoluminescence; SE: secondary electrons; BSE: Backscattered electrons. Bars: (**a**) 10 µm, (**b**) 12 µm, (**c**), 10 µm, (**d**,**e**) 1 µm.

<

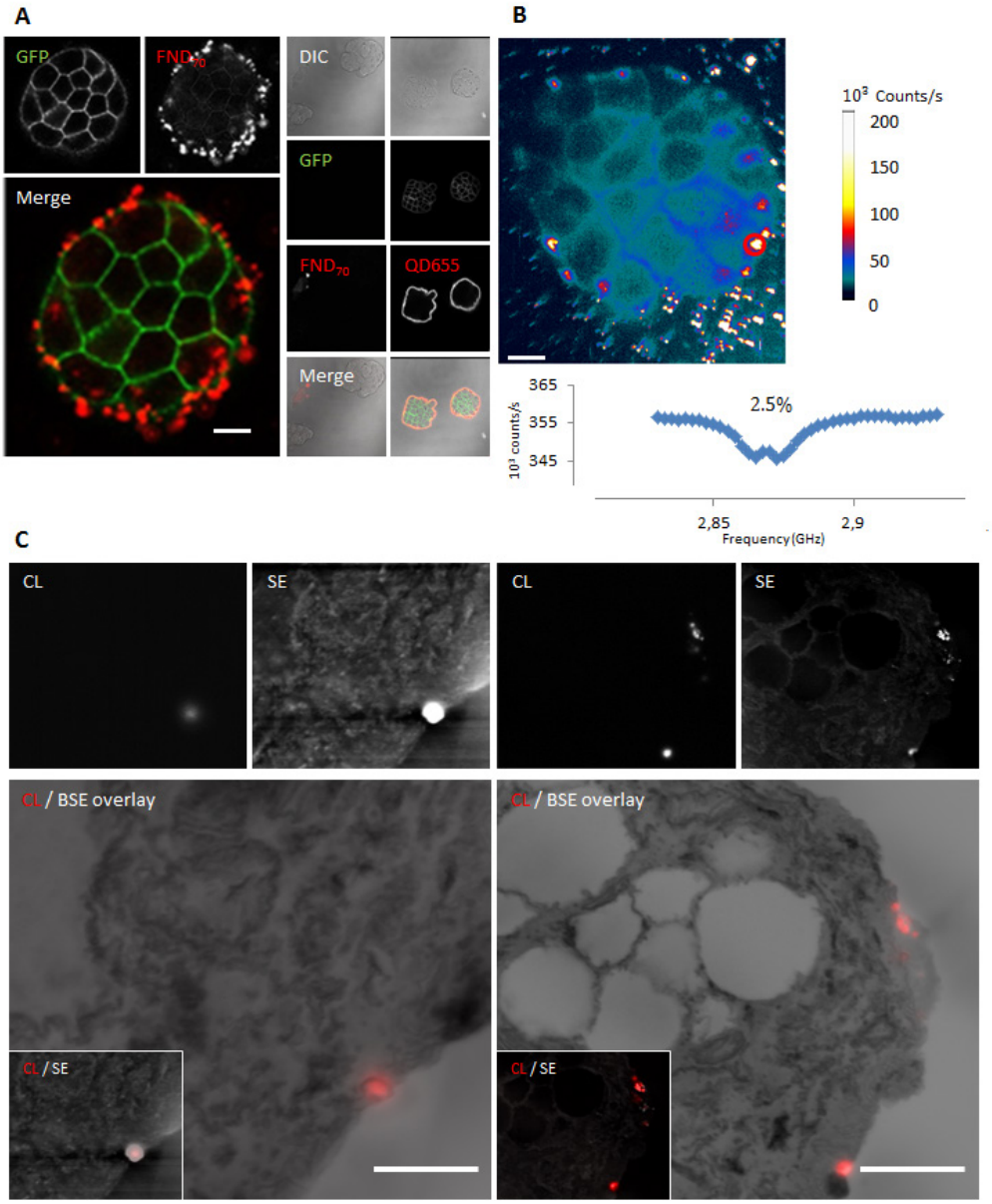

Figure 4. Multimodal analysis of FND_{70} immunolabeling of EpCAM-GFP HT29 cells. (**A**) Streptavidin-conjugated FND_{70} labels at the outside of a HT29 cell cluster. The context of different cells within the cluster is shown by GFP. Negative controls (left column) and positive controls (right column; QD655) are shown. No FND_{70} labeling of non-transfected negative controls is observed, context is shown by diffraction interference contrast (DIC) as EpCAM-GFP is absent. (**B**) Magnetic resonance spectra where taken at the bright spots identified as diamonds. The lower part of the figure shows the spectrum taken at the circled spot. 2.5% is the contrast between the resonance line and the background for 1 run. (**C**) CL, SE and the CL overlaid with BSE images of FND_{70} labeling an HT29 cell cluster at the cell surface. Note that in the right image single FND_{70} particles are resolved with CL. Abbreviations as in Figure 3. Bars: (**A**,**B**) 25 µm, (**C**) 1 µm.

FND_{70} allows immunolabeling and superresolution detection

Given the notion that FND_{40} particles are detectable with CL and EM at high resolution in uptake assays, FND_{70} was conjugated to streptavidin for generic immunolabeling application. As a proof of principle we immuno-targeted the extracellular domain of EpCAM-GFP expressed by HT29 cells[27] (**Figure 4A**) using a pre-embedding approach without permeabilization to maintain both antigenicity and ultrastructure. Immunolabeling was successful as compared to non-EpCAM-GFP expressing control cells, but sparse compared to smaller QD655 particles (~10 nm). On the other hand, FND_{70} can be used in ODMR (**Figure 4B**). Overlap of the EpCAM positive and FND positive pixels for the cell cluster of Figure 4A was 22.9%. This imaging mode not only allows proofing that the optical signal comes from diamond particles but also opens up the possibility to measure chemicals or certain properties in the surrounding of the particles via ODMR. Moreover, immunolabeling was detected with CL in EM samples and overlaid with BSE data for high resolution localization (**Figure 4C**). Again, FNDs also stand out in SE detection. Also very dim or even non-fluorescent nanodiamonds, e.g., due to a lack of CL-active defect centers, show up in SE. On the other hand, only surface exposed particles, would be visible in SE, as for deeper (> few nanometers) lying FNDs, the low energy SEs cannot escape the sample. CL of FNDs for superresolution imaging has mostly been explored using single particles[5,40] even with detecting individual defect centers within one nanodiamond.[39] Here, we show for the first time CL of relatively small-sized FNDs within a biological context (Figures 1d,e and 3c), compared to what others have shown before[24] to achieve superresolution imaging. Bio-application of CL correlation with EM has been applied before with different nanoparticles, but size was often an issue.[9,10]

Conclusions

FNDs have the advantage that they are stable and bleach resistant. They remain fluorescent after osmium fixation, and can also be detected using CL in samples for analysis with EM or integrated microscopes. The CL allows better localization based on the electron beam excitation rather than on the diffraction-limited light detection. Also, FNDs can be used to generate optically detected magnetic resonance signals allowing nanoscale magnetometry. We show proof-of-principle that all these FND properties can be used with small 40 nm and 70 nm particles using uptake assays or immunolabeling. Given the progress made in the last 10 years by using other nanoparticles, e.g., quantum dots, and labels for bioapplications, our results provide a first lead to further develop FNDs for life science research. This might include smaller, differently conjugated or more homogenous particle distributions. Our proof-of-principle of using multi-modal imaging with small FNDs demonstrates (i) fluorescence in EM prepared samples, (ii) CL, (iii) SE and BSD detection, and (iv) magnetometry detection, which will open up possibilities to gain additional information on the magnetic surrounding of the particles.

References

1. de Boer, P., Hoogenboom, J. P. & Giepmans, B. N. G. Correlated light and electron microscopy: ultrastructure lights up! *Nat. Methods* **12,** 503–513 (2015).
2. Niitsuma, J. I., Oikawa, H., Kimura, E., Ushiki, T. & Sekiguchi, T. Cathodoluminescence investigation of organic materials. *J. Electron Microsc. (Tokyo).* **54,** 325–330 (2005).
3. Nisman, R., Dellaire, G., Ren, Y., Li, R. & Bazett-Jones, D. P. Application of quantum dots as probes for correlative fluorescence, conventional, and energy-filtered transmission electron microscopy. *J. Histochem. Cytochem.* **52,** 13–8 (2004).
4. Giepmans, B. N. G., Deerinck, T. J., Smarr, B. L., Jones, Y. Z. & Ellisman, M. H. Correlated light and electron microscopic imaging of multiple endogenous proteins using Quantum dots. *Nat. Methods* **2,** 743–749 (2005).
5. Glenn, D. R. *et al.* Correlative light and electron microscopy using cathodoluminescence from nanoparticles with distinguishable colours. *Sci. Rep.* **2,** 865 (2012).
6. Narváez, A. C. *et al.* Cathodoluminescence Microscopy of nanostructures on glass substrates. *Opt. Express* **21,** 29968 (2013).
7. Morrison, I. E. G. *et al.* Multicolour correlative imaging using phosphor probes. *J. Chem. Biol.* **8,** 169–177 (2015).
8. Furukawa, T. *et al.* High-resolution microscopy for biological specimens via cathodoluminescence of Eu- and Zn-doped Y_2O_3nanophosphors. *Opt. Express* **21,** 25655 (2013).
9. Fukushima, S. *et al.* Y2O3: TM,Yb nanophosphors for correlative upconversion luminescence and cathodoluminescence imaging. *Micron* **67,** 90–95 (2014).
10. Fukushima, S. *et al.* Correlative near-infrared light and cathodoluminescence microscopy using Y2O3:Ln, Yb (Ln = Tm, Er) nanophosphors for multiscale, multicolour bioimaging. **6,** 25950 (2016).
11. Schirhagl, R., Chang, K., Loretz, M. & Degen, C. L. Nitrogen-vacancy centers in diamond: nanoscale sensors for physics and biology. *Annu. Rev. Phys. Chem.* **65,** 83–105 (2014).
12. Zhu, Y. *et al.* The biocompatibility of nanodiamonds and their application in drug delivery systems. *Theranostics* **2,** 302–312 (2012).
13. Mohan, N., Chen, C. S., Hsieh, H. H., Wu, Y. C. & Chang, H. C. In vivo imaging and toxicity assessments of fluorescent nanodiamonds in caenorhabditis elegans. *Nano Lett.* **10,** 3692–3699 (2010).
14. Nagl, A., Hemelaar, S. R. & Schirhagl, R. Improving Surface and Defect Center Chemistry of Fluorescent Nano-Diamonds for Imaging Purposes – A Review. *Anal. Bioanal. Chem.* (2015). doi:10.1007/s00216-015-8849-1
15. Faklaris, O. *et al.* Detection of single photoluminescent diamond nanoparticles in cells and study of the internalization pathway. *Small* **4,** 2236–2239 (2008).
16. McGuinness, L. P. *et al.* Quantum measurement and orientation tracking of fluorescent nanodiamonds inside living cells. *Nat. Nanotechnol.* **6,** 358–363 (2011).
17. Pope, I. *et al.* Coherent anti-Stokes Raman scattering microscopy of single nanodiamonds. *Nat. Nanotechnol.* **9,** 940–946 (2014).
18. Hemelaar, S. R. *et al.* The interaction of fluorescent nanodiamond probes with cellular media. *Microchim. Acta* 1–9 (2017). doi:10.1007/s00604-017-2086-6
19. Balasubramanian, G. *et al.* Nanoscale imaging magnetometry with diamond spins under ambient conditions. *Nature* **455,** 648–651 (2008).

20. Van Oort, E. & Glasbeek, M. Electric-field-induced modulation of spin echoes of N-V centers in diamond. *Chem. Phys. Lett.* **168,** 529–532 (1990).
21. Acosta, V. M. *et al.* Temperature dependence of the nitrogen-vacancy magnetic resonance in diamond. *Phys. Rev. Lett.* **104,** (2010).
22. Müller, T. *et al.* Wide-range electrical tunability of single-photon emission from chromium-based colour centers in diamond. *New J. Phys.* **13,** (2011).
23. Zhang, H. *et al.* Silicon-vacancy color centers in nanodiamonds: Cathodoluminescence imaging markers in the near infrared. *Small* **10,** 1908–1913 (2014).
24. Nagarajan, S. *et al.* Simultaneous cathodoluminescence and electron microscopy cytometry of cellular vesicles labeled with fluorescent nanodiamonds. *Nanoscale* **8,** 11588–11594 (2016).
25. Nawa, Y. *et al.* Multi-color imaging of fluorescent nanodiamonds in living HeLa cells using direct electron-beam excitation. *ChemPhysChem* **15,** 721–726 (2014).
26. Ong, S. Y., Chipaux, M., Nagl, A. & Schirhagl, R. Shape and crystallographic orientation of nanodiamonds for quantum sensing. *Phys. Chem. Chem. Phys.* (2017).
27. De Leij, L., Helrich, W., Stein, R. & Mattes, M. J. SCLC cluster2 antibodies detect the pancarcinoma/epithelial glycoprotein EGP2. *Int. J. Cancer* **57,** 60–63 (1994).
28. Schnell, U., Kuipers, J. & Giepmans, B. N. G. EpCAM proteolysis: new fragments with distinct functions? *Biosci. Rep.* **33,** e00030 (2013).
29. Schindelin, J. *et al.* Fiji: an open-source platform for biological-image analysis. *Nat. Methods* **9,** 676–682 (2012).
30. Loretz, M., Pezzagna, S., Meijer, J. & Degen, C. L. Nanoscale nuclear magnetic resonance with a 1.9-nm-deep nitrogen-vacancy sensor. *Appl. Phys. Lett.* **104,** (2014).
31. Ofori-Okai, B. K. *et al.* Spin properties of very shallow nitrogen vacancy defects in diamond. *Phys. Rev. B - Condens. Matter Mater. Phys.* **86,** (2012).
32. Chipaux, M. *et al.* Magnetic imaging with an ensemble of Nitrogen Vacancy centers in diamond. *arXiv* 10 (2014). doi:10.1140/epjd/e2015-60080-1
33. Lin, H. H. *et al.* Tracking and Finding Slow-Proliferating/Quiescent Cancer Stem Cells with Fluorescent Nanodiamonds. *Small* **11,** 4394–4402 (2015).
34. Chu, Z. *et al.* Rapid endosomal escape of prickly nanodiamonds: implications for gene delivery. *Sci. Rep.* **5,** 11661 (2015).
35. Peddie, C. J. *et al.* Correlative and integrated light and electron microscopy of in-resin GFP fluorescence, used to localise diacylglycerol in mammalian cells. *Ultramicroscopy* **143,** 3–14 (2014).
36. Paez-Segala, M. G. *et al.* Fixation-resistant photoactivatable fluorescent proteins for CLEM. *Nat. Methods* **12,** 215–218 (2015).
37. Kukulski, W. *et al.* Precise, Correlated Fluorescence Microscopy and Electron Tomography of Lowicryl Sections Using Fluorescent Fiducial Markers. *Methods Cell Biol.* **111,** 235–257 (2012).
38. Kukulski, W. *et al.* Correlated fluorescence and 3D electron microscopy with high sensitivity and spatial precision. *J. Cell Biol.* **192,** 111–119 (2011).
39. Ascarelli, P. *et al.* Secondary electron emission from diamond: Physical modeling and application to scanning electron microscopy. *J. Appl. Phys.* **89,** 689–696 (2001).
40. Tizei, L. H. G. & Kociak, M. Spectrally and spatially resolved cathodoluminescence of nanodiamonds: local variations of the NV(0) emission properties. *Nanotechnology* **23,** 175702 (2012).

Supplementary information

Supplementary text S1: Quantification of diamonds in cells

In order to quantify internalized particles we have developed a script to be used in the image analysis software FIJI (Fiji Is Just ImageJ, https://fiji.sc/). The analysis was divided into three phases: Cell Selection, Masking and Particle Analysis. During the first phase, the images were visually inspected and random cells were selected for the analysis. Cells in which aggregates associated with the cell membrane were rejected to prevent false positive results. The images were composed of several slices (z-stacks), the cell's region was defined in all the three dimensions. In the horizontal plane, the selection considered an area containing only the cell of interest. In the height, the first and last slices containing the cell were identified. As a result, the first phase defines a volume that holds only the cell of interest. In the Masking phase, that volume is molded in order to resemble the shape of the cell. The image is converted to binary (using the Isodata algorithm to calculate the threshold)[1] then the cell's perimeter is detected in every slice. To find the inner volume of the cell, the program shrinks the cell's region in order to exclude the cell membrane from the analysis. The final step uses a special function of Fiji, which analyzes the particles found in a region. Applying this function to the masked image, it is possible to directly obtain the amount of particles (connected components) in the specified region. The performance of this process is set mainly by the parameter "threshold". The threshold is used to separate the background light from the signal emitted by the FNDs. Every pixel with intensity less than the threshold is assumed as background and deleted from the image (set as black) while every pixel with an intensity greater or equal than the threshold is assumed as part of a particle. To find an adequate value for this parameter, the image was visually inspected and different values were probed. Finally, the choice was made in favor of removing more background signal, but without deleting particles clearly identified, which showed no signal inside cells without FNDs. As a result, the process provides the number of particles, which are found in every analyzed cell.

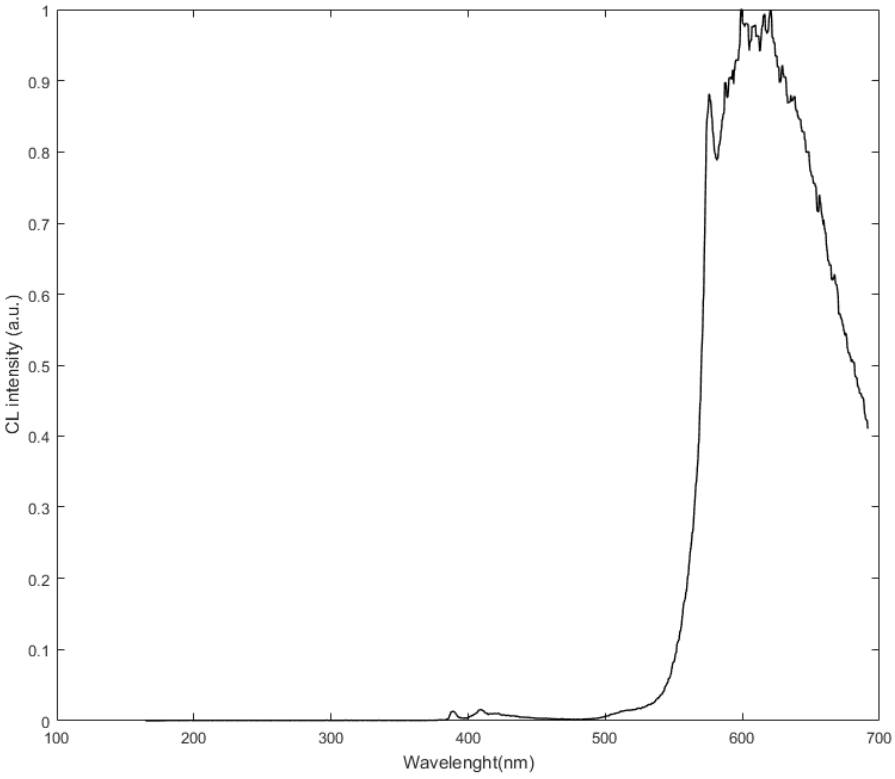

Supplementary Figure 1: Cathodoluminescence spectrum from NV0 recorded while exciting with the electron beam

References

1. Torrano, A. a *et al.* A fast analysis method to quantify nanoparticle uptake on a single cell level. *Nanomedicine* **8,** 1815–1828 (2013).

Discussion

Simon R. Hemelaar

"Simon builds a fluorescent nanodiamond foundation"

Scientific Relevance

Fluorescent nanodiamonds have been identified for some time to be powerful and promising nanoscale probes.[1] FNDs have been used in the field of quantum physics,[2] spectroscopy[3] and biology.[4,5] The diamond particles can be used to measure a large variety of quantities inside the cells, such as temperature,[6] redox state or pH.[7] Although the theory of these analyses has been there for quite some years, the biology aspect remained a hurdle for the world of diamond magnetometry. This thesis covers part of the most recent advances in the field of *in vitro* fluorescent nanodiamond applications.

Compatibility

The Nitrogen-Vacancy (NV) center in diamond particles is the most important copmonent when it comes to quantum measurements. Its sensitivity for electron spins is rather high, but its range is limited to tens of nanometers. With a particle which is shaped like a flake[8] and which has a diameter of average 70 nm (meaning that it is longer and wider than it is high), limits the measureable surrounding. To make sure that the diamond particle can get close enough to its target, it is important that it is not surrounded by other diamond particles. The process of aggregation describes particles sticking together to form a more stable agglomeration, reducing the measurable distance and obscuring the signal, by having more NV-centers in different directions. In **Chapter 2** we tackled the aggregation behavior of diamonds in cellular medium, by adding serum proteins. Although the proteins decrease the diamond's sensing range, the prevention of aggregation is highly beneficial. Colloidally stable particles improve the uptake into cells which are otherwise less likely to take up particles because of the particle size. Some cell lines however, such as HT29 colon carcinoma cells or yeast cells, do not even take up colloidally stable diamond nanoparticles. Several different coatings including vesicles such as liposomes or charged proteins[9] can be utilized to trick cells into taking up a wide range of particles. Yeast cells have a double barrier to overcome; external to the cell membrane which is also present in mammalian cells, the cell wall proves an even tougher hurdle to overcome. In this case the coating approach alone is not sufficient and more invasive techniques need to be utilized. Such techniques are validated in **Chapter 3.** We adopted a method for the transfection of yeast cells to allow diamond uptake. Then we devised a software based method to give a relative estimate of the internalized diamonds. This relative measure gives a success rate for the transformation technique. Although exactly quantifying the number of diamonds is limited by the current techniques, it would be very useful in trying to get single diamonds into cells. This could be estimated by measuring the average intensity of a single particle and comparing it to a bright spot / aggregate in a sample. However, these techniques are not both as high throughput and easy to carry out as the technique noted here before. Transformation of the yeast cells does not show any direct effect on the viability of the cells. Analysis of specific genetic and protein alterations should prove if the diamonds and the technique have no adverse effect

on yeast cells. In mammalian cells, genetic and proteomic changes appear to remain to a minimum after diamond uptake, as shown in **Chapter 4**.

Applications

As mentioned before, the possible uses of FNDs in intracellular quantum measurements are numerous. However, when an internalized diamond particle is at a random position within the cell the usefulness of the measurements is limited. Targeting the nanodiamonds towards specific cell organelles has multiple advantages. First, it makes searching for the diamond in a confocal image easier, when only the nuclear envelope has to be examined, for example. In addition, it allows for very localized analyses. Therefore, in **Chapter 5,** we investigated successful targeting of nanodiamond particles using adsorbed primary antibodies. After 24 hours of incubation, the majority of diamond particles resides near the nuclear region. The targeting of nanodiamonds has also been proven in **Chapter 6**, where extracellular domains of transmembrane proteins were labelled. Here also another unique characteristic of diamonds and NV-centers was proven: the conservation of fluorescence after Epon embedding. Normally, when researchers do an immunological staining and subsequently prepare their samples for electron microscopy, the fluorescent dye is destroyed and hence the immunological information is lost. Employing an antibody-FND targeting strategy, this problem of damaged dyes will be one of the past.

Alternatives to NV containing diamond nanoparticles

This thesis revolved around the nanodiamond with a nitrogen vacancy defect inside. There are notably more diamond defects which can be utilized for quantum measurements. The Silicon Vacancy defect (SiV) differs from the NV in its light emission; it has a very narrow Zero-Phonon Line (part of light spectrum where there suddenly is a relatively high intensity of emitted photons), where approximately 70% of its fluorescence is generated. This makes it ideal in single photon applications such as quantum key distribution.[10,11] However, it has not the same remarkable properties as can be found in NV-centers such as the possibility to use it at room temperature, and the relatively long coherence spin time of ODMR measurements under these conditions. The field of quantum measurements using diamond defects is relatively young, and the characteristics of other defects are still being recorded.[12–14] Although these defects differ in their applications from the nitrogen vacancy center and require different measurement setups, they can all be realized in nanodiamond particles. This means that the results of **Chapters 2-5** are also likely to be applicable to these research domains, paving the way for even more intracellular quantum measurements. Apart from diamond defects there are also other potential materials such as silicon carbide, which can host defects that also can be used in quantum measurements.[15] So far, however, the NV-centers holds the record in sensitivity and outperform other defects with regard to quantum sensing.

Opportunities in biological systems – use in people and animals

Clinicians often pose us the question: "How are you going to utilize it in humans?" The goal of our research has so far been to establish this technique *in vitro* and not (yet) to utilize the fluorescent nanodiamonds in live animal cells. However, there are some potential targets in animals for research topics. Before progressing to this kind of research, there are prerequisites which need to be met. Focussing less on biological safety, as we can expect that the diamond should be compatible (**Chapter 4**). First, the tissue surrounding the diamond should be transparent enough to allow emission and excitation of the diamond. Second, the background fluorescence should be at a low enough level that the fluctuations of the NV-center could still be detected. These prerequisites were met by the *C. elegans* model of Mohan[4] or could be combined with the glass window in mice, as demonstrated by Xu.[16]

Future directions of this research group

Detection of free radicals using T1 measurements will soon be demonstrated as a proof of principle in our laboratory. Utilizing other pulsing schemes will give more information on the characteristics of the free radicals. For example, Double Electron-Electron Resonance (DEER) allows the differentiation between species of radicals, to separate for example $ONOO^-$ from *OH and O_2^{-}.[17] Furthermore, our radical sensing technique could be used to analyze the mechanisms of drugs in scavenging or producing free radicals, with precise information of location, species, lifetime and target. When these experiments can be performed in a high throughput and reliable manner, this research group, and indeed the field, should focus on carrying out more sensitive magnetometry measurements. As all atoms that are visible with conventional magnetic resonance techniques (with a non-zero spin) can be detected, a similar map as produced in MRI techniques can be made, but then with nanoscale resolution. This would for example allow to follow the process of protein folding in real time, or the transcription of proteins from mRNA. The pinnacle of this biological research field will be to make a complete 3D map of a cell, using either moving or evenly distributed nanodiamonds in a cell.

References

1. Schirhagl, R., Chang, K., Loretz, M. & Degen, C. L. Nitrogen-vacancy centers in diamond: nanoscale sensors for physics and biology. *Annu. Rev. Phys. Chem.* **65,** 83–105 (2014).
2. Hensen, B. *et al.* Loophole-free Bell inequality violation using electron spins separated by 1.3 kilometres. *Nature* **526,** 682–686 (2015).
3. Pope, I. *et al.* Coherent anti-Stokes Raman scattering microscopy of single nanodiamonds. *Nat. Nanotechnol.* **9,** 940–946 (2014).
4. Mohan, N., Chen, C. S., Hsieh, H. H., Wu, Y. C. & Chang, H. C. In vivo imaging and toxicity assessments of fluorescent nanodiamonds in caenorhabditis elegans. *Nano Lett.* **10,** 3692–3699 (2010).
5. Haziza, S. *et al.* Fluorescent nanodiamond tracking reveals intraneuronal transport abnormalities induced by brain-disease-related genetic risk factors. *Nat. Nanotechnol.* **12,** 322–328 (2016).
6. Kucsko, G. *et al.* Nanometre-scale thermometry in a living cell. *Nature* **500,** 54–8 (2013).
7. Rendler, T. *et al.* Optical imaging of localized chemical events using programmable diamond quantum nanosensors. *Nat. Commun.* **8,** 14701 (2017).
8. Ong, S. Y., Chipaux, M., Nagl, A. & Schirhagl, R. Shape and crystallographic orientation of nanodiamonds for quantum sensing. *Phys. Chem. Chem. Phys.* (2017). doi:10.1039/C6CP07431F
9. Zheng, T. *et al.* Recombinant Protein Polymers for Colloidal Stabilization and Improvement of Cellular Uptake of Diamond Nanosensors. *Anal. Chem.* **89,** 12812–12820 (2017).
10. Leifgen, M. *et al.* Evaluation of nitrogen- and silicon-vacancy defect centers as single photon sources in quantum key distribution. *New J. Phys.* **16,** (2014).
11. Neu, E. *et al.* Single photon emission from silicon-vacancy colour centers in chemical vapour deposition nano-diamonds on iridium. *New J. Phys.* **13,** (2011).
12. Jelezko, F. & Wrachtrup, J. Single defect centers in diamond: A review. *Physica Status Solidi (A) Applications and Materials Science* **203,** 3207–3225 (2006).
13. Shaw, M. J. *et al.* Importance of quantum tunneling in vacancy-hydrogen complexes in diamond. *Phys. Rev. Lett.* **95,** (2005).
14. Morfa, A. J. *et al.* Single-photon emission and quantum characterization of zinc oxide defects. *Nano Lett.* **12,** (2012).
15. Koehl, W. F., Buckley, B. B., Heremans, F. J., Calusine, G. & Awschalom, D. D. Room temperature coherent control of defect spin qubits in silicon carbide. *Nature* **479,** 84–87 (2011).
16. Xu, H.-T., Pan, F., Yang, G. & Gan, W.-B. Choice of cranial window type for in vivo imaging affects dendritic spine turnover in the cortex. *Nat. Neurosci.* **10,** 549–551 (2007).
17. Mamin, H. J., Sherwood, M. H. & Rugar, D. Detecting external electron spins using nitrogen-vacancy centers. *Phys. Rev. B - Condens. Matter Mater. Phys.* **86,** (2012).

Summary / Samenvatting

Simon R. Hemelaar

Summary

Fluorescent NanoDiamonds (FNDs) are a promising new biosensor. They are chemically synthesized diamond particles with a diameter between 10 and a couple 100 nanometers (1 nanometer is 1 millionth of a millimeter). These particles consist (mainly) of carbon. Thus they share several key properties with bulk diamonds. For example, they are pressure resistant, have sharp edges and are chemically inert. Inside, two neighboring carbon atoms are replaced. One is replaced by a nitrogen atom, another by a vacancy, this is called the nitrogen vacancy (NV) center. The centers can be produced by irradiation and one diamond can contain one or more (up to thousands) of NV-centers. This 'defect' in the diamond gives it a wide range of interesting properties. First and foremost, the center is fluorescent, meaning that it can emit a certain color of light (in this case red) when shined upon with a different color of light (in this case yellow green). This property can be utilized in confocal microscopy, where different wavelengths (colors) of light are used to image structures of interest. The diamonds also can emit their red light when excited by an electron beam, which is what happens in electron microscopy, this technique is called cathodoluminescence. But wait, there's more! The emitted red light of the diamond can be influenced by several parameters such as its magnetic surrounding, the temperature and pressure, to name a few.

This means that by observing the (fluctuations in the) light from a fluorescent nanodiamond, you can trace back the magnetic surrounding. This will then allow you to make a molecular map of certain species within a couple of nanometers of the diamond. In our research lab, we want to use Fluorescent NanoDiamonds to detect molecules of interest inside cells. There are however a couple of obstacles which need to be overcome before this can be used in a high throughput manner.

In **Chapter 1** a scientific background is sketched and the gaps in research concerning FNDs are revealed. Specific focus lies on the different kind of diamonds and the mechanism of the Nitrogen-Vacancy center, as well as different quantum sensing techniques to detect the influences on its fluorescence. Further, primary literature concerning nanodiamonds and biology is discussed. Finally, the aims of this thesis are introduced.

One of the first problems we encountered was the aggregation of FNDs in cellular media. Aggregation can be caused by multiple parameters, such as the ionic balance or the size of particles. We found that fluorescent nanodiamonds tended to cluster together in medium which is used to culture cells, producing aggregates which were up to a 100 fold bigger in diameter than a single particle. These aggregates are formed by interaction of the diamond surface with a combination of proteins and salts in the cellular medium. The analysis of this aggregation process and the prevention of it are discussed in **Chapter 2.** By collecting the aggregated complexes from medium, we could determine the protein composition on these aggregates. This revealed an even distribution of iso-electric points (the overall charge of a

protein), ruling out the option that the aggregation was driven by only proteins with a specific charge. Next we analyzed the surface of the aggregated diamonds using X-Ray Photoelectron Spectroscopy (XPS), which can detect the elements on a specific surface. We found that salts greatly contribute to the formation of larger aggregates. Ultimately, we showed that aggregation was caused by an interplay of salts and proteins and it could be prevented using Fetal Bovine Serum. Fetal Bovine Serum, one of the major components (10%) of normal medium for cells to grow in, can be used to adhere a thin protein corona on the surface of the diamond particles before the particles are added to the full medium. Because the serum is already used in cellular media, it does not introduce any unwanted compounds. Using dynamic light scattering, we observed that the size of diamonds only increased roughly 30%, greatly counteracting the size increase of the aggregates. This is an important step in FND research, because it is of high relevance that the diamond can get as close as possible to the molecules of interest.

A physical obstacle which needs to be overcome for some cell types is the cell wall. Present in yeast, bacterial and plant cells, the cell wall is a structural layer on the outside of the cell membrane. It makes cells more rigid and allows for a better control of osmolarity and transport of molecules. This also results in the absence of FND uptake. **Chapter 3** discusses different methods of manipulating yeast cells in taking up nanodiamond particles. An analysis of different physical conditions, such as keeping the cells in the dark during the diamond uptake period, shows no changes in uptake. So the cells must be further 'persuaded' by a process of chemical or electrical cell wall disruption. A mixture of chemicals or a sequence of electric pulses was tested to increase uptake. The electrical transformation resulted in a high amount of cell death, with levels of viability decreasing to approximately 1%, while not showing the clear increase in diamond uptake we hoped for. Chemical transformation is less invasive, while the uptake of nanodiamonds increases significantly. The uptake is estimated using a protocol written for FIJI software, which can also be used for quantifying other (fluorescent) particles.

The (loss off) viability is often considered as a hallmark for the health of the cell. For our measurements it is of the utmost importance that cells apart from surviving the process also still behave in a normal fashion. To this end we performed a more elaborate evaluation of influences on the cell biology including non-fatal influences. In **Chapter 4,** we incubated HeLa cells, a model cell line for cancer research, with different sizes, shapes and concentrations of diamonds at different time points. We also included diamond aggregates to see if the aggregates or the prevention measures suggested in **Chapter 2** affected the cells health in any way. The HeLa cells were evaluated on different parameters for the quality of their internal homeostasis. Metabolic activity, overall free radical production, changes in genetic behavior and up or down regulation of proteins were correlated to the amount of uptaken diamond particles. The nanodiamonds did not change normal cell homeostasis and it can be concluded that they are safe for use, especially at common working concentrations for magnetometry (around 1 µg/ml).

In **Chapter 5** we have resolved an interesting question in the targeting of diamond particles. It has been disputed that covalent immobilization works better to attach antibodies on the surface of nanodiamonds than physical adsorption. Here we have put this to the test and found that both approaches can be favorable in specific situations, by targeting the cellular nucleus. We have tested a wide range of different antibody diamond concentration ratio's, incubation times and various protocol adjustments to target the nucleus as efficient as possible. By making Euclidian Distance Maps of our confocal images, we were able to compare the distance of a particle to the nucleus between different conditions. When using adsorbed antibody-diamonds, one can incubate these with cells for a prolonged time, about 24 hours, and then find the majority of the diamond particles within close range of the nucleus. When using cells which are fixated, which more closely resembles the traditional methods of immunostaining, diamond particles which are covalently bound to a secondary antibody show more promising results. In addition, using our homebuilt confocal microscope, we designed a way to precisely follow the diamond particle as it moves inside a cell and make a trajectory of this path. By using mathematical equations in special software, we can display and measure a wide range of parameters which tell something about how the diamond particle is moving exactly.

One important use of nanodiamonds, as mentioned before, is their possibility to be excited using an electron beam. In **Chapter 6,** we used fluorescent nanodiamonds for two different biological goals. First, we wanted to visualize uptake of nanodiamonds in macrophages. Second, we connected diamonds indirectly to antibodies, utilizing them as an immunological label. Streptavidin was adsorbed on the surface of FNDs, and this was used to link to biotin. The biotin streptavidin connection is a famous one in biology and is a very hard to disrupt non-covalent bond. The biotin was conjugated to a secondary antibody. These secondary antibodies are relatively cheap and react with the outward directing domain on the antibody from a specific species of animal. The primary antibody used here was against a transmembrane protein of a cell called HT29. In this colon carcinoma cell, the protein called EpCAM was overexpressed and fused to a Green Fluorescent Protein (GFP). This allowed simultaneous visualization of the EpCAM and the fluorescence of the nanodiamond, giving a measure for the quality of the immunological labeling. Adsorbing streptavidin on the surface of the diamond particles allows the diamonds to be used for any indirect immunological labeling and greatly increases its usefulness. All samples we gained from these experiments were imaged in three different setups: (1) a conventional confocal microscope, (2) a homebuilt confocal microscope / magnetometer and (3) an integrated electron microscope. In the conventional confocal microscope, we observed that the nanodiamonds and GFP were present before the preparation for electron microscopy, but only the nanodiamonds were visible after. This happens during the process of post fixation (part of the preparation protocol) in which Osmium tetroxide is used. A chemical which destroys the fluorescence from fluorescent proteins or organic dyes. Since the NV-center is inside the extremely resistant nanodiamond particle, its fluorescence is retained. In our homebuilt microscope we could see that even after this preparation, there was still the possibility to make an Optically Detected

Magnetic Resonance spectrum, which is signatory for the NV-center. Finally, in the integrated electron microscope, we demonstrated that we could not only identify the nanodiamonds using secondary electron detection, but also with the cathodoluminescent signal. With both modalities we could resolve single particles.

Finally, in **Chapter 7**, the results of this thesis are discussed in the light of recent findings. The alternatives for fluorescent nanodiamonds are discussed and the implications of these results are extrapolated to other particles and fields. In the end, an outlook is on future directions for this field of research and an ultimate goal is proposed.

Samenvatting

Fluorescente nanodiamanten (FNDs) zijn een nieuwe en veelbelovende biosensor. Het zijn chemische geproduceerde diamantdeeltjes met een diameter tussen 10 en een paar 100 nanometer (1 nanometer is 1 miljoenste van een millimeter). Deze deeltjes bestaan (voornamelijk) uit koolstof. Vandaar dat ze verscheidene belangrijke eigenschappen delen met grotere diamanten. Ze kunnen bijvoorbeeld beiden goed tegen druk, hebben scherpe randen en zijn chemisch non-reactief. In onze nanodiamanten zijn twee naastgelegen koolstof atomen vervangen; één is vervangen door een stikstof atoom, de andere door een leegte. Dit wordt het Nitrogen-Vacancy (NV) center genoemd. De centers kunnen geproduceerd worden door bestraling en een enkele diamant kan één of meer (tot duizenden) NV-centers bevatten. Dit 'defect' in de diamant geeft een breed scala aan interessante eigenschappen. Ten eerste is het center fluorescent, wat betekent dat het een bepaalde kleur licht kan uitstralen (in dit geval rood) wanneer er op geschenen wordt met een andere kleur licht (in dit geval geelgroen). Deze eigenschap kan gebruikt worden in confocale microscopie, waar verschillende golflengten (kleuren) licht worden gebruikt om interessante structuren te visualiseren. De diamanten kunnen hun rode licht ook uitstralen wanneer ze geactiveerd worden door een elektronenstraal, zoals in elektronenmicroscopie. Deze techniek heet cathodoluminescentie. Maar wacht, er is meer! Het uitgestraalde rode licht van de diamanten kan beïnvloed worden door bepaalde parameters zoals de magnetische omgeving, de temperatuur en de druk, om er een paar te noemen.

Dit betekent dat door het observeren van (schommelingen in het) licht van fluorescente nanodiamanten, je de magnetische omgeving kan herleiden. Dit geeft de mogelijkheid om een moleculaire kaart van interessante structuren binnen een paar nanometer van de diamant te maken. In ons onderzoekslab willen we fluorescente nanodiamanten gebruiken om specifieke moleculen in cellen te detecteren. Er zijn echter een aantal obstakels welke overwonnen moeten worden, voordat we dit op een efficiënte manier kunnen gebruiken.

In **Hoofdstuk 1** wordt een wetenschappelijke achtergrond geschetst en worden de hiaten in het onderzoek rondom FNDs blootgelegd. Er ligt een specifieke focus op de verschillende soorten diamanten en het mechanisme van het Nitrogen-Vacancy center, evenals verschillende kwantum meettechnieken om de schommelingen in de fluorescentie te detecteren. De primaire literatuur rondom nanodiamanten en biologie worden eveneens bediscussieerd. Tenslotte worden de doelen van deze thesis geïntroduceerd.

Één van de eerste problemen die we ervoeren was de aggregatie van FNDs in medium voor cellen. Aggregatie kan verschillende oorzaken hebben, zoals de ionenbalans of de grootte van de deeltjes. Wij ontdekten dat de fluorescente nanodiamanten beginnen te clusteren wanneer ze werden gemengd in medium dat voor het groeien van cellen gebruikt wordt. Dit leverde aggregaten op die tot 100 keer groter waren in diameter dan een enkel deeltje. Deze aggregaten vormden zich door interactie

van het diamantoppervlak met een combinatie van eiwitten en zouten in het celkweekmedium. De analyse van het aggregatieproces en de preventie ervan worden bediscussieerd in **Hoofdstuk 2.** Door het verzamelen van geaggregeerde complexen uit het medium konden we de compositie hiervan bepalen. Dit onthulde dat er een gelijke verdeling was van iso-elektrische ladingen (de gemiddelde lading van een eiwit), wat bewees dat de aggregatie niet alleen veroorzaakt werd door eiwitten met één specifieke lading. Vervolgens analyseerden we het oppervlak van de geaggregeerde diamanten met X-Ray Photoelectron Spectroscopie (XPS), wat specifieke elementen op een oppervlak kan detecteren. We vonden dat zouten voor een groot deel bijdroegen aan de vorming van grotere aggregaten. Uiteindelijk lieten we zien dat de aggregatie veroorzaakt wordt door een samenspel aan zouten en eiwitten en dat deze voorkomen kan worden met behulp van foetaal kalfserum (Fetal Bovine Serum, FBS). FBS, één van de basis ingrediënten (10%) van normaal celkweekmedium, kan gebruikt worden om een dunne eiwit corona op het oppervlak van diamantdeeltjes te organiseren voordat de deeltjes toegevoegd worden aan het volledige medium. Omdat het serum al een onderdeel is van het kweekmedium, introduceert het geen ongewilde stoffen. Met een techniek bekend als dynamische licht verstrooiing vonden we dat de grootte van de diamantdeeltjes diameter maar 30% toenam dat en het aggregatie probleem grotendeels kon worden teruggedraaid. Dit is een zeer belangrijke stap in het FND onderzoek, omdat het van groot belang is dat de diamant zo dichtbij interessante moleculen moet kunnen komen als mogelijk is.

Een fysiek obstakel dat moet worden overwonnen in sommige cellen is de celwand. Aanwezig in gist-, bacterie- en plantcellen. De celwand bestaat uit een structurele laag aan de buitenkant van de celmembraan. Het maakt cellen steviger en geeft ze meer controle over de waterbalans en het transport van moleculen in en uit de cel. Hierdoor nemen deze cellen ook geen nanodiamanten op. **Hoofdstuk 3** bespreekt verschillende methoden om gistcellen te motiveren om nanodiamantdeeltjes op te nemen. Een analyse van verschillende fysieke condities, zoals het houden van de cellen in het donker gedurende de opnameperiode, liet geen veranderingen in de opname zien. Dit betekende dat de cellen 'overgehaald' moesten worden met een chemische of elektrische verstoring van de celwand. Daarom werden een mix van chemicaliën en een serie elektrische pulsen getest om de opname te verhogen. De elektrische transformatie resulteerde in een hoge celdood, met een levensvatbaarheid van 1% van de cellen, terwijl het niet de grote diamantopname toonde waar we op gehoopt hadden. Chemische transformatie was minder stressvol, terwijl de diamantopname significant verhoogd wordt. De opname werd geschat met een protocol dat geschreven was voor FIJI software, welke ook gebruikt kan worden voor het kwantificeren van toekomstige andere (fluorescente) deeltjes.

Het (verlies van) levensvatbaarheid wordt vaak gezien als het kenmerk voor de gezondheid van een cel. Voor ons is het van het hoogste belang dat cellen los van overleven, zich ook nog steeds op een normale manier gedragen. Vandaar dat wij een uitgebreide evaluatie hebben uitgevoerd van de invloeden van nanodiamanten op de

celbiologie, rekening houdend met ook niet fatale gevolgen. In **Hoofdstuk 4** hebben we HeLa cellen, een gerenommeerd model voor kankeronderzoek, geïncubeerd met verschillende groottes, vormen en concentraties van nanodiamanten, met verschillende tijdsspannen. We hebben ook geaggregeerde nanodiamanten gebruikt om te zien of de aggregaten of de voorgestelde preventiemaatregel uit **Hoofdstuk 2** de gezondheid van de cellen op een negatieve manier beïnvloeden. De HeLa cellen werden geëvalueerd op verschillende parameters om de kwaliteit van hun interne homeostase te kunnen beoordelen. De metabolische activiteit, de totale productie van radicalen, veranderingen in genetisch gedrag en de regulering van eiwitten werden gecorreleerd aan het aantal geschatte opgenomen diamantdeeltjes. De nanodiamanten hadden geen invloed op de normale homeostase van de cel en kunnen beschouwd worden als veilig in gebruik, zeker wanneer het gebruikt wordt in gebruikelijke concentraties voor magnetometrie (rond 1 µg/ml).

In **Hoofdstuk 5** hebben we een interessante vraag opgelost in het veld van het sturen van diamantdeeltjes. In dit veld wordt stevig gediscussieerd of het covalent hechten van antilichamen op het oppervlakte van nanodiamanten beter werkt dan fysische adsorptie. Hier hebben wij dit vergeleken en gevonden dat beide methodes werken in specifieke situaties, waarbij wij op de nucleus van de cel aangestuurd hebben. We hebben een grote variatie aan verschillende antilichaam-diamant concentratieratio's, incubatietijden en verschillende protocolaanpassingen getest om de diamant zo efficiënt mogelijk bij de celkern te krijgen. Door het maken van Euclidian Distance Maps van onze confocale beelden, konden wij de afstand van de deeltjes tot de nucleus in de verschillende condities vergelijken. Door middel van geadsorbeerde antilichaam-diamanten kan men deze na een lange incubatie tijd, ongeveer 24 uur, grotendeels terugvinden in kort bereik van de nucleus. Wanneer cellen worden gebruikt die gefixeerd zijn (een techniek die meer lijkt op traditionele immunohistologie) laten diamanten die covalent gebonden zijn aan een secundair antilichaam veelbelovende resultaten zien. Daarbij hebben we met onze zelfgebouwde confocale microscoop een protocol ontworpen om de diamant heel precies te volgen bij zijn reis door de cel en daarmee een traject te maken van het pad dat de diamant aflegt. Met behulp van wiskundige vergelijken in speciale software konden we een grote variëteit aan parameters beschouwen die ons meer vertellen over de exacte bewegingen die het diamantdeeltje in de cel maakt.

Een belangrijke eigenschap van fluorescente nanodiamanten, zoals initieel genoemd, is de mogelijkheid om geactiveerd te worden met een elektronenstraal. In **Hoofdstuk 6** hebben we fluorescente nanodiamanten gebruikt om een licht te schijnen op twee verschillende biologische vraagstukken. Ten eerste wilden we de opname van nanodiamanten in macrofagen visualiseren. Ten tweede hebben we de diamanten op een indirecte manier verbonden aan antilichamen, zodat we ze konden utiliseren als een immunologisch label. Streptavidine werd geadsorbeerd op het oppervlak van FNDs, en dit werd gebruikt om het te verbinden aan biotine. De biotine-streptavidine verbinding is beroemd binnen de biologie om zijn zeer moeilijk te verbreken connectie. Het gebruikte Biotine was geconjugeerd aan een secundair

antilichaam. Deze secundaire antilichamen zijn relatief goedkoop en reageren met het naar buiten gerichte dierspecifieke domein van een primair antilichaam. Het primaire antilichaam was gericht tegen een transmembraan eiwit van een cellijn die HT29 genoemd wordt. In deze coloncarcinoom cel wordt het eiwit EpCAM extra veel geproduceerd. In dit geval was EpCAM ook gefuseerd met een groen fluorescent eiwit (GFP), waardoor de visualisering van EpCAM en de visualisering van de nanodiamanten tegelijkertijd mogelijk was. Hiermee kon een maat gegeven worden aan de kwaliteit van de immunologische labeling. Adsorptie van streptavidine op het oppervlak van diamantdeeltjes vergroot de bruikbaarheid van de diamantcomplexen enorm, omdat het gebruikt kan worden om ieder antilichaam met een biotine label aan te tonen. Alle samples die we verkregen van deze experimenten werden gevisualiseerd in drie verschillende opzetten: (1) een traditionele confocale microscoop, (2) een zelf gebouwde confocale microscoop / magnetometer en (3) een geïntegreerde elektronenmicroscoop. In de traditionele confocale microscope vonden we dat de nanodiamanten en het GFP beiden zichtbaar waren vooraf aan de bewerkingen voor elektronenmicroscopie, maar dat alleen de nanodiamanten zichtbaar waren naderhand. Dit komt omdat gedurende het bewerkingsprotocol een post-fixatie stap moet worden uitgevoerd, in welke Osmium tetroxide gebruikt wordt. Deze stof vernietigt de werking van normale fluorescerende eiwitten en organische kleurstoffen. Omdat het NV-center zich bevindt binnenin de extreem resistente nanodiamant, blijft de fluorescentie behouden. In onze zelfgebouwde microscoop konden we zien dat zelfs na deze bereiding het nog steeds mogelijk was om een Optically Detected Magnetic Resonance spectrum te maken, een soort unieke handtekening voor het Nitrogen-Vancy center. Uiteindelijk hebben we gedemonstreerd dat in de geïntegreerde elektronenmicroscoop, we niet alleen de nanodiamanten konden identificeren met secundaire elektronen, maar ook met het cathodoluminescente signaal. Met beide detectie technieken konden we enkele (niet geaggregeerde deeltjes onderscheiden.

Tot slot hebben we deze resultaten bediscussieerd in het licht van recente bevindingen, in **Hoofdstuk 7.** De alternatieven voor fluorescente nanodiamanten worden daar beschouwd en de implicaties van deze resultaten worden geëxtrapoleerd naar andere deeltjes en andere velden van onderzoek. Aan het einde wordt een vooruitzicht gegeven met aanwijzingen voor toekomstige richtingen in dit onderzoeksveld en een ultiem einddoel wordt voorgesteld.

Geachte lezer, dear reader,

You have made it all the way to the end of the thesis (or just skipped most of it to see if your name ended up in the list). This might well be the most important part of my whole thesis, as I can express my gratitude to those without whom this thesis would not have existed in the first place. The fact that my thesis is finished within 4 years and that I have been able to do so many different cool things is the result of a lot of different people who in any small or tremendously large way helped, motivated, supported, lectured, pushed, entertained and intoxicated me. And to all of you I want to give a huge THANK YOU! Thank you big-big![1]

Dear **Romana**, I still very well remember our first meeting, which I later thought of as the most peculiar job interview I ever had. I think we talked 30 minutes about my profile and the PhD position and the remaining two hours about building a Lego Death Star with your lab. Without you I would have never finished my PhD as quick as it is done now. You have ever been so helpful in career advice and always put your (PhD) students and postdocs in the highest priority. I hope you will have a lot more success stories and happy PhD students in the future, show them how it's done!

Not so long ago, in the summer of 2018, **Go** joined this project as co-promotor. I am very glad to have such an enthusiastic scientist strenghten my promotion team and hope he will lead our group to more clinical approaches of research.

I would also like to express my very warm gratitude to the reading committee of my thesis. **Henny**, thank you for being a part as the representative of the department. I am also very grateful to have met **Lou** during my time in the Gopher board and am happy that you accepted to read and weigh my thesis. And of course I was delighted when **François**, who is a big name in the biological nanodiamond field, accepted to be part of my reading committee as well.

Thanks also to the department head **Henk**, for giving us so much freedom in the organization of my thesis and the facilitation of the process.

In addition I would like to express my gratitude to **Nora,** who so awesomely designed all the chapter arts which you see throughout this thesis and the cover art, it has become a lot easier to explain with these illustrations.

This work is the result of a huge amount of synergy within our research group. **Mayeul** and **Felipe** were the people who I have spent almost my whole PhD with and who helped me out in the understanding of physics and programming. **Yori** was the next to join our group and I am very happy that we could share our interest in the multiverse and portals! **Thamir** has invested a huge amount of time in getting

[1] For those I forget to mention, make sure to let me know and there will be a nice ice-cold beer waiting for you.

Chapter 5 finished in time, to which I owe him a great debt. Although **Kiran** and me were grew up in the same village (Nuenen city!) we only got to really know each other in Groningen due to the many projects and not-so-work-related discussions we had together. I had the privilege to meet **Aryan**, who learned me so much about Indonesia, introduced me to her family and was always around to play with Cheddy (our cat). In October of 2017 four new people arrived to come and work in our research group, and I am very happy to have been working with them for the last year. **Charles** has helped me a lot with his programming skills and career advice. Without **Alina** I would not have been able to produce Chapter 5, her never ending computer skills and likewise social communications really made the last months fly. The coming of **Yuchen** was also the start of an era of nicknames, thanks to him I have been a DJ, an IKEA employee and nameless other professions. My Hasselt partner in crime, **Linyan**, is the biggest socializing monster in our group with whom I have been happy to drink countless beers. I am also very happy to have met **Viraj**, an excellent chemist who takes our group on new scientific adventures. I'm sorry to have only have had a short time with **Claudia** and **Rokshana**, while we were in the department simultaneously, I have come to know them as very enthusiastic PhD students.

Over the past few years I have had the privilege to tutor or work together in some way or another with a lot of bright and fun students. So I want to give a big shout out to: **François, Monique, Nienke, Anne, Femke, Andreas, Melissa, David, Johnny, Sona, Sophie, Manon, Else, Babujhi, Severin, Hugo, Mirthe, Bas-Peter, Freya, Julie, Jean-Paul, Nicolas, Citra, Ilja, Ruben, Leyla, Neda and Anam**.

During my four years I have collaborated with a lot of different people from different departments. Most importantly, **Daniele Novarina** helped me a lot with setting up the first yeast experiments. **Pascal de Boer** and **Ben Giepmans** were important collaborators during our cathodoluminescence projects. I also have had wonderful help from and discussions with **Duco Kramer, Jan Visser, Harrie Kampinga, Philip Born** and **Muriel Mari.**

Over the past years I have seen the department of Biomedical Engineering change a lot. The amount of PhD students first decreased and then doubled a couple of times over. I want to thank all of those hard working young scientists. Especially I want to express my gratitude to those who accompanied me during the drinking of coffee or beer: **Philipp, Joe (Qihui), JP (Jiapeng), Rebecca, René, Hilde, Anna (Chongxia), Raquel, Vera, Jeroen, Gwenda, Sara (Lu), Abigail, Edwin, Isabelle, Yoshi, Damla** and **Colin (Wubbalubbadubdub).** I have been helped out countless times by the awesome technical supporting staff of the department, give it up for: **Minie, Ed, Betsy, Willy, Gesinda, Melissa, Willem, Marianne, Reinier, Chris, Hans, Joop, René, Jelly and Corien.** A special thanks go to **Ina** who (wo)mans the secretariat, but more importantly, always is available for a friendly chat! During the staff meetings (and also outside) I have had a lot of interesting interactions with the whole scientific staff of our department: **Prashant, Roel, Theo, Inge, Patrick, Wya, Jelmer, Sarthak, Brandon** and **Daniëlle.**

After I moved to Groningen, I soon got involved in the Groningen Organisation for PhD Education and Recreation (GOPHER). Through Gopher I have made a lot of friends and organized a ton of activities. I want to especially thank the following people for the great times: **Linda, Keri, Christel, Wouter, Ni, Brenda, Els, Antonija, Daniela and Eric.** During one of those many epic GOPHER parties I also met **Maarten**, with whom I have had the pleasure to cook big chunks of meat, drink ample whiskies and have strangely philosophical discussions. Soon after the start of my PhD, I participated in an overnight workshop which lead to the amazing **Allersmaborg Group**, and to my special friendship with **Michael** and **Mirjam**, who were always there for me and pushed my culinary skills in uncharted territory. To release the extra energy build-up during my PhD I started playing baseball, thanks gents of **Caribe HB3 OG**, we had a ball! And last but not least, my squash / waving buddy, Jamaican rock 'n rolls star and every-day-very-busy friend **Halewijn!**

En ook uit Nijmegen zijn jullie met grote getalen 'North of the Wall' gekomen om te kijken hoe de vikingen hier leven. Er ging geen jaar voorbij zonder meerdere bezoeken van mijn homeboys van **M.H.D. Ferus Ebrius**, van piepjong tot oud kwamen ze hier allemaal de 11e Oceaan, Het Gouden Fust of de Schieters bewonderen, dank jullie wel! Nog meer traditie vinden we terug in het jaarlijkse bezoek van **ASV Pap in de Beanen,** hoewel ik van jullie bezoekjes / onze reizen in Europa toch elke keer een week moest herstellen, heeft het me altijd gemotiveerd om mijn werk dan maar van tevoren af te hebben! Ook de buddies van het oude **MFVN bestuur** moeten we niet vergeten, of jullie nu hier kwamen gewoon om een beetje te hangen of om te stappen, het was altijd Machtig Mooi!

In Utrecht woont mijn BFF **Caspar,** die mij talloze keren van een gezellige dag of goed advies voorzien heeft, met zijn altijd relaxte instelling. I'm also in great debt to the amazing **Rebekah Burrow** for all the wonderful stays in London and warm friendship and checking this thesis.

Ook gaat mijn hart uit naar de hele familie **Höppener / Lempens.** Over de afgelopen jaren hebben jullie mij met open armen ontvangen in jullie familie en ik heb me vanaf het begin af aan ontzettend thuis gevoeld. **Marijke** en **Frank,** ik denk met zoveel plezier telkens terug aan de vakanties in India en Afrika, ik ben heel blij en dankbaar dat jullie me daarnaartoe meegenomen hebben!

Lieve **familie**, jullie hebben de afgelopen jaren mij bij elke bocht in mijn onderzoek ondersteund, en waren altijd bereid te luisteren naar mijn presentaties of naar mijn geëmmer over dingen die niet zo goed gingen. **Oma,** ik ben ontzettend blij dat ik nog altijd met open armen ontvangen wordt aan het Bovenste Eind en dat u altijd in bent voor een belletje. Dat geldt natuurlijk ook voor **Marlou** en **Leon,** die altijd een kaarsje opsteken als ik een uitdaging tegemoet ga en onze kat veel te veel verwennen.

Pap en **mam,** hoe ingewikkeld is het om goed uit te drukken waar ik jullie allemaal wel niet dankbaar voor ben. Ik ben jullie dankbaar voor alles, van begin tot eind. Dat begon natuurlijk al ver voor de start van mijn PhD, maar ik wil toch graag een paar onderdelen uitlichten die mij erg aan het hart gaan. **Papa,** ik heb ontzettend veel gehad aan al je adviezen over het krijgen van de promotieplek tot aan het omgaan met teleurstellingen. Doordat jij me zo gepusht hebt, heb ik er veel meer uitgehaald dan ik vooraf mogelijk had geacht. **Mama,** jij stond altijd klaar om zo in de auto te springen om weer naar Groningen af te rijden, als de (weers)omstandigheden het maar toelieten (knipoog)! Je was altijd geïnteresseerd in mijn ontwikkelingen en ik vond de bezoekjes die je bracht aan Groningen heel speciaal. Je hebt met al je zorgzaamheid heel erg veel bijgedragen aan mijn promotie en mijn ontwikkeling als mens.

Ik ben ook heel erg blij met alle bezoekjes die ik van en naar **Joris** heb gehad. Het leuke aan een broer hebben is dat je altijd op hetzelfde punt kunt verder gaan als waar je gebleven was. Ons uitstapje naar Engeland was er één om nooit te vergeten en getuigd van de hechte band van ons broederschap. Bedankt voor alle miljoen miljard tags op Facebook onder de belachelijk lekkere burgers en andere voedsel bacchanalen!

5 jaar geleden ontmoette ik in Boston op de vooravond van Independence Day een meisje. Ik viel meteen voor haar, het waren haar ogen. **Marthe** ik ben onwijs blij dat wij bij elkaar zijn gekomen en gebleven. De laatste twee jaar, dat we eindelijk samen konden wonen, waren de gelukkigste van mijn leven. Ik vind het fantastisch dat je mij op nieuwe manieren naar de wereld leert kijken en dat we zo kunnen genieten van al onze ondernemingen samen. Ik kijk gigantisch uit naar al onze volgende avonturen! Ik hou van jou.

About the author

Simon Hemelaar was born on the 24th of April 1989 in Weert, the Netherlands. After graduating from the Lorentz Casimir Lyceum in Eindhoven in 2007, he started his bachelor in Biomedical Sciences at the Radboud University Nijmegen. During his bachelor degree he completed a clinical research internship at the Intensive Care Research unit at the Radboud University Medical Center under supervision of dr. B. Ramakers and prof. dr. P. Picckers, concerning the role of adenosine during septic shock. One month after the start of his Master in Toxicology in 2010, Simon started a sabbatical year to govern the local student association. In 2012, he successfully finished a Malaria Research internship at the London School of Hygiene and Tropical Medicine in collaboration with dr. T. Bousema and prof. dr. C. Sutherland identifying the parameters for Malaria hotspots in developing countries, sponsored by the Erasmus foundation, resulting in a publication in the Malaria Journal. After he finished his courses following a minor in Pathobiology, Simon went to the Boston Children's Hospital (Harvard University) to uncover the role of the Wilms-Tumor 1 protein in chronic kidney disease in the group of dr. J. Kreidberg, in collaboration with dr. S. Ettou and prof dr. R. Bindels. This research was subsidized by the Nijmegen University Funding Foundation (SNUF) and the Dutch Kidney Foundation.

Following his graduation in 2013, Simon started his PhD in Groningen at the Bioanalysis Research Group led by Romana Schirhagl at the Biomedical Engineering department of the University Medical Center Groningen, in 2014. In his project Simon laid the groundwork for the use of Fluorescent Nanodiamonds in a wide array of cell biology settings. Next to his research, he was a board member of the Groningen Organization for PhD Education and Recreation (GOPHER) from 2014 to 2016, he organized the 2015 PhD Day and was a PhD representative at departmental meetings. During his PhD he has won several awards and prizes. In 2017 Simon got a personal scholarship for a new research line from the Jan Cornelis de Cock foundation. In the same year he got a Young Scholarship Award from the International Conference on Diamond and Carbon Materials, for his oral and poster presentation at the conference in Gothenburg. A year later, in 2018 Simon was awarded the Brilliant Poster Award at the SBDD XXIII Diamond Workshop at the conference in Hasselt. Finally, as he has always been interested in making his research accessible to a layman audience, Simon was a Finalist of the Three Minute Thesis Competition at the University of Groningen. In the second half of 2018 Simon obtained his PhD degree from the University of Groningen. He's currently employed as a post-doc lecturer at the University of Groningen teaching microscopy and surface charactarizatin.

Bibliography

2014 Mosha, J.F., Sturrock, H.J.W., Greenwood, B., Sutherland, C.J., Gadalla, N.B., Atwal, S., **Hemelaar, S.R.**, Brown, J.M., Drakeley, C., Kibiki, G., Bousema, T., Chandramohan, D. & Gosling, R.D. Hot spot or not: a comparison of spatial statistical methods to predict prospective malaria infections. *Malar. J.* **13**, 53 (2014).

2015 Nagl, A., **Hemelaar, S. R.** & Schirhagl, R. Improving Surface and Defect Center Chemistry of Fluorescent Nano-Diamonds for Imaging Purposes – A Review. *Anal. Bioanal. Chem.* (2015). doi:10.1007/s00216-015-8849-1

2017 **Hemelaar, S.R.**, Nagl, A., Bigot, F., Rodríguez-García, M.M., de Vries, M.P., Chipaux, M.S. & Schirhagl, R. The interaction of fluorescent nanodiamond probes with cellular media. *Microchim. Acta* 1–9 (2017). doi:10.1007/s00604-017-2086-6

Hemelaar, S.R., de Boer, P., Chipaux, M., Zuidema, W., Hamoh, T., Martinez, F.P., Nagl, A., Hoogenboom, J.P., Giepmans, B.N.G. & Schirhagl, R. Nanodiamonds as multi-purpose labels for microscopy. *Sci. Rep.* **7**, 720 (2017).

Hemelaar, S.R., van der Laan, K.J., Hinterding, S.R., Koot, M.V., Ellermann, E., Perona-Martinez, F.P., Roig, D., Hommelet, S., Novarina, D., Takahashi, H., Chang, M. & Schirhagl, R. Generally Applicable Transformation Protocols for Fluorescent Nanodiamond Internalization into Cells. *Sci. Rep.* **7**, (2017).

2018 **Hemelaar, S.R.**, Saspaanithy, B., L'Hommelet, S. R. M., Perona Martinez, F., van der Laan, K. J. & Schirhagl, R. The Response of HeLa Cells to Fluorescent NanoDiamond Uptake. *Sensors* **18**, 355 (2018).

Chipaux M.S., van der Laan, K.J., **Hemelaar, S.R.**, Hasani, M., Zheng, T. & Schirhagl, R. Nanodiamonds and Their Applications in Cells. *Small* **14**, (2018).